

Thermal, Hydraulic and Mechanical Properties of Sealing Materials

NWMO TR-2009-20

December 2009

A. Man and J.B. Martino

Atomic Energy of Canada Limited

nwmo

NUCLEAR WASTE
MANAGEMENT
ORGANIZATION

SOCIÉTÉ DE GESTION
DES DÉCHETS
NUCLÉAIRES



Nuclear Waste Management Organization
22 St. Clair Avenue East, 6th Floor
Toronto, Ontario
M4T 2S3
Canada

Tel: 416-934-9814
Web: www.nwmo.ca

Thermal, Hydraulic and Mechanical Properties of Sealing Materials

NWMO TR-2009-20

December 2009

A. Man and J.B. Martino
Atomic Energy of Canada Limited

Disclaimer:

This report does not necessarily reflect the views or position of the Nuclear Waste Management Organization, its directors, officers, employees and agents (the "NWMO") and unless otherwise specifically stated, is made available to the public by the NWMO for information only. The contents of this report reflect the views of the author(s) who are solely responsible for the text and its conclusions as well as the accuracy of any data used in its creation. The NWMO does not make any warranty, express or implied, or assume any legal liability or responsibility for the accuracy, completeness, or usefulness of any information disclosed, or represent that the use of any information would not infringe privately owned rights. Any reference to a specific commercial product, process or service by trade name, trademark, manufacturer, or otherwise, does not constitute or imply its endorsement, recommendation, or preference by NWMO.

ABSTRACT

Title: Thermal, Hydraulic and Mechanical Properties of Sealing Materials
Report No.: NWMO TR-2009-20
Author(s): A. Man, J.B. Martino
Company: Atomic Energy of Canada Limited
Date: December 2009

Abstract

A large amount of work has been invested in developing an understating of the properties of materials used in engineered barrier systems for used nuclear fuel isolation in Canada and internationally. Clay-based sealing materials have been designated by function and material composition. The proposed clay based sealing materials for use in Canada include: Light Backfill (LBF), Dense Backfill (DBF), Gap Fill (GF), Bentonite-Sand Buffer (BSB) and Highly Compacted Bentonite (HCB). Cement based material is primarily designated as concrete and specifically low alkalinity concrete, but cement based materials may also be used in grouting applications. Properties and behaviour of these materials are required to evaluate and model the performance of the overall repository sealing system.

The known properties and behaviour of these materials are summarized from various programs. As all natural materials vary, the details of the materials are identified when available. Not all properties of these materials have been determined, and these are identified as knowledge gaps to guide future material testing programs.

TABLE OF CONTENTS

	<u>Page</u>
ABSTRACT	v
1. INTRODUCTION.....	1
1.1 CLAY-BASED MATERIALS	4
1.2 CEMENT-BASED MATERIALS.....	6
2. THERMAL PROPERTIES	8
2.1 THERMAL PROPERTIES OF BENTONITE-SAND BUFFER	8
2.2 THERMAL PROPERTIES OF LIGHT BACKFILL.....	10
2.3 THERMAL PROPERTIES OF HIGHLY COMPACTED BENTONITE	10
2.4 THERMAL PROPERTIES OF GAP FILL.....	12
2.5 THERMAL PROPERTIES OF DENSE BACKFILL	12
2.6 THERMAL PROPERTIES OF LOW ALKALINITY CONCRETE	13
2.7 THERMAL PROPERTIES OF LOW ALKALINITY CEMENTITIOUS GROUT	13
2.8 SUMMARY OF THERMAL PROPERTIES.....	13
3. HYDRAULIC PROPERTIES	14
3.1 HYDRAULIC PROPERTIES OF BENTONITE-SAND BUFFER.....	14
3.1.1 Soil-Water Characteristic Curve.....	14
3.2 Hydraulic Conductivity	16
3.3 HYDRAULIC PROPERTIES OF LIGHT BACKFILL	20
3.4 HYDRAULIC PROPERTIES OF HIGHLY COMPACTED BENTONITE	20
3.4.1 Soil-Water Characteristic Curve.....	20
3.4.2 Hydraulic Conductivity.....	22
3.5 HYDRAULIC PROPERTIES OF GAP FILL	22
3.5.1 Soil-Water Characteristic Curve.....	22
3.5.2 Hydraulic Conductivity.....	23
3.6 HYDRAULIC PROPERTIES OF DENSE BACKFILL.....	23
3.6.1 Soil-Water Characteristic Curve.....	23
3.6.2 Hydraulic Conductivity.....	23
3.7 HYDRAULIC PROPERTIES OF LOW ALKALINITY CONCRETE	25
3.8 HYDRAULIC PROPERTIES OF LOW ALKALINITY CEMENTIOUS GROUT ...	25
3.9 SUMMARY OF HYDRAULIC PROPERTIES	26
4. MECHANICAL PROPERTIES.....	26
4.1 BACKGROUND.....	26
4.1.1 Linear Elastic Model.....	27
4.1.2 Mohr-Coulomb Models.....	28
4.1.3 Critical State Models	29
4.2 MECHANICAL PROPERTIES OF BENTONITE-SAND BUFFER.....	36
4.2.1 Strength Envelope	37
4.2.2 Elastic Parameters.....	42
4.2.3 Hardening Behaviour	43
4.2.4 Yield Loci and Flow Rule.....	47
4.2.5 Unsaturated Conditions	49

4.2.5.1	Strength Envelope	49
4.2.5.2	Elastic Parameters.....	57
4.2.5.3	Hardening Behaviour	62
4.2.5.4	Yield Loci and Flow Rule.....	64
4.2.6	Swelling Behaviour	72
4.3	MECHANICAL PROPERTIES OF LIGHT BACKFILL	72
4.3.1	Strength Envelope	73
4.3.2	Elastic Parameters.....	77
4.3.3	Hardening Behaviour	79
4.3.4	Yield Loci and Flow Rule.....	84
4.3.5	Unsaturated Conditions	85
4.3.6	Swelling Behaviour	85
4.4	MECHANICAL PROPERTIES OF HIGHLY COMPACTED BENTONITE	85
4.4.1	Strength Envelope	86
4.4.2	Elastic Parameters.....	86
4.4.3	Hardening Behaviour	86
4.4.4	Yield Loci and Flow Rule.....	88
4.4.5	Unsaturated Conditions	89
4.4.6	Swelling Behaviour	89
4.5	MECHANICAL PROPERTIES OF GAP FILL	93
4.5.1	Strength Envelope	93
4.5.2	Elastic Parameters.....	93
4.5.3	Hardening Behaviour	94
4.5.4	Yield Loci and Flow Rule.....	94
4.5.5	Unsaturated Conditions	94
4.5.6	Swelling Behaviour	96
4.6	MECHANICAL PROPERTIES OF DENSE BACKFILL.....	101
4.6.1	Strength Envelope	102
4.6.2	Elastic Parameters.....	104
4.6.3	Hardening Behaviour	104
4.6.4	Yield Loci and Flow Rule.....	107
4.6.5	Unsaturated Conditions	107
4.6.6	Swelling Behaviour	107
4.7	MECHANICAL PROPERTIES OF LOW ALKALINITY CONCRETE.....	108
4.8	MECHANICAL PROPERTIES OF LOW ALKALINITY CEMENTIOUS GROUT	116
4.9	SUMMARY OF MECHANICAL PROPERTIES	117
5.	KNOWLEDGE GAP SUMMARY.....	119
6.	CONCLUSIONS.....	123
	ACKNOWLEDGEMENTS	124
	REFERENCES	125

LIST OF TABLES

	<u>Page</u>
Table 1: Summary of General Properties (after Russell and Simmons 2003)	7
Table 2: Typical Relative Densities and Specific Heat Capacities of Constituent Materials for Sealing Materials (after Baumgartner 2006e)	10
Table 3: Coefficient of Thermal Expansion for MX-80 Na-Bentonite (after Börgesson et al. 1988).....	12
Table 4: Summary of Thermal Properties	13
Table 5: Summary of As-Placed Hydraulic Properties.....	26
Table 6: Values of M^b and ϕ^b for Bentonite-Sand Buffer (after Wiebe et al. 1998)	50
Table 7: Matrix of Triaxial Tests Completed on Light Backfill made with Fresh Water as the Pore Fluid (after Blatz et al. 2008).....	73
Table 8: Matrix of Triaxial Tests being Completed on Light Backfill with Saline Water (227 g/L CaCl_2) as the Pore Fluid	73
Table 9: Strength Parameters for Light Backfill.....	75
Table 10: Deformation Parameters for Light Backfill made with Fresh Water as the Pore Fluid (after Blatz et al. 2008;).....	79
Table 11: Summary of Compression Index (C_c) and Swelling Index (C_s) for LBF under Various Pore Fluid Conditions (Priyanto et al. 2008b)	81
Table 12: Summary of Compression Index (C_c) and Swelling Index (C_s) for Highly Compacted Bentonite under Various Pore Fluid Conditions (Priyanto et al. 2008b) ..	87
Table 13: Matrix of Triaxial Tests on Dense Backfill Made With Fresh Water as the Pore Fluid (Blatz et al. 2008)	101
Table 14: Strength Parameters for Dense Backfill	102
Table 15: Preliminary Deformation Parameters for Dense Backfill (after Blatz et al. 2008).....	104
Table 16: Summary of Compression Index (C_c) and Swelling Index (C_s) for Dense Backfill Under Various Pore Fluid Conditions (Priyanto et al. 2008b)	106
Table 17: Comparison of Material Content of High Performance Concrete Types	109
Table 18: Mechanical Properties Comparison of Standard High Performance Concrete and Low Heat High Performance Concrete	111
Table 19: Average Unconfined Compressive Strength Values (MPa)	112
Table 20: Properties of UF41-14-4 Low Alkalinity Grout	117
Table 21: Summary of Mechanical Properties.....	118
Table 22: Repository Sealing Systems	120

LIST OF FIGURES

	<u>Page</u>
Figure 1: Proposed Sealing Materials for use in a Deep Geological Repository for the (a) Horizontal Tunnel Placement and (b) In-floor (NUKEM 2003) Placement Cross-sectional Geometry	3
Figure 2: Thermal Conductivity of 50:50 wt% Bentonite-Sand Buffer (BSB) (Wan 1996; Graham et al. 1997) and Estimated Range of Values for Highly Compacted Bentonite Clay (HCB) (derived from Villar 2002; JNC 2000; Börgesson et al. 1994). Note: Label units are dry densities (ρ_d) (after Baumgartner 2006e)	8

continued...

LIST OF FIGURES (continued)

	<u>Page</u>
Figure 3: Specific Heat Capacity for Highly Compacted Bentonite as a Function of Saturation. Note: Label units are dry densities (ρ_d) (after Baumgartner 2006e).....	11
Figure 4: Soil-Water Characteristic Curve for Highly Compacted Ca-Bentonite (after Villar 2002) and for 50:50 Bentonite-Sand Buffer (after Wan 1996) Under the Free-Volume Boundary Condition. Note: no direct correlation between the two horizontal axes.....	15
Figure 5: Soil-Water Characteristic Curve of Bentonite-Sand Buffer made with a Variety of Bentonites, Determined using Several Measurement Techniques (after Priyanto 2007).....	16
Figure 6: Hydraulic Conductivity as a Function of Effective Montmorillonite Dry Density and Total Dissolved Solids (TDS) for Saturated Smectite-Based Sealing Materials. Note: TDS is based on NaCl solutions (after Dixon 2002).....	18
Figure 7: Hydraulic Conductivity of Bentonite-Sand Buffer.....	19
Figure 8: Hydraulic Conductivity of Bentonite and Bentonite Sand Mixture (after Priyanto et al. 2008b).....	19
Figure 9: Soil-Water Characteristic Curves for Highly Compacted Bentonite (MX-80) under the Constant-Volume Boundary Condition (unpublished data). Note: regression fits by van Genuchten et al. (1991) (after Baumgartner 2006e).....	21
Figure 10: The Relationship Between Gap Fill Effective Montmorillonite Dry Density (EMDD) and the Resulting Average EMDD of the System (after Dixon et al. 2005).....	23
Figure 11: Hydraulic Conductivity of Dense Backfill (after Dixon et al. 2002).....	24
Figure 12: Classification of Mechanical Constitutive Models for Clay (after Priyanto 2007).....	27
Figure 13: Mohr-Coulomb Model for Saturated Soil (after Terzaghi 1936).....	28
Figure 14: Mohr-Coulomb Model for Unsaturated Soil (after Fredlund and Morgenstern 1977).....	29
Figure 15: Modified Cam-clay Model (after Roscoe and Burland 1968; Priyanto 2007).....	32
Figure 16: The Basic Barcelona Model (BBM): (a) p,q-space; (b) p,s-space; (c) V,ln p-space; and (d) V,ln s-space (after Alonso et al. 1990; Priyanto 2007).....	32
Figure 17: The Basic Barcelona Model (BBM) Yield Surface (after Alonso et al. 1990; Priyanto 2007).....	33
Figure 18: The Yield Surface for the BExM Model (after Alonso et al. 1990; Priyanto 2007).....	33
Figure 19: Coupling Yield Surfaces in p,s-Space (after Tang and Graham 2002; Delage and Graham 1996; Alonso et al. 1990; Priyanto 2007).....	34
Figure 20: Yield Surfaces on p,s-Space for the BBM and the BGM (after Priyanto 2007).....	34
Figure 21: Planar Critical State Surface (after Wiebe et al. 1998; Blatz and Graham 2003; Priyanto 2007).....	35
Figure 22: Critical State Slope as a Function of Suction in BGM (after Blatz and Graham 2003; Priyanto 2007).....	35
Figure 23: Critical State Slope as a Function of Suction in the BGM (after Blatz and Graham 2003; Priyanto 2007).....	36
Figure 24: Summary of Strength Envelopes at Various Temperatures. Note: top = peak, bottom = end-of-test (after Lingnau 1993).....	40
Figure 25: Summary of Shear Strength Results (after Yarechewski 1993).....	41
Figure 26: Summary of Critical State Lines in V_c vs. $\log p'$ -Space (after Lingnau 1993).....	41
Figure 27: Summary of Critical State Lines in V_c vs. $\ln p'$ -Space (after Yarechewski 1993).....	42

continued...

LIST OF FIGURES (continued)

	<u>Page</u>
Figure 28: Summary of Hardening Behaviour of Bentonite-Sand Buffer in V_c vs. in p' -Space (after Wan 1987)	46
Figure 29: Summary of Normal Consolidation Lines for Bentonite-Sand Buffer (after Yarechewski 1993).....	47
Figure 30: Yield Data, Normalized with Respect to p'_c , for Low ($\rho_d = 1.49 \text{ Mg/m}^3$) and High Density ($\rho_d = 1.67 \text{ Mg/m}^3$) Bentonite-Sand Buffer (after Oswell 1991).....	48
Figure 31: Plastic Strain Increment Vectors for Low ($\rho_D = 1.49 \text{ Mg/m}^3$) and High Density ($\rho_D = 1.67 \text{ Mg/m}^3$) Bentonite-Sand Buffer Indicating Non-Associated Flow (after Oswell 1991).....	48
Figure 32: Typical Stress-Strain Curves for Low Temperature and Pressure (Top) and High Temperature and Pressure (Bottom) (after Wiebe et al. 1998)	50
Figure 33: Boundary Surface for the Peak Strength of Unsaturated Bentonite-Sand Buffer (after Wiebe et al. 1998).....	51
Figure 34: Peak Strength Envelopes at Various Suctions (after Blatz 2000).....	52
Figure 35: Peak Strength Envelopes at Various Cell Pressures (after Blatz 2000)	52
Figure 36: Large Strain Strengths at Varying Suction (after Blatz 2000).....	53
Figure 37: Summary of Critical State M Values for Varying Suction (after Blatz 2000).....	53
Figure 38: N Values for Bentonite-Sand Buffer Made with Wyoming and Saskatchewan Bentonite at Varying Suctions (after Anderson 2003 which referenced Ferris 2000 and Blatz 2000)	54
Figure 39: Summary of Critical State M Values for Varying Suction (after Tang 1999)	54
Figure 40: Comparison of Triaxial Testing Results Conducted on Specimens prepared by Blatz (2000) and on Specimens from a Large Scale in Situ Experiment (after Blatz 2000).....	55
Figure 41: Peak Strength vs. Suction for a Range of Salt Concentrations in the Pore Fluid (after Tang 1999)	56
Figure 42: Tensile Strength of Bentonite-Sand Buffer as a Function of Total Suction (after Tang 1999)	56
Figure 43: Effect of Total Suction and Confining Pressure on Young's Modulus at 26°C, 65°C and 100°C (after Wiebe 1998).....	58
Figure 44: Young's Modulus vs. Degree of Saturation (after Tang 1999).....	59
Figure 45: Young's Modulus vs. Degree of Saturation for Two Different Concentrations of NaCl in the Pore Fluid (after Tang 1999).....	59
Figure 46: Bentonite-Sand Buffer Stiffness for Varying Cell Pressure and Suction (after Blatz 2000).....	61
Figure 47: Comparison of Interpreted E Values (after Blatz 2000).....	61
Figure 48: κ Values for Bentonite-Sand Buffer at Varying Suction (after Anderson 2003).....	62
Figure 49: Volume Change with Mean Stress and Total Suction (after Tang 1999).....	63
Figure 50: Hardening Line (λ) Parameters for Bentonite-Sand Buffer at Varying Suctions (after Anderson 2003)	63
Figure 51: Conceptual Elastic-Plastic Model for Unsaturated Soils showing the State Boundary Surface in p,q,s -Space (after Tang and Graham 2002).....	65
Figure 52: Two Series of Tests Examined by Tang and Graham (2002) in p,q,s -Space. Note: for clarity, data points from only one test are shown (after Tang and Graham 2002).....	65

continued...

LIST OF FIGURES (continued)

	<u>Page</u>
Figure 53: Normalized Yield Data for Bentonite-Sand Buffer. Series 1 was prepared with an initial suction of 4 MPa (as-compacted), and Series 2 was prepared with an initial suction of 6 MPa (after Tang and Graham 2002)	66
Figure 54: Expansion of the Yield Locus in p,s-Space (after Tang and Graham 2002)	66
Figure 55: Modelled LY and T-line Based on Experimental Results. Note: CSF represents Critical State Failure (after Blatz and Graham 2003)	67
Figure 56: Three-Dimensional p,q,s Model (after Blatz and Graham 2003)	68
Figure 57: Three-dimensional Volume State Surface for Bentonite-Sand Buffer in p,s, V-Space (after Blatz and Graham 2003)	68
Figure 58: Shrinkage Curves Showing Suction Induced Yielding for Bentonite-Sand Buffer made with Wyoming and Saskatchewan Bentonite (after Anderson 2003).....	69
Figure 59: Load-Yield (LY) Lines for Bentonite-Sand Buffer made with Wyoming and Saskatchewan Bentonite (after Anderson 2003)	70
Figure 60: Normalized Peak Strengths for Bentonite-Sand Buffer made with Wyoming and Saskatchewan Bentonite, Defining Yield Loci for Varying Suction (after Anderson 2003) .	70
Figure 61: Results of Infiltration Test on Compacted Bentonite-Sand-Buffer on p,w,V-Space (after Siemens 2006).....	71
Figure 62: Critical State (Solid Line) and Peak (Dashed Line) Strength Envelopes for LBF made with Fresh (Distilled, Deionized) Water as the Pore Fluid (after Blatz et al. 2008) ...	75
Figure 63: Strength Results for Light Backfill Made with Saline (227 g/L) Pore Fluid Compared to the Results for Light Backfill Made with Fresh Pore Water	76
Figure 64: Light Backfill Specimen GS-LB05 (prepared with Fresh Water) used to Calculate Cam Clay Parameters κ and λ . Bulk Modulus was estimated from the same portion of the curve as κ (modified from Blatz et al. 2008)	78
Figure 65: Isotropic Consolidation Data from Drained Tests on Light Backfill (prepared with Fresh Water) used for the Determination of Cam Clay λ Parameter. Note: the plot was established by combining the end-of-consolidation data from the tests shown (from Blatz et al. 2008).....	80
Figure 66: The Effect of CaCl ₂ and NaCl Solution to the Compression Index (C _c) and Swelling Index (C _s) of Light Backfill (after Priyanto et al. 2008b)	82
Figure 67: Relationship of Compression Index (C _c) and Swelling Index (C _s) and TDS of Solution (after Priyanto et al. 2008b)	83
Figure 68: 1-D Constrained Moduli as a Function of Effective Montmorillonite Dry Density for Samples made with Fresh Water and Saline Water for the Loading Path (after Baumgartner et al. 2008; Priyanto et al. 2008b)	84
Figure 69: Normalized Yield Loci for LBF	85
Figure 70: The Effect of CaCl ₂ and NaCl Solution to the Compression Index (C _c) and Swelling Index (C _s) of Highly Compacted Bentonite (after Priyanto et al. 2008b)	88
Figure 71: Swelling Pressure as a Function of Effective Montmorillonite Dry Density and Total Dissolved Solids (TDS) for Saturated Smectite-based Sealing Materials. Note: TDS is based on NaCl solutions (after Baumgartner 2006e).....	90
Figure 72: Swelling Pressure of MX-80 Bentonite as a Function of Effective Montmorillonite Dry Density and Total Dissolved Solids (TDS) (after SKI 2005; Hedin 2004). Note: Concentration and TDS are based on NaCl solutions	91

continued...

LIST OF FIGURES (concluded)

	<u>Page</u>
Figure 73: The Effect of CaCl ₂ Concentration in Pore Liquid on the Swelling Pressure of Highly Compacted Bentonite (after Priyanto et al. 2008b).....	93
Figure 74: Stress Path Followed during Wetting of Gap fill at Constant Loading (after Hoffmann et al. 2007).....	95
Figure 75: Stress Path Followed during Wetting of Gap fill at Constant Volume (after Hoffmann et al. 2007).....	95
Figure 76: Pellet and Granule Free Swell Tests in Distilled Deionized Water (after Kjartanson et al. 2005).....	97
Figure 77: Pellet and Granule Free Swell Tests in 100 g/L NaCl Solution (after Kjartanson et al. 2005).....	97
Figure 78: Pellet and Granule Free Swell Tests in 100 g/L CaCl ₂ Solution (after Kjartanson et al. 2005).....	98
Figure 79: Swelling Pressure of Gap Fill in 100 g/L TDS Solution (after Kjartanson et al. 2003).....	98
Figure 80: Swelling Strain versus Vertical Stress for Gap Fill for a Range of Dry Density (after Hoffmann et al. 2007).....	99
Figure 81: Swelling Pressure of Gap fill made with MX-80 Pellets Saturated with 0.2 mol/L NaCl Solution (after Karnland et al. 2008).....	99
Figure 82: Swelling Pressure of Compacted FoCa Bentonite Powder and Powder/Pellet Mixtures (after Imbert and Villar 2006) (solid line shows relationship for FoCa samples).....	100
Figure 83: Critical State (Solid Line) and Peak (Dashed Line) Strength Envelopes for Dense Backfill made with Fresh (Distilled, Deionized) Water.....	103
Figure 84: Combined End-of-Test Isotropic Consolidation Data for Dense Backfill (after Blatz et al. 2008).....	105
Figure 85: The Effect of CaCl ₂ and NaCl Solution on (a) the Compression Index (Cc) and (b) Swelling Index (Cs) of Dense Backfill (after Priyanto et al. 2008b).....	106
Figure 86: Normalized Yield Locus for DBF.....	107
Figure 87: Unconfined Compressive Strength of Low Heat High Performance Concrete (LHHPC), Standard High Performance Concrete (SHPC), Pulverized Fly Ash Concrete (PFAC) Mixes (a) Laboratory Cured Cylinders (b) Cored Samples from Blocks.....	110
Figure 88: Unconfined Compressive Strength of Low Heat High Performance Concrete (LHHPC), Standard High Performance Concrete (SHPC), Pulverized Fly Ash Concrete (PFAC) Mixes (a) Laboratory Cured Cylinders (b) Cored Samples from Blocks.....	114

1. INTRODUCTION

The Government of Canada (NRCan 2007) has accepted the Nuclear Waste Management Organization's (NWMO) recommendation of Adaptive Phased Management as the long-term management approach for Canada's used nuclear fuel (2005). Adaptive Phased Management (APM) includes the isolation and containment of used nuclear fuel in a suitable rock formation, such as crystalline rock or sedimentary rock.

The APM approach includes:

- centralized containment and isolation of the used fuel in a deep geologic repository (DGR) in suitable rock formations, such as the crystalline rock of the Canadian Shield or sedimentary rock;
- flexibility in the pace and manner of implementation through a phased decision-making process, supported by a program of continuous learning, research and development;
- continuous monitoring of the used fuel to support engineering design and confirmation of the safety and performance of the repository; and
- potential for retrieval of the used fuel for an extended period, until such time as a future society makes a decision on the final closure and the appropriate form and duration of post-closure monitoring.

The interim storage phase ensures that the used nuclear fuel will be monitored and remain retrievable, and is also designed to take advantage of emerging energy technologies, including the possibility of recycling the fuel.

Research and development (R&D) has been underway in Canada since 1978 (Joint Statement 1978) to develop an acceptable approach for the management of Canada's used nuclear fuel. Since 2005, this R&D has focussed on the development of the required technologies for the implementation of a deep geological repository as one feature of the Adaptive Phased Management approach (NWMO 2005, NRCan 2007). Ontario Power Generation (OPG) and Atomic Energy of Canada Limited (AECL) are also considering the use of deep geologic repositories for the isolation of low- and intermediate-level radioactive wastes.

A large amount of work has been invested in developing an understanding of the properties of the materials used in engineered barrier systems in Canada and internationally. The engineered barriers that comprise the overall repository sealing system include the:

- placement room sealing system (Baumgartner 2006a);
- bulkhead sealing system (Baumgartner 2006b);
- tunnel, service area, shaft and ramp sealing system (Baumgartner 2006c); and
- borehole sealing system (Baumgartner 2006d).

Multiple sealing-system components may be used in an emplacement-room sealing system (Figure 1) as part of a Deep Geologic Repository (DGR) for used nuclear fuel as proposed by Ontario Power Generation's third case study (Gierszewski et al. 2004). This includes the Horizontal Tunnel Placement method (Baumgartner 2005) and the In Floor Method (NUKEM 2003). The repository-sealing system will include components comprised of both clay-based and cement-based materials. In order to understand the mechanical response of the

components, and their combined effects, the properties of each component material need to be determined under the geochemical conditions expected in a DGR.

This report builds on an earlier report titled “Generic thermal-hydraulic-mechanical (THM) data for sealing materials – Volume 1: Soil-water relationships” (Baumgartner 2006e). Baumgartner (2006e) included general descriptive relationships, hydraulic properties, swelling properties and thermal properties available at the time of writing for the clay-based sealing materials. This report compiles and summarizes the information and adds a further review of the literature on the thermal-hydraulic-mechanical properties of unsaturated clay-based sealing materials.

An extensive list of references is provided. The known properties of these materials are summarized from various research programs. As all natural materials vary, the details of the materials are identified when available. The information presented in this document states the relevant test conditions and types of constitutive models used. To prevent the use of any parameter out of context, the reader is advised to consider the relevant conditions and if uncertain, consult the original research.

The purpose of this report is to summarize the currently available information on material properties and behaviour that are relevant to the sealing materials being considered by NWMO. This information is required to evaluate and model the performance of the repository sealing system. Missing information is identified as knowledge gaps to identify further characterization needs; this will guide future materials testing programs.

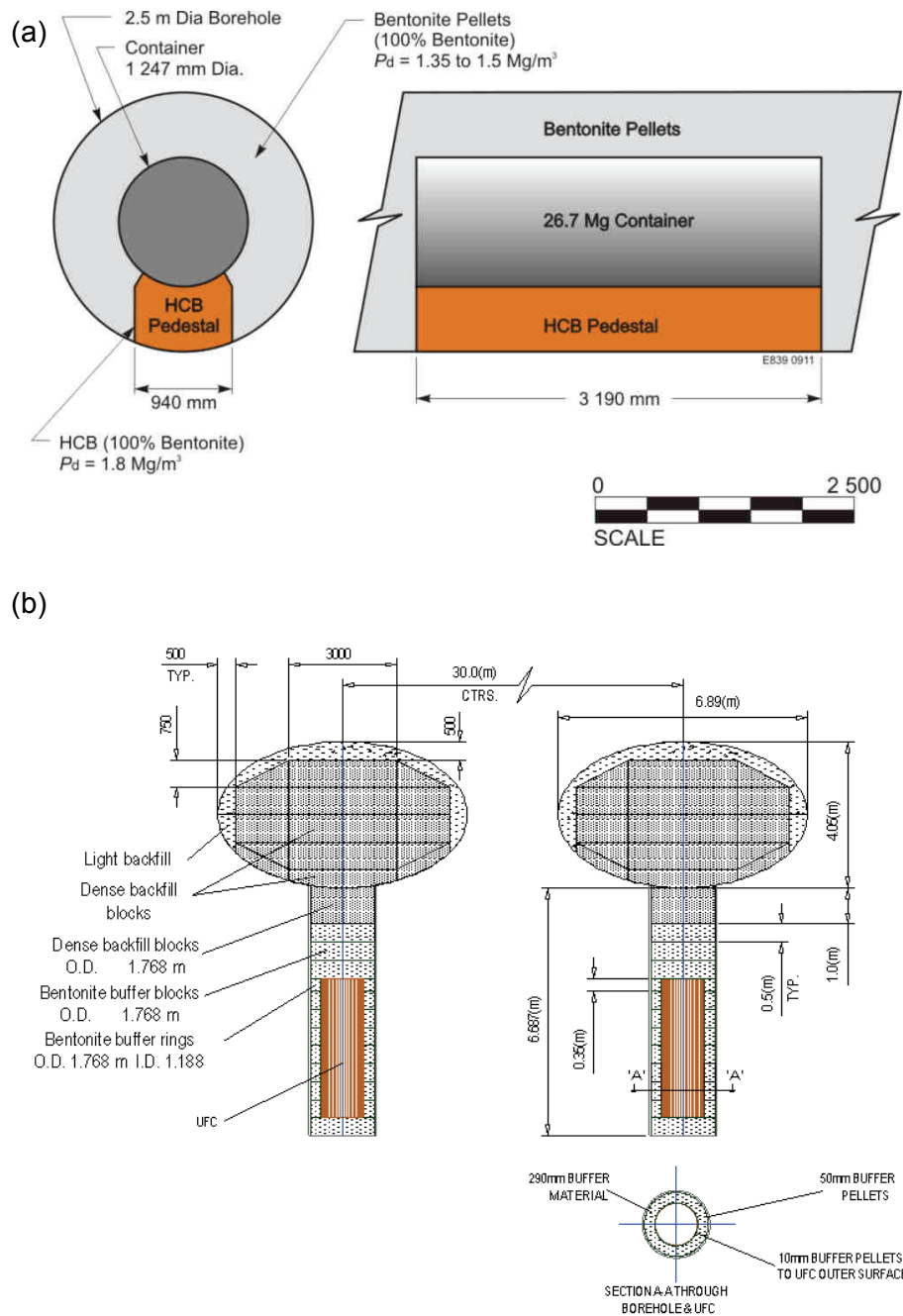


Figure 1: Proposed Sealing Materials for use in a Deep Geological Repository for the (a) Horizontal Tunnel Placement and (b) In-floor (NUKEM 2003) Placement Cross-sectional Geometry

1.1 CLAY-BASED MATERIALS

Potential clay-based materials have been designated as (Russell and Simmons 2003):

- Bentonite-Sand Buffer (BSB) – a mixture of bentonite clay and silica sand, installed either at high dry density by *in situ* compaction or as prefabricated blocks;
- Light Backfill (LBF) – a mixture of bentonite clay and silica sand, likely installed in the form of dense pellets at low-to-medium dry density;
- Highly compacted bentonite (HCB) – 100% bentonite clay installed either at high dry density by *in situ* compaction or as prefabricated blocks;
- Gap Fill (GF) – either bentonite clay, possibly fabricated in the form of dense pellets, silica sand or some combination of the two, which are likely to be installed at low-to-medium average dry density; and
- Dense Backfill (DBF) – a mixture of lake clay, crushed host rock and bentonite clay, installed either at high dry density by *in situ* compaction or as prefabricated blocks.

A summary of the general as-placed properties of these materials is included in Table 1. Each material has a specific purpose, as shown in Figure 1. BSB and HCB provide a low hydraulic conductivity barrier immediately surrounding the used fuel canisters that is capable of swelling and self-sealing. The addition of sand in BSB increases the thermal conductivity of the material relative to pure bentonite to assist in heat transfer from the used fuel. DBF may be used in the emplacement rooms and/or for sealing access tunnels and shafts. LBF and GF are intended for placement in areas where mechanical compaction will be difficult and will swell into any voids as it saturates.

The THM properties and behaviour of clay based sealing materials are dependent on density and water content of the materials. Baumgartner (2006e) provides a detailed discussion of the soil phase relationships in Volume 1 of this report series. A summary of these important factors is presented here for completeness.

The dry density (ρ_d) of a mixture of soil constituents can be expressed as follows (Baumgartner 2006e):

$$\rho_d = \frac{M_s}{V} = \frac{M_s}{(V_s + V_v)} = \frac{\sum_{i=1}^n M_{si}}{\left(\sum_{i=1}^n (V_{si}) + V_v \right)} = \frac{\sum_{i=1}^n M_{si}}{\left[\sum_{i=1}^n \left(\frac{M_{si}}{(G_{si} \cdot \rho_w)} \right) + V_v \right]} \quad (1)$$

where: V = total volume (m^3);
 V_{si} = volume occupied by solid component i (m^3);
 V_v = void volume (m^3);
 M_s = total mass of solids (kg)
 M_{si} = mass of solid constituent material i (no units); and
 G_{si} = specific gravity of solid constituent i (no units).

In the past, the mixture of bentonite clay and aggregates was characterized by the clay fraction as being the active component in the mixture (Dixon and Gray 1985). Thus, the term clay dry density (ρ_{cd}) or effective clay dry density (ECDD) was derived and is expressed as follows (Baumgartner 2006e):

$$ECDD = \rho_{cd} = \frac{M_c}{(V_c + V_v)} = \frac{f_c \cdot \rho_d}{\left[1 - \left(\frac{(1 - f_c) \cdot \rho_d}{G_a \cdot \rho_w}\right)\right]} \quad (2)$$

where M_c = expressed as mass per unit volume of clay component (kg/m^3);
 V_c = volume occupied by clay component (m^3);
 f_c = mass fraction of clay in dry solids (no units); and
 G_a = specific gravity of aggregate component (no units).

An extension of this concept is to consider the amount of swelling clay (smectite) in the clay fraction of a given clay. The smectite minerals (the most commonly present smectite mineral is the clay mineral montmorillonite) incorporate available water into their layered mineral structure (hence its swelling ability) and dominate the clay fraction in the commercially marketed swelling clays called bentonite. The smectite content in bentonite varies with source deposit and even within a single source. The term effective montmorillonite dry density (EMDD) was derived to provide a normalizing parameter for use in describing several key behavioural properties (e.g. swelling pressure and hydraulic conductivity) (Baumgartner and Snider 2002, JNC 2000a) to single out the role of montmorillonite in soil behaviour and is expressed as follows (Baumgartner 2006e):

$$EMDD = \rho_{md} = \frac{M_m}{(V_m + V_v)} = \frac{f_m \cdot f_c \cdot \rho_d}{\left[1 - \left(\frac{(1 - f_c) \cdot \rho_d}{G_a \cdot \rho_w}\right) - \left(\frac{(1 - f_m) \cdot f_c \cdot \rho_d}{G_n \cdot \rho_w}\right)\right]} \quad (3)$$

where M_m = expressed as mass per unit volume of montmorillonite component (kg/m^3);
 V_m = volume occupied by montmorillonite component (m^3);
 f_m = mass fraction of montmorillonite in clay fraction f_c (no units); and
 G_n = specific gravity of non-montmorillonite component in clay, typically 2.64 to 2.70 (no units).

The above ECDD and EMDD relationships are useful for normalizing the hydraulic and swelling behaviours of bentonite and aggregate mixtures on a common basis under saturated conditions (Baumgartner 2006e).

Throughout the life of a repository sealing system, water content of the clay-based materials will undergo a transition from as-placed, unsaturated conditions to saturated conditions as the groundwater flow regime rebounds. Following placement, the material will be subject to heating from the waste, initially with moisture movement away from the canister. Over time, wetting occurs as the host formation supplies water to the materials. As the system becomes saturated, the materials with higher EMDD values will swell and compress materials with lower EMDD values. This may be accompanied by a change in pore fluid chemistry within the material.

The thermal, hydraulic and mechanical properties of the clay based sealing materials are largely dependent on water content, which in turn is influenced by heating. As such, the system is coupled in terms of thermal, hydraulic and mechanical (THM) conditions. In order to effectively model the THM behaviour of the sealing system, the THM properties of each material are required for the range of conditions expected in the repository.

1.2 CEMENT-BASED MATERIALS

Cement-based materials are those that use Portland cement as part of their binder material. In engineered barrier systems, the primary use of cement-based material is for massive restraint plugs. Cement-based materials may also be used for engineering expedients; cement-based materials can include floors, shotcrete for tunnel support, grouts to reduce hydraulic conductivity in natural fracturing and in excavation damaged zones, and constructing underground structures.

The mode of placing the concrete material for an engineered barrier system has not yet been specified, but large concrete units have been successfully poured in place with no cold joints that could provide a flow pathway through a restraint unit or reduce its stability (Chandler et al. 2002; Martino et al. 2008).

Although grout is generally considered an engineering expedient rather than a sealing material, the development of grout and other cement-based engineering expedients falls into the category of materials development and so are described in this report. Furthermore, grout will eventually be required to decommission the network of investigation and monitoring boreholes surrounding a repository to prevent short-circuiting of the groundwater flow regime.

Concrete used in repository sealing systems will be in contact with clay-based sealing materials. The general concern with concrete-clay interactions is the effect of concrete degradation products on clay swelling potential and the elevated pH of concrete reducing the swelling ability of clays. This was shown by Oscarson et al. (1997), who demonstrated that high pH concrete leachates affected clay minerals.

In regular concretes, cement dissolution releases mainly Na, K, OH (early), and Ca, OH (later). The initial high Na and K concentrations are a consequence of the non-restricted solubility of NaOH and KOH present in freshly hydrated cement. The following increasing/high Ca concentration is a result of $\text{Ca}(\text{OH})_2$ solubility (Metcalf and Walker 2004). Pusch (1982) studied the chemical interaction of clay buffer materials and concrete in low temperature systems (approximately 15°C). In that study, the trend was for calcium to leach from the concrete into the clay, largely due to the higher concentration of calcium in the concrete. This leaching has the effect of increasing porosity and permeability, and decreasing strength of the concrete.

Because of the potential effect of a high alkaline plume from concrete, low alkalinity type concrete is recommended for repository use to maintain the desirable properties of clays (Bodén et al. 2001). Cement-based materials for use in a Canadian deep geologic repository for used nuclear fuel are designated as low alkalinity materials to minimize the interaction with the swelling clay based materials (Martino 2006). Vieno (2004) also suggests the redox stability of spent fuel is questionable if it comes in contact with a high pH solution. It was noted that the

spent fuel itself also contains alkaline and earth-alkaline metals, notably cesium, which, when released from the fuel, may increase the pH inside the canister.

Low alkalinity (also called low pH) concrete, or LAC, can have various formulations and are achieved by substituting a silica-based pozzolan (e.g. fly ash, silica fume) for a portion of the cement in the binder. The reference material in Canada is the Low Heat High Performance Concrete (Gray and Shenton 1998). The binder is 25% Sulphate Resistant Portland cement, 25% silica fume and 25% silica flour (ground silica), these substitutions produce a pH of less than 10, while normal concrete has a pH of 12 or higher (Chandler et al. 2002). Other formulations to produce low alkalinity concrete are possible. In terms of pH, a cement-based material must have a pH of less than 11 to be accepted as low pH to ensure proper function of engineered barrier systems (Baumgartner 2006a, b, d; Arenius et al. 2008).

Table 1: Summary of General Properties (after Russell and Simmons 2003)

Property	Bentonite-Sand Buffer (BSB)	Light Backfill (LBF)	Highly Compacted Bentonite (HCB)	Gap Fill (GF)	Dense Backfill (DBF)	Concrete	Grout
Composition	50% bentonite 50% sand	50% bentonite 50% sand	100% bentonite	100% pelletised bentonite	5% bentonite 25% glacial clay 70% crushed rock	low-heat high-performance concrete (LHHPC)	low alkalinity cementitious grout
EMDD ¹ (kg/m ³)	1,150	1,000	1,500	1,250	800	-	-
Dry density (kg/m ³)	1,690	1,240	1,610	1,400	2,120	-	-
As placed density (kg/m ³)	1,980	1,400	1,950	1,410	2,280	2,430	-
Saturated density (kg/m ³)	2,060	1,780	2,010	1,880	2,330	-	-
As placed porosity (%)	38	55	41	49	22	15	-
As placed saturation (%)	80	33	65	6	80	50	-
Initial gravimetric water content (%)	18.5	15	17	2	8.5	3	-
Saturated gravimetric water content (%)	23	46	26	36	10.6	6	-

¹ Effective Montmorillonite Dry Density = (mass of bentonite * smectite fraction)/(volume of voids + volume of smectite minerals)

2. THERMAL PROPERTIES

Volume 1 of this report series (Baumgartner 2006e) presents the details of the available thermal properties of the clay based sealing materials described by Russell and Simmons (2003). For completeness, the information provided in Volume 1 is summarized in the following sections, supplemented by new information where possible. Additionally, the available thermal properties of concrete and cementitious grout are summarized.

Included parameters are:

- Thermal Conductivity, λ – a measure of a substance's ability to transfer heat (W/(m·K));
- Specific Heat Capacity, c – the amount of heat required to raise the temperature of one gram of a material by 1°C (J/(kg·K); and
- Coefficient of Linear Thermal Expansion, α – the amount of volume strain per unit increase in temperature (1/°K).

2.1 THERMAL PROPERTIES OF BENTONITE-SAND BUFFER

The thermal conductivity of BSB is well characterized, ranging from approximately 0.75 W/(m·K) at 0% saturation to approximately 2.0 W/(m·K) at 100% saturation (Figure 2) (Wan 1996). The as-placed thermal conductivity of BSB is 1.9 W/(m·K) at 80% saturation. Note that the presence of silica sand in BSB increases its thermal conductivity relative to HCB.

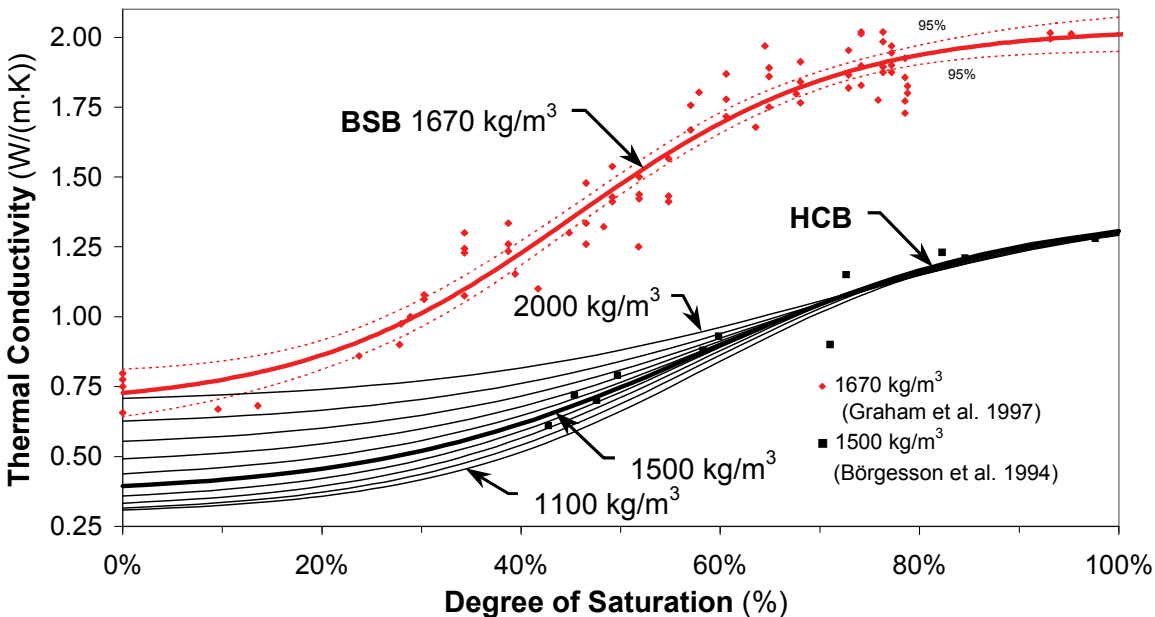


Figure 2: Thermal Conductivity of 50:50 wt% Bentonite-Sand Buffer (BSB) (Wan 1996; Graham et al. 1997) and Estimated Range of Values for Highly Compacted Bentonite Clay (HCB) (derived from Villar 2002; JNC 2000; Börgesson et al. 1994). Note: Label units are dry densities (ρ_d) (after Baumgartner 2006e)

Baumgartner 2006e provides the equation of the curve fit for BSB in the form of the Boltzmann sigmoid curve as follows:

$$\lambda = A_1 + \frac{(A_2 - A_1)}{1 + e^{\left(\frac{V_{50} - S}{m}\right)}} \quad (4)$$

where A_1 = value of λ for the degree of saturation (S) = 0%;
 A_2 = value of λ for the degree of saturation (S) = 100%;
 V_{50} = regression parameter; and
 m = regression parameter.

For BSB with a dry density of 1670 kg/m^3 , the Boltzmann sigmoid fitted parameters are as follows:

A_1 = 0.68 W/(m·K);
 A_2 = 2.03 W/(m·K);
 V_{50} = 0.4524; and
 m = 0.1357.

The specific heat capacity of a given sealing material comprised of a mixture of materials can be calculated knowing the specific heat capacity of the individual components (each of which will generally fall within the range of 700 to 1100 J/(kg·K)) and the mass fractions of each component. The addition of water to the sealing materials increases the overall effective specific heat capacities since water has a high specific heat capacity (i.e., 4186 J/(kg·K)). The specific heat capacity, c , for a sealing-system component as a function of water content, w is defined by the following (Baumgartner 2006e):

$$c = \frac{[(f_1 \cdot c_1) + (f_2 \cdot c_2) + \dots + (f_n \cdot c_n) + w \cdot c_w]}{1 + w} = \frac{w \cdot c_w + \sum_{i=1}^n (f_i \cdot c_i)}{1 + w} \quad (5)$$

where f_i = mass fraction of solid constituent material;
 c_i = specific heat capacity of solid constituent material (J/(kg·K));
 w = water content;
 c_w = specific heat capacity of water (i.e., 4186 J/(kg·K)); and
 n = number of constituent materials in sealing-component mixture.

Equation 5 can be rewritten in terms of the degree of saturation (S) as follows (Baumgartner 2006e):

$$c = \frac{S \cdot \left(\sum_{i=1}^n G_s \cdot \rho_w - \rho_d \right) \cdot c_w + \sum_{i=1}^n G_s \cdot \rho_d \cdot \sum_{i=1}^n (f_i \cdot c_i)}{\left[\sum_{i=1}^n G_s \cdot \rho_d + S \cdot \left(\sum_{i=1}^n G_s \cdot \rho_w - \rho_d \right) \right]} \quad (6)$$

where G_s is the specific gravity of the soil particles and S is the degree of saturation. Using this approach, and the appropriate specific heat capacity values provided in Table 2, the specific heat capacity for BSB is 767 J/(kg·K) (silica sand and Avonlea bentonite). This same approach will be used for other sealing materials comprised of a mixture of different components.

Table 2: Typical Relative Densities and Specific Heat Capacities of Constituent Materials for Sealing Materials (after Baumgartner 2006e)

Constituent Material	Specific Gravity	Specific Heat Capacity (J/(kg·K))
Lac du Bonnet Granite	2.62	845
Silica Sand	2.65	733
Avonlea Bentonite Clay	2.76	800
MX-80 Bentonite Clay	2.75	800
Lake Agassiz Clay	2.71	800

Information regarding the coefficient of thermal expansion for BSB was not available.

2.2 THERMAL PROPERTIES OF LIGHT BACKFILL

The thermal properties of LBF can be expected to be similar to BSB. However, testing is required to confirm the thermal properties of the material at its specified density.

2.3 THERMAL PROPERTIES OF HIGHLY COMPACTED BENTONITE

The lower family of curves in Figure 2 show thermal conductivity values for Wyoming Na-bentonite (i.e. MX-80) with dry densities ranging from 1,100 kg/m³ to 2,000 kg/m³. As for BSB, increasing water content increases thermal conductivity of the material. It also shows that increasing the dry density of a sealing-system component, which increases the number and area of interparticle contacts, improves its effective thermal conductivity (Villar 2002; Graham et al.1997; Börgesson et al.1994). The as-placed thermal conductivity of HCB is 0.94 W/(m·K) at 65% saturation.

The fitted values of the Boltzmann sigmoid parameters (Equation 4) describing the family of curves for MX-80 bentonite of variable dry density (ρ_d) are listed below (Baumgartner 2006e).

$$A_1 = 5.17 \times 10^{-7} \rho_d^2 - 1.16 \times 10^{-3} \rho_d + 0.94 \quad (7)$$

$$A_2 = 8.25 \times 10^{-5} \rho_d + 1.26 \quad (8)$$

$$V_{50} = 2.75 \times 10^{-7} \rho_d^2 - 7.28 \times 10^{-4} \rho_d + 1.057 \quad (9)$$

$$m = 5.42 \times 10^{-5} \rho_d + 0.0847 \quad (10)$$

Thermal conductivity testing on Black Hills bentonite and Avonlea bentonite yielded values that plot above the family of curves in Baumgartner (2006e) with results that suggest a more linear fit to the data. Black Hills bentonite has a reported thermal conductivity of 0.7 W/(m·K) to 1.1 W/(m·K) at 20% to 30% water content. Avonlea bentonite has a reported thermal conductivity of 0.6 W/(m·K) to 0.9 W/(m·K) at 26% to 33% water content (Radhakrishna 1984).

Cho et al. (2002) used a linear fit to relate water content, w , to the thermal conductivity of a variety of bentonites including MX-80, Kunigel, and Kyungju bentonite at three different dry densities. These equations are listed below.

$$\lambda = 0.0306w + 0.2286 \quad (\rho_d \text{ 1.4 Mg/m}^3) \quad (11)$$

$$\lambda = 0.0345w + 0.4318 \quad (\rho_d \text{ 1.6 Mg/m}^3) \quad (12)$$

$$\lambda = 0.0584w + 0.4738 \quad (\rho_d \text{ 1.8 Mg/m}^3) \quad (13)$$

Although the data presented by Cho et al. (2002) shows differences between the various sources of bentonite, these equations are for the entire data set and do not reflect those differences.

JNC (2000a) reported a thermal conductivity of 0.96 W/(m·K) and a specific heat capacity of 580 J/(kg·K) for Kunigel bentonite with a dry density of 1.8 Mg/m³.

Baumgartner (2006e) calculated a family of curves for the specific heat capacity of HCB as functions of dry density as shown in Figure 3, i.e. for 100% bentonite.

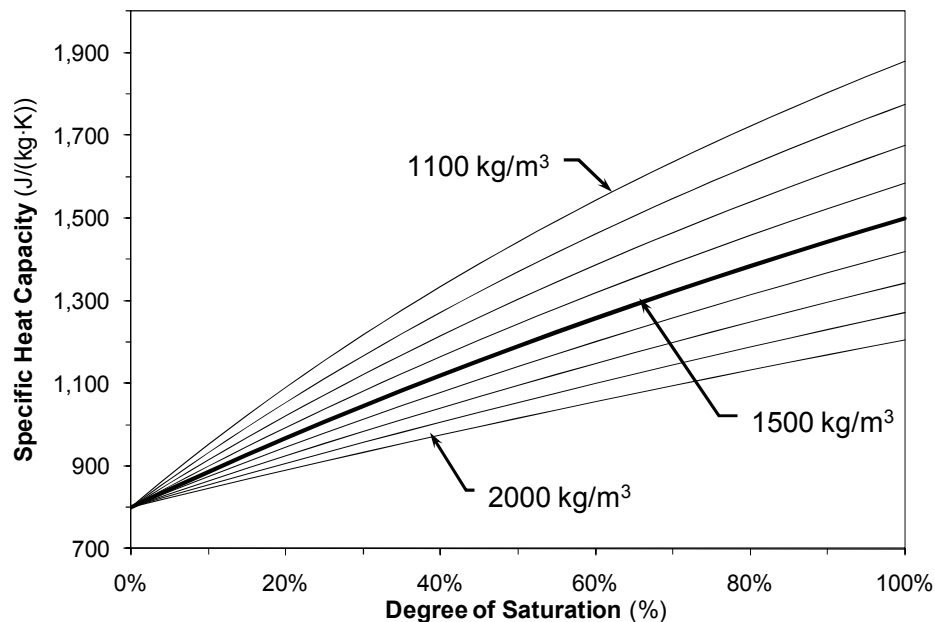


Figure 3: Specific Heat Capacity for Highly Compacted Bentonite as a Function of Saturation. Note: Label units are dry densities (ρ_d) (after Baumgartner 2006e).

Börgesson et al. (1988) reported the coefficient of thermal expansion for MX-80 bentonite. Their results are summarized on Table 3 for a temperature range of 20°C to 60°C. The values show a change within the same order of magnitude suggesting little variation in expansivity for the water contents tested.

Table 3: Coefficient of Thermal Expansion for MX-80 Na-Bentonite (after Börgesson et al. 1988)

Dry Density (Mg/m ³)	Water Content (%)	EMDD (Mg/m ³)	Coefficient of Thermal Expansion (1/°K)
1.2	13	1.02	3.1 x 10 ⁻⁴
1.5	33	1.31	3.0 x 10 ⁻⁴
1.65	27	1.47	2.2 x 10 ⁻⁴

2.4 THERMAL PROPERTIES OF GAP FILL

The thermal properties of GF can be inferred from tests conducted on MX-80 bentonite at the specified dry density or EMDD for GF (i.e. dry density = 1.40 Mg/m³, EMDD = 1.25 Mg/m³). For example, Figure 2 includes a curve for the applicable dry density of GF. The as-placed thermal conductivity of GF is 0.38 W/(m·K) at 6% saturation. Equations 4 to 7 and Figure 3 can be used to estimate the specific heat capacity of GF.

2.5 THERMAL PROPERTIES OF DENSE BACKFILL

The DBF (Table 1), defined in Russell and Simmons 2003, has not been thermally tested to date.

Baumgartner (2006e) provides an estimate of specific heat capacity of 832 J/(kg·K) for DBF at 0% saturation. The method for calculating the specific heat capacity for component materials is based on the specific heat capacity of the individual components that comprise DBF (Table 2) and uses equations [5] and [6]. However, this approach requires uniformity of the material components used in the engineered barrier material.

Some thermal properties testing has been conducted on similar mixtures of bentonite and crushed rock. Radhakrishna (1984) tested a 50:50 mixture of Black Hills bentonite and crushed granite. This material had a thermal conductivity of 1.60 W/(m·K) at a dry density of 1.88 Mg/m³ and a water content of 16%. Decreasing the bentonite content to 25% increased the thermal conductivity of the material to 2.10 W/(m·K) at a dry density of 2.08 Mg/m³ and a water content of 10%.

Engelhardt and Finsterle (2003) tested 30:70 bentonite:crushed rock mixtures. Bentonites tested included a sodium bentonite from Wyoming (Volclay or MX-80) and a calcium bentonite from Germany (Calcigel). The crushed rock consisted of diorite gravel with particles no larger than 5 mm. Water contents of 30% and 40% were used for the mixtures made with Calcigel

and Volclay, respectively. The Calcigel mixture was compacted to a dry density of 1.6 Mg/m³, and the Volclay mixture was compacted to a dry density of 1.4 Mg/m³. The materials had thermal conductivities in the order of 1.6 W/(m·K) to 2.2 W/(m·K) for the mixtures made with Calcigel and Volclay, respectively. Specific heat capacity of the material was 810 J/(kg·K) and 1020 J/(kg·K) for the mixtures made with Calcigel and Volclay, respectively.

2.6 THERMAL PROPERTIES OF LOW ALKALINITY CONCRETE

Thermal properties of low alkalinity concrete are a current knowledge gap. Thermal conductivity, specific heat capacity and thermal expansion are the important thermal properties to be determined. Limited information is available on LHHPC thermal properties, and the number of tests and test conditions required to produce these values is unknown. Therefore, testing to determine the thermal properties of low alkalinity concrete is required.

2.7 THERMAL PROPERTIES OF LOW ALKALINITY CEMENTITOUS GROUT

A low alkalinity grout has not been developed using Canadian materials. In terms of pH, a material must have a pH of less than 11 to be accepted as low pH to ensure proper function of engineered barrier systems (Arenius et al. 2008,). A Canadian grout was designated a high performance grout for use in repositories (Onofrei et al. 1993), but it has a pH of 11.5 to 11.9 in laboratory tests and so is not a low pH grout by this definition.

Thermal properties of low alkalinity cementitious grout are a current knowledge gap. Testing to determine the thermal properties of low alkalinity cementitious grout is required.

2.8 SUMMARY OF THERMAL PROPERTIES

Table 4 provides a summary of thermal properties for the various sealing materials based on their as-placed conditions provided in Table 1.

Table 4: Summary of Thermal Properties

Property ¹	BSB	LBF	HCB	GF	DBF	Concrete	Grout
Thermal Conductivity, λ W/(m·K)	1.9 (Figure 2, Eqn. 4, 7-10)	TBD	0.9 (Figure 2, Eqn. 1, 4-7)	0.38 (Figure 2, Eqn. 4, 7-10)	TBD	TBD	TBD
Specific Heat Capacity ² , α J/(kg·K)	1,650	1,348	1,285	870	1,562	TBD	TBD
Thermal Expansion, c 1/°K	TBD	TBD	3×10^{-4}	3×10^{-4}	TBD	TBD	TBD

Note: ¹ - Thermal properties based on the as-placed properties presented in Table 1

² - Calculated based on specific heat capacity of the individual components (Baumgartner 2006 using equation 6)

TBD – to be determined

The estimated alteration of smectite to illite is <10% over one million years at anticipated repository temperatures (i.e., <100°C). Work is being initiated on collecting thermal conductivities for certain sealing-system components at varying dry densities and degrees of saturation, and specific heats derived from material composition and degree of saturation, however the range of materials and conditions of materials must be expanded.

3. HYDRAULIC PROPERTIES

Volume 1 of this report series (Baumgartner 2006e) presents the details of the available hydraulic properties of the clay based sealing materials described by Russell and Simmons (2003). For completeness, the information provided in Volume 1 is summarized in the following sections, supplemented by new information where possible. Additionally, the available hydraulic properties of concrete and cementitious grout are summarized.

Included parameters are:

- Soil Water Characteristic Curve, SWCC – the relation between total suction potential (S_r) and water content (w) of a given soil; and
- Saturated Hydraulic Conductivity, K_{sat} – from Darcy's Law (m/s).

No rigorous measurements or theory for hydraulic conductivity under unsaturated conditions have been developed. Unsaturated hydraulic conductivity is generally estimated using the SWCC relationship.

3.1 HYDRAULIC PROPERTIES OF BENTONITE-SAND BUFFER

3.1.1 Soil-Water Characteristic Curve

The Soil-Water Characteristic Curve (SWCC) for BSB defines the relationship of gravimetric water content (w) or degree of saturation (S) versus suction (s). The total suction (s), present in this material is defined as the difference between pore air pressure (u_a) and pore water pressure (u_w) (i.e., $s = u_a - u_w$). It should be noted that suction is generally expressed as a positive value, corresponding to a negative pore water pressure. The SWCC for bentonite based sealing materials displays hysteretic behaviour for drying and wetting cycles, likely attributable to microstructural changes induced by internal wetting or drying processes.

Figure 4 shows the SWCC for BSB under a free-volume boundary condition (i.e. the bentonite is allowed to swell freely) (Villar 2002, Wan 1996). In these tests, suction is not measured directly, but is calculated using the Kelvin equation with a measured relative humidity (vapour pressure) in the samples. This figure shows that the $EMDD_{FS}^1$ decreases under free swelling conditions as the water content in the smectite fraction of the soil (also known as the effective montmorillonite water content, where $EMWC = \text{mass of dry montmorillonite solids/mass of water}$) increases, even though they are not along the same path due to hysteresis effects associated with the smectite “aggregate” or “ped” microstructures (Villar 2002; Wan 1996). Wan (1996) found that saturation approached 100% when suction decreased to small values during free swell. Because of large scatter associated with degree of saturation, Wan (1996)

¹ $EMDD_{FS}$ is defined as the EMDD under the free swell (FS) boundary condition.

concluded that suction was dependent upon only water content and not upon saturation. Villar draws a different line between Suction and degree of saturation than the one drawn in Figure 4 and concludes that “The data obtained show that the degree of saturation cannot be related to a single value of total suction”.

Regression analyses of the free-volume data in Figure 4 suggests the total suction potential (s) relationship to effective montmorillonite water content for 50:50 bentonite:sand buffer (BSB) (EMWC) is as follows (after Wan 1996):

$$s = 592e^{-16.7EMWC} \quad (14)$$

Priyanto (2007) summarized the SWCC results for BSB made with a variety of bentonites (Wan 1996; Wiebe 1998; Tang 1999; Blatz 2000; and Anderson 2002), using several suction measurement techniques. These results along with models established by Wan (1996), Baltz (2000) and Priyanto (2007) are shown on Figure 5.

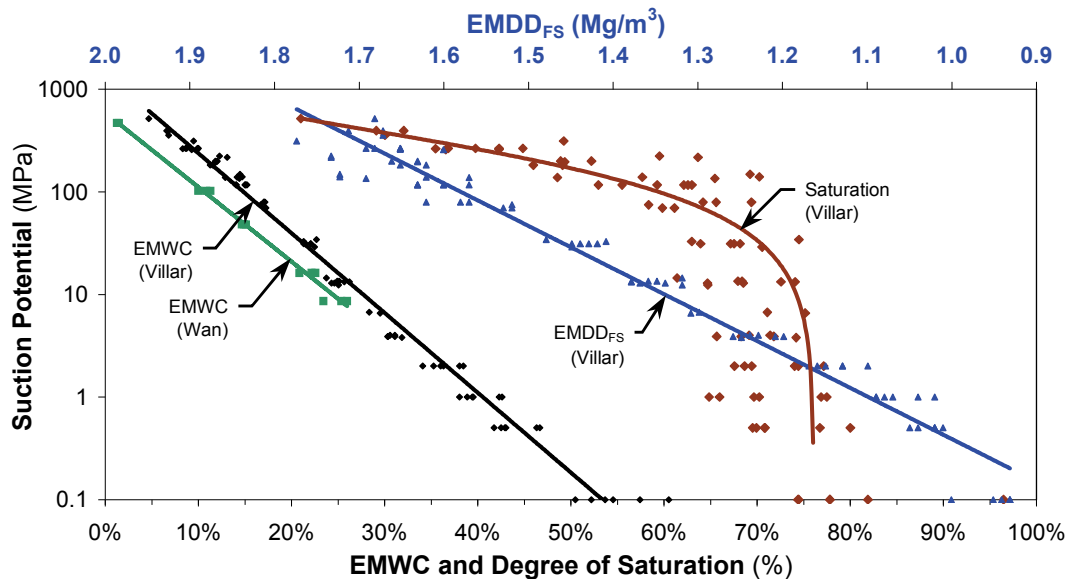


Figure 4: Soil-Water Characteristic Curve for Highly Compacted Ca-Bentonite (after Villar 2002) and for 50:50 Bentonite-Sand Buffer (after Wan 1996) under the Free-Volume Boundary Condition. Note: No direct correlation between the two horizontal axes.

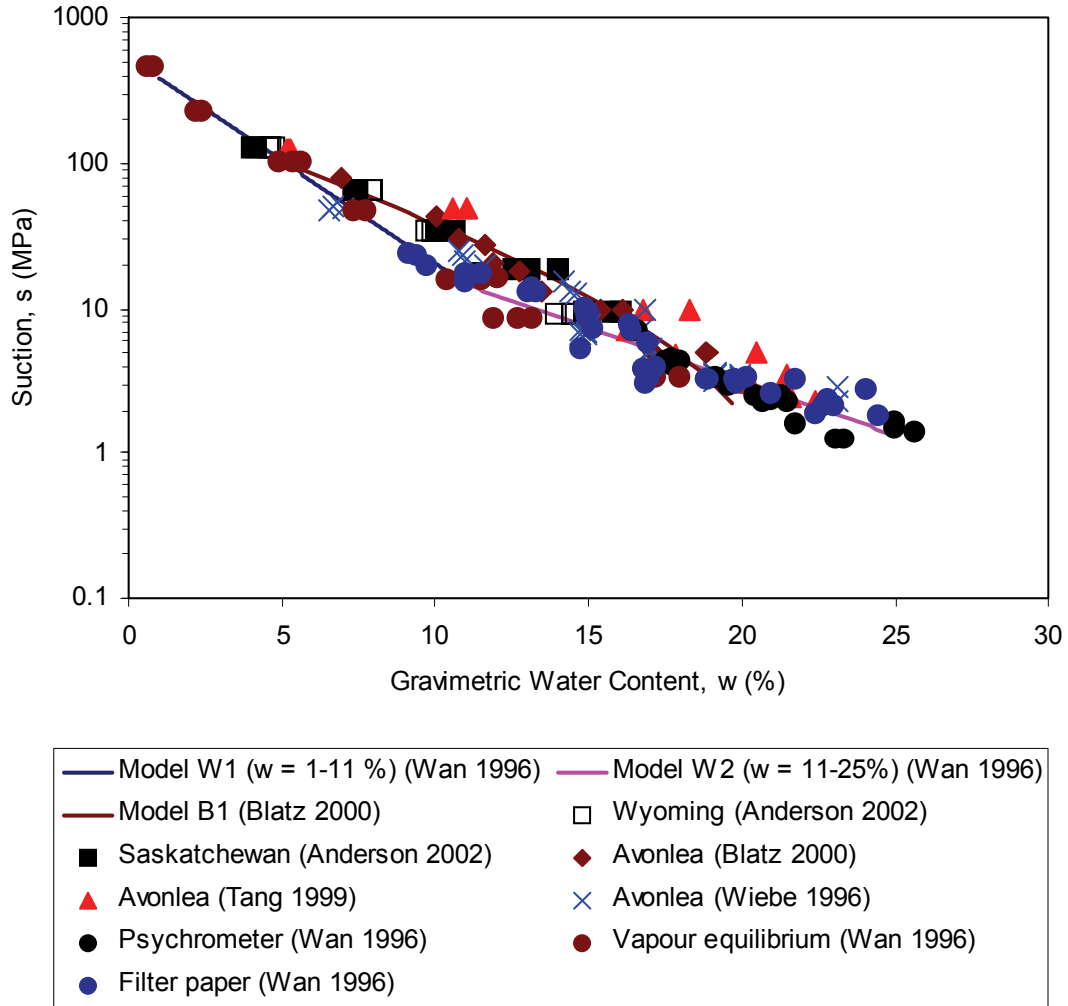


Figure 5: Soil-Water Characteristic Curve of Bentonite-Sand Buffer made with a Variety of Bentonites, Determined using Several Measurement Techniques (after Priyanto 2007)

The above SWCCs were determined from shrinkage tests, and therefore are the “drying curve”. Since hysteresis is expected, infiltration tests were completed by Siemens (2007) in order to provide the “wetting curve”. Siemens (2007) provides some data that support a three dimensional SWCC with gravimetric water content, suction and specific volume as the axes. The data was from wetting tests, however, the equations were not presented. The interested reader is directed to the original document.

3.2 Hydraulic Conductivity

The hydraulic conductivity of bentonite based sealing materials is dependent on the dry density and the montmorillonite content of the bentonite (which varies between different source locations) (Dixon et al. 2002; Baumgartner and Snider 2002). Figure 6 illustrates hydraulic conductivity values for bentonite based sealing materials expressed as a function of EMDD.

The data points in Figure 6 are a database of hydraulic conductivities collected from the international literature as well as from AECL's tests on a range of North American bentonites. (Included, for example are: Avonlea bentonite, Sealbond illite, MX-80 bentonite, and 50:50 BSB made with Avonlea bentonite and silica sand.) The EMDD values span the range of the materials specified by Russell and Simmons (2003).

It is noted that the wide scatter in data is largely attributed to large variations in the $\text{Na}^+/\text{Ca}^{2+}$ cation ratios and inherent salt contents of the different-source bentonites, for which no compensation has been attempted. The fitted hydraulic conductivity for a wide range of Na-bentonites in fresh water (i.e., deionized-distilled water added to natural bentonite) is (Baumgartner 2006e):

$$K = 9.0 \times 10^{-10} e^{-6.18\text{EMDD}} \quad (15)$$

The hydraulic conductivity of bentonite is affected by the salinity of the groundwater. The study conducted by Dixon (2000) showed that increasing salinity increases hydraulic conductivity. Figure 6 shows hydraulic conductivity as a function of EMDD and total dissolved solids (TDS) for saturated smectite-based sealing materials. Empirical fitting equations for differing salinities are expressed as total dissolved solids (TDS) for NaCl solutions as follows:

$$35\text{-}60 \text{ g/L} \quad K = 4.75 \times 10^{-12} \text{EMDD}^{-9.68} \quad (16)$$

$$100 \text{ g/L} \quad K = 5.1 \times 10^{-11} \text{EMDD}^{-13.6} \quad (17)$$

$$350 \text{ g/L} \quad K = 2.5 \times 10^{-10} \text{EMDD}^{-15.8} \quad (18)$$

Note that Equations 16 to 18 are power functions selected to approximately converge with the fresh-water line (Equation 15) (Baumgartner 2006e).

For comparison, the saturated hydraulic conductivity of a 70:30 bentonite sand mixture (EMDD = 0.9 Mg/m³) made with Kunigel bentonite is 4.5×10^{-13} m/s at room temperature (JNC 2000a).

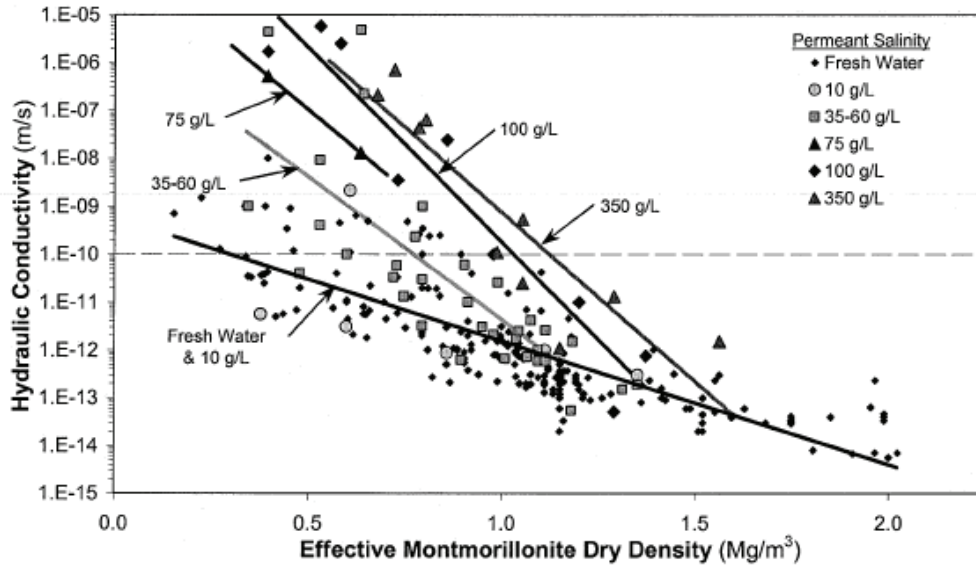


Figure 6: Hydraulic Conductivity as a Function of Effective Montmorillonite Dry Density and Total Dissolved Solids (TDS) for Saturated Smectite-Based Sealing Materials. Note: TDS is based on NaCl solutions (after Dixon 2002)

Figure 7 shows the hydraulic conductivity of both 100% bentonite and bentonite-sand mixtures (e.g., BSB or LBF) for saturated conditions. The data consists of the results from permeability tests conducted by Dixon (1995), data from a literature review conducted by Dixon (1995), and the results of 1D-consolidation tests (Baumgartner et al. 2008, Priyanto et al. 2008b). Note that the hydraulic conductivity from 1D-consolidation tests (Baumgartner et al. 2008, Priyanto et al. 2008b) is comparable to the constant volume permeability tests (Dixon 1995).

The equation describing the relationship between saturated hydraulic conductivity and porosity (n) for bentonite and bentonite-sand mixture after Dixon et al. (1999) is:

$$\text{Log}(k_w^{\text{sat}}) = 4.537 \cdot n - 14.597 \quad (19)$$

This equation considers both 100% bentonite and bentonite-sand mixtures. Figure 8 considers only the bentonite-sand mixture data separately. The best-fit equation for BSB (having R^2 of 0.6017) is:

$$k_w^{\text{sat}} = 3 \cdot 10^{-15} \cdot e^{13.41n} \quad (20)$$

This relationship can be used to define the saturated permeability of the BSB material.

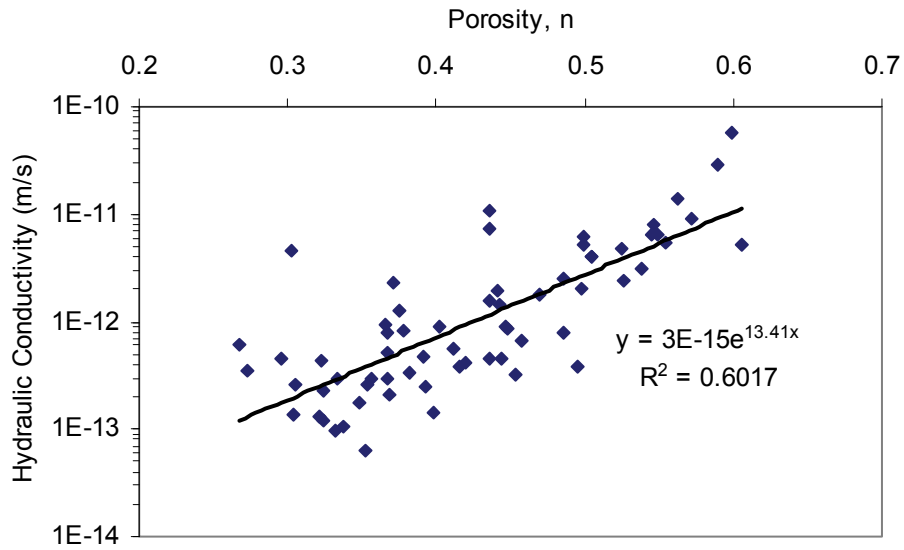


Figure 7: Hydraulic Conductivity of Bentonite-Sand Buffer

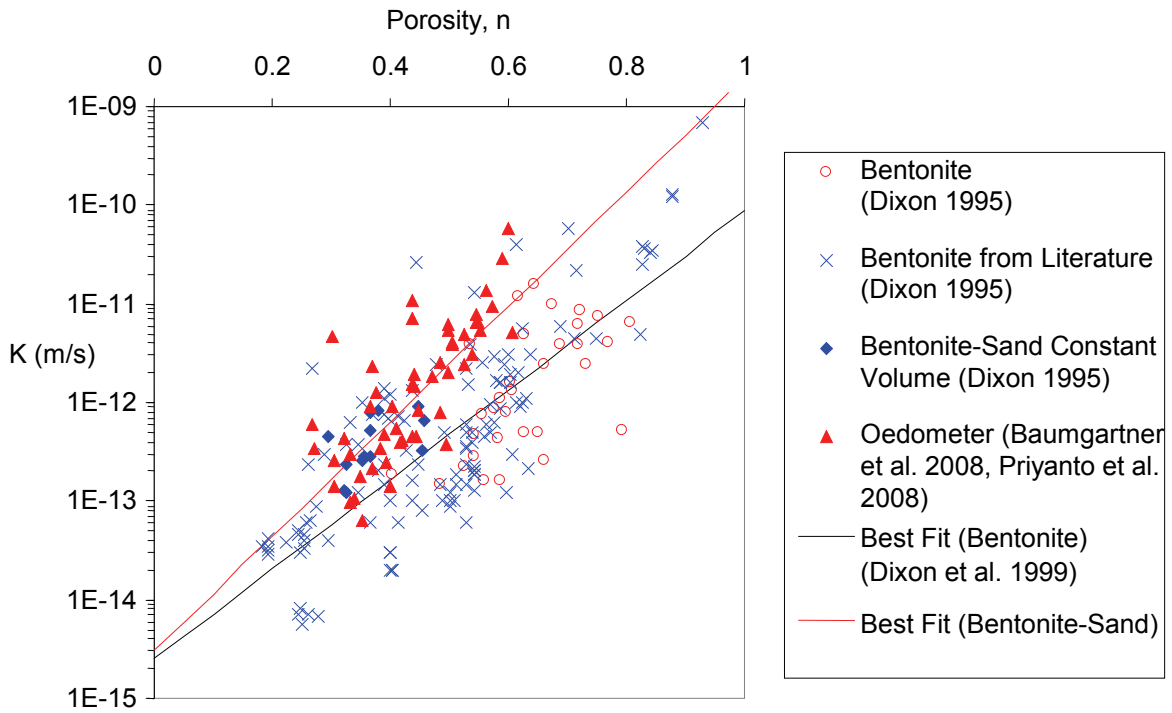


Figure 8: Hydraulic Conductivity of Bentonite and Bentonite Sand Mixture (after Priyanto et al. 2008b)

3.3 HYDRAULIC PROPERTIES OF LIGHT BACKFILL

Hydraulic properties for LBF can be inferred from testing of BSB under the appropriate dry density or EMDD conditions (Figure 4 and Figure 5), since LBF properties have not yet been directly tested. It is possible that mechanical and hydraulic properties of this material may be different than BSB as a result of the lower degree of compaction applied to it, and potential differences in pore structure associated with this.

It is expected that the shape of the SWCC will be similar for LBF and BSB. However, the parameters for LBF will be different. Further, the information presented in Figure 4 and Figure 5 was obtained from shrinkage tests, thus yielding a “drying curve”. Infiltration tests, as completed by Siemens (2007) are also required to provide the “wetting curve”. Hysteresis is expected between drying and wetting conditions.

3.4 HYDRAULIC PROPERTIES OF HIGHLY COMPACTED BENTONITE

3.4.1 Soil-Water Characteristic Curve

Figure 4 shows the SWCC for HCB made with a Ca-bentonite from Cabo de Gata, Spain under a free-volume boundary (Villar 2002). Regression analyses of the free-volume data in Figure 4 suggest the total suction potential (s) relationship to effective montmorillonite water content (EMWC) for Ca-bentonite is as follows (after Villar 2002):

$$s = 1427e^{-17.9EMWC} \quad (21)$$

This regression line is similar to that of Wan (1996) for BSB using Avonlea bentonite, but since it is for pure bentonite it covers a wider range of water contents.

Based on Ca-bentonite data (after Villar 2002), the total suction potential can be correlated to the $EMDD_{FS}$ (Figure 4), as follows:

$$s = 1.79 \times 10^{-5} e^{9.6EMDD_{FS}} \quad (22)$$

Based on the constant-volume SWCC boundary condition, that prevents the soil sample from swelling as water is taken up, the EMDD of the sample remains constant as EMWC increases (Blatz and Siemens 2005; Villar 2002). The degree of saturation does reach 100%, including in a humid atmosphere, and the total suction potential can be expressed as a function of the degree of saturation (S) for modelling purposes at fixed values for the EMDD as shown in Figure 9. The constant-volume data in Figure 9 are fit in a regression analysis to the form of the van Genuchten et al. (1991) equation, as follows:

$$S = \frac{1}{[1 + (\alpha \cdot s)^n]^m} \quad (23a)$$

where α , n and m are regression parameters, or solving for total suction potential (s):

$$s = \frac{\left[(S^{-1})^m - 1 \right]^{-n}}{\alpha} \quad (23b)$$

The regression parameters α , n and m for MX-80 bentonite are further estimated as functions of the EMDD as a first approximation to generate the family of curves in Figure 9, as follows:

$$\alpha = 0.0775 \cdot \text{EMDD}^2 - 0.308 \cdot \text{EMDD} + 0.311 \quad (24)$$

$$n = 1.56 \cdot \text{EMDD} - 0.873 \quad (25)$$

$$m = 0.311 \cdot \text{EMDD} + 0.226 \quad (26)$$

For the constant-volume case, it is important to note that the suction potential is a function of the degree of saturation and EMDD, however these correlations are empirical estimates only and do not directly relate to phenomenological behaviour. The van Genuchten et al. (1991) equation is not meant for use with swelling clays. If swelling is prevented by external constraint, then its use may have some merit. The theoretical relationship for suction potential (s) as a function of EMWC is applicable to free-volume and constant-volume conditions for modelling purposes provided that the resulting differences in EMDD are taken into account.

Dueck (2004) conducted a laboratory study of the hydro-mechanical properties of HCB made with MX-80. The study investigated the impact of factors such as void ratio, degree of saturation, boundary conditions and external load on suction. The SWCC relationship presented by Dueck was provided in terms of Relative Humidity (RH) versus gravimetric water content (w). The interested reader is directed to Dueck (2004) for the equations.

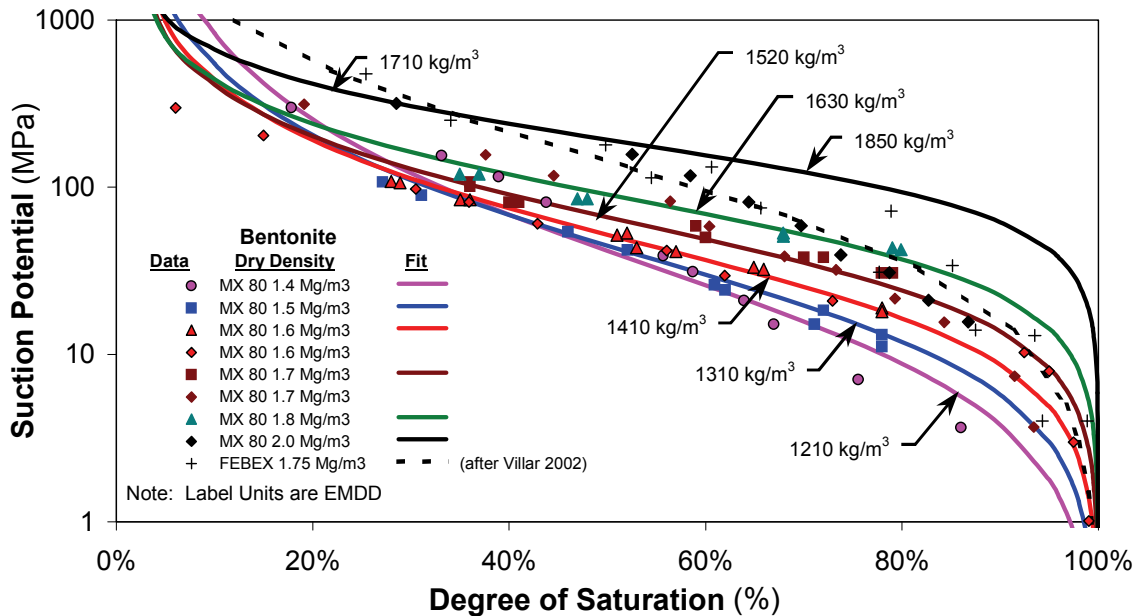


Figure 9: Soil-Water Characteristic Curves for Highly Compacted Bentonite (MX-80) under the Constant-Volume Boundary Condition (unpublished data). Note: Regression fits by van Genuchten et al. (1991) (after Baumgartner 2006e)

3.4.2 Hydraulic Conductivity

Figure 6 and Figure 8 shows the hydraulic conductivity of 100% bentonite for saturated conditions. The equation describing the relationship of saturated hydraulic conductivity and porosity (n) equations for bentonite and bentonite-sand mixture after Dixon et al. (1999) is:

$$\text{Log}(k_w^{\text{sat}}) = 4.537 \cdot n - 14.597 \quad (27)$$

Equation 27 represents the Dixon et al. (1999) data in Figure 8. For comparison, the saturated hydraulic conductivity of Kunigel bentonite (EMDD = 1.34 Mg/m³) is 2.5 x 10⁻¹⁴ m/s at room temperature (JNC 2000a).

The influence of initial degree of saturation, back pressuring, permeant salinity (in contrast to lower density materials), flow direction, bacterial activity, and hydraulic gradient changes on the flux measured were all examined and found to be insignificant in densely compacted bentonites (Dixon 2002).

Available experimental and natural analogue data on bentonite exposed to high temperatures indicate that the hydraulic properties of the material will not be compromised at temperatures less than 120°C (Wersin et al. 2007).

3.5 HYDRAULIC PROPERTIES OF GAP FILL

3.5.1 Soil-Water Characteristic Curve

Further testing is required to determine the SWCC for GF. This should include both shrinkage (drying) and infiltration (wetting) tests. It is expected that the behaviour of GF will be complex due to the presence of large voids and/or fines between the pellets.

Hydraulic properties obtained from testing of HCB can be inferred for GF under the appropriate dry density or EMDD conditions (Figure 6). Figure 10 shows an example of the relationship developed between the initial GF EMDD to the final average system EMDD for the in-floor borehole emplacement concept with the dimensions defined by NUKEM (2003) (after saturation for several pellet densities). On defining of a reference geometry with dimensional specifications, it is possible to develop a set of system density predictions for a given range of HCB densities and thereby test the potential suitability of the system.

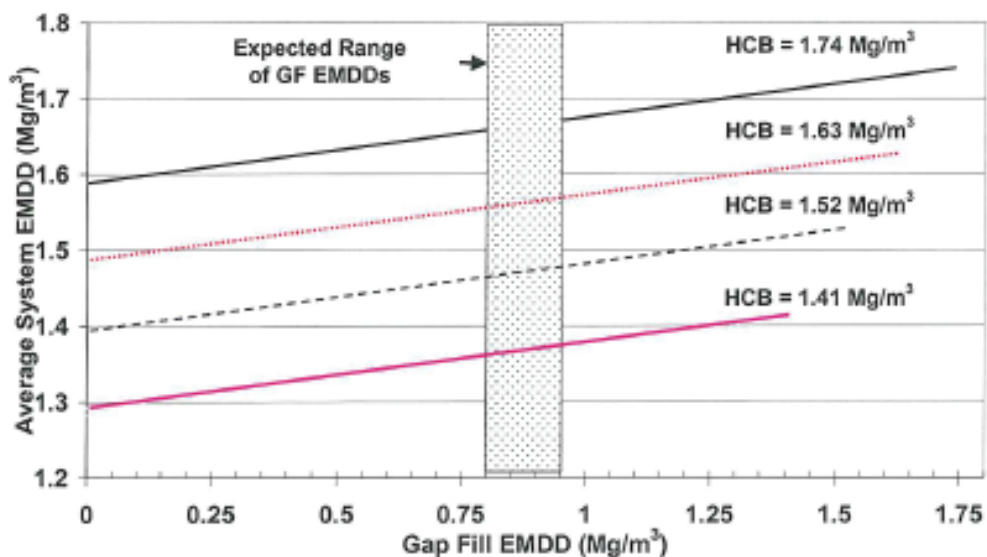


Figure 10: The Relationship Between Gap Fill Effective Montmorillonite Dry Density (EMDD) and the resulting Average EMDD of the System (after Dixon et al. 2005)

3.5.2 Hydraulic Conductivity

Dixon et al. (2002) indicated that bentonites with EMDD values similar to GF are sensitive to changes in pore fluid chemistry, with significant increases in hydraulic conductivity resulting from the increase in total dissolved solids (TDS) concentration (Figure 6).

In Figure 6, the EMDD needs to be greater than $\sim 1.05 \text{ Mg/m}^3$ to give a hydraulic conductivity $< 10^{-10} \text{ m/s}$ with a permeant salinity of 100 g/L. The EMDD values shown in Figure 10 indicate that the average system conditions would have acceptable hydraulic conductivity values for the as-placed GF EMDD values. Smaller numbers of tests done on MX-80 and Febex bentonites have been reported by Hoffman et al. (2007) and Karnland et al. (2008). Their results show low hydraulic conductivities for these materials at the densities considered for repository use and suggest that the resulting hydraulic conductivity of GF will be lower (i.e. on the order of 10^{-12} to 10^{-13} m/s) that indicated by correlation with EMDD (Figure 6).

3.6 HYDRAULIC PROPERTIES OF DENSE BACKFILL

3.6.1 Soil-Water Characteristic Curve

No information is available regarding the SWCC of DBF. This is the subject of ongoing testing.

3.6.2 Hydraulic Conductivity

Dixon et al. (2002) reported the results of hydraulic conductivity testing of DBF. The results are summarized in Figure 11. Included are DBF mixtures being considered for the Canadian and

Swedish programs. The Canadian EIS-type backfill was a 75% crushed granite – 25% glacial lake clay mixture and the Modified DBF was a later compositional change that had the DBF composed of 70% crushed granite, 25% glacial lake clay and 5% bentonite clay. The ellipses shown in Figure 13 show the anticipated range of density and hydraulic conductivity that could be expected for the two Canadian DBF compositions. The original DBF could, under certain circumstances, exhibit $k > 10^{-10}$ m/s, and the modified DBF would maintain an adequately low hydraulic conductivity for the range of conditions expected for a repository. The limited data available on this material indicates that Canadian DBF is not highly sensitive to changes in pore fluid chemistry. This is likely due to DBF's high dry density in combination with a high fines content (the fines content being the main determinant in defining k for these materials).

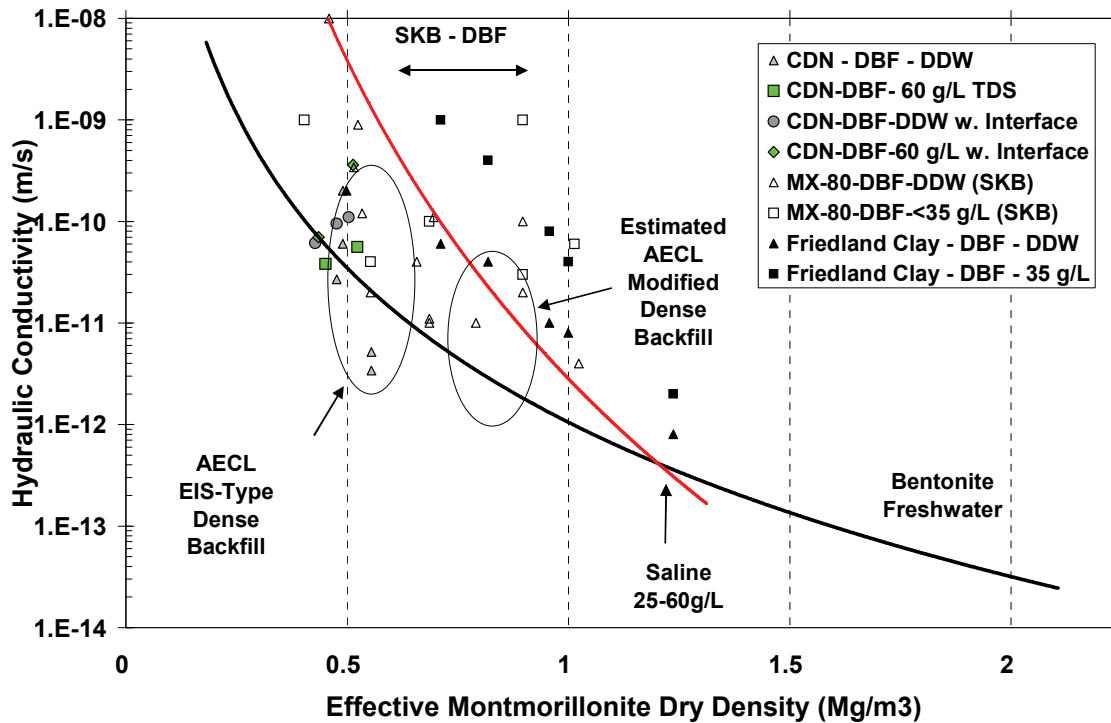


Figure 11: Hydraulic Conductivity of Dense Backfill (after Dixon et al. 2002)

For comparison, Engelhardt and Finsterle (2003) tested 30:70 bentonite:crushed rock mixtures. Bentonites tested included a sodium bentonite from Wyoming (Volclay, or MX-80) and a calcium bentonite from Germany (Calcigel). The crushed rock consisted of diorite gravel with particles no larger than 5 mm. The Calcigel mixture was compacted to a dry density of 1.6 Mg/m^3 (estimated EMDD = 1.1 Mg/m^3), and the Volclay (MX-80) mixture was compacted to a dry density of 1.4 Mg/m^3 (EMDD = 1.21 Mg/m^3). Saturated hydraulic conductivity was 1.64×10^{-11} m/s for the mixture made with Volclay and 4.93×10^{-9} m/s for the mixture made with Calcigel. Cho et al. (1995) measured slightly higher hydraulic conductivity values on mixtures of calcium bentonite and limestone at similar dry densities (i.e., 3×10^{-9} m/s and 2.5×10^{-8} m/s at dry densities of 1.5 Mg/m^3 (40% of clay content) and 1.6 Mg/m^3 (30% of clay content), respectively).

3.7 HYDRAULIC PROPERTIES OF LOW ALKALINITY CONCRETE

A number of laboratory tests were conducted on LHHPC prior to the Tunnel Sealing Experiment (TSX) but the arrangement and age of the concrete of those tests are not known. The TSX included a mass pour of low-heat high-performance concrete (LHHPC). Testing of cores from the TSX did not produce repeatable results, as the aggregate size was too large for the available apparatus.

The results of *in situ* hydraulic testing in the TSX bulkhead, showed a higher transmissivity towards the perimeter. The central portion of the mass had a hydraulic conductivity in the order 10^{-15} m/s and the exterior was in the order of 1 to 1.5 orders of magnitude larger (10^{-13} m/s) (Martino et al. 2008). This suggests that microcracks may have developed due to drying in the curing process near the perimeter of the bulkhead. The exact cause, including the role of adjacent materials (host rock, tunnel fill, open tunnel), and localized drying conditions while curing was not strictly controlled, except for water application to the face to the bulkhead. This effect represents a knowledge gap.

The LHHPC should be subjected to different laboratory curing conditions and the permeability compared to what could reasonably be expected in a repository environment in a more controlled laboratory environment. This is linked to other issues including; durability, mix design, shotcrete design, curing in warm environments, material compatibility in a sedimentary host rocks, and developing mix designs and/or placement methods to reduce the potential for shrinkage or incomplete curing during hydration were identified as knowledge gaps.

Concrete curing is influenced by its environment and this in turn impacts on its hydraulic properties. Testing to determine what hydraulic conductivity can reasonably be achieved in a given condition of temperature and available humidity should be conducted.

3.8 HYDRAULIC PROPERTIES OF LOW ALKALINITY CEMENTIOUS GROUT

A low alkalinity cementitious grout (LACG), that meets current definitions of low pH ($\text{pH} < 11$) has not been developed using Canadian materials. A grout with a pH greater than 11 (11.5 to 11.9) was developed using 90% concrete and 10% silica fume. The hydraulic conductivity of 90/10 grout is expected to be as low as 10^{-14} m/s (Onofrei et al. 1991) but the methodology and conditions of testing are not described.

A low pH, high performance cementitious grout has been developed with the ability to penetrate fine fractures of less than 100 μm , and is called UF41-14-4 (Arenius et al. 2008) in Europe and hydraulic properties are given as 10^{-13} m/s (Kuosa and Oranite 2008). A similar low pH grout was developed for use in large aperture fractures (Kronl6f 2005).

Based on the European work, a silica fume and cement-based grout, with a superplasticizer should be able to achieve the necessary pH value, and be able to penetrate fractures; however development work using Canadian materials must be done.

The development of a low pH grout using materials available in Canada is recommended.

3.9 SUMMARY OF HYDRAULIC PROPERTIES

The following table provides a summary of hydraulic properties for the various sealing materials.

Table 5: Summary of As-Placed Hydraulic Properties

Property	BSB	LBF	HCB	GF	DBF	Concrete	Grout
Hydraulic Conductivity (Saturated) ms^{-1}	10^{-13}	10^{-11}	10^{-14}	10^{-13}	10^{-11}	Depends on curing conditions 10^{-13} to 10^{-15}	European 10^{-13}
SWCC	Figures 4,5		Figures 4,5		TBD	NA	NA

Note: TBD – to be determined
NA – not applicable

4. MECHANICAL PROPERTIES

4.1 BACKGROUND

Mechanical properties can be influenced by both the thermal and hydraulic properties. Furthermore, due to diffuse double layer effects, pore fluid chemistry will also influence the mechanical behaviour of the clay-based sealing materials. The mechanical properties of concrete are influenced more by moisture and temperature related effects during the curing process. However, as low alkalinity concrete differs chemically from normal concrete, an understanding of linkages between thermal, hydraulic and mechanical properties needs to be developed.

For clay-based materials, the mechanical parameters of interest primarily arise from three general categories of constitutive models that are used to describe the mechanical behaviour of soils. These include the linear elastic model, the Mohr-Coulomb model, and the critical state model. Each category of model can be applied to saturated and unsaturated soil. Concrete is commonly modeled using the linear elastic model. Figure 12 illustrates several subcategories of these models.

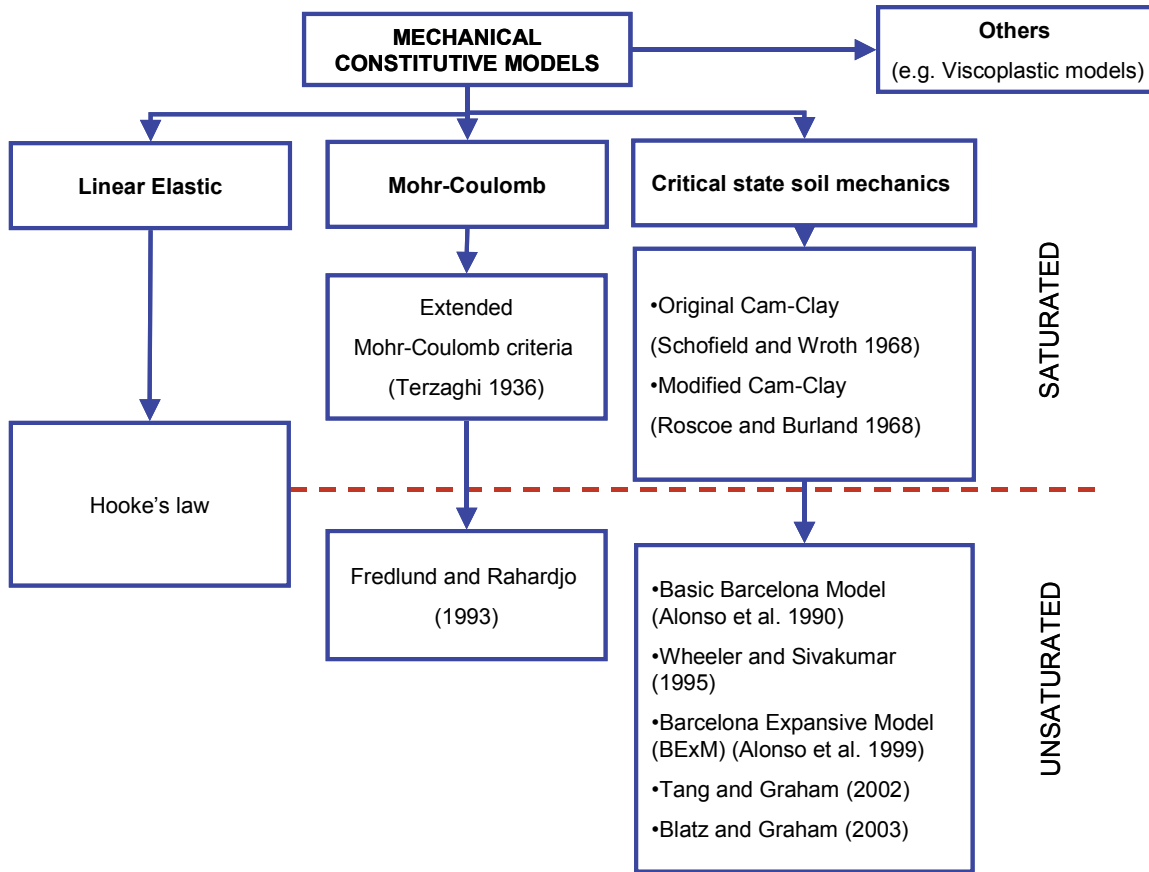


Figure 12: Classification of Mechanical Constitutive Models for Clay (after Priyanto 2007)

The associated stress-deformation parameters of each of these constitutive models are typically determined through triaxial testing. Oedometer testing provides one-dimensional consolidation characteristics of a given material that can be used to support critical state models. The following sections summarize the constitutive models, prior to presentation of the mechanical parameters available for each material.

4.1.1 Linear Elastic Model

Although soil is not purely linear elastic, a linear elastic model can be used to model soil behaviour in some cases (Davis and Selvadurai 1995). The linear elastic model follows Hooke's law and requires at least two parameters (i.e., Young's modulus E or bulk modulus K ; and Poisson's ratio ν or shear modulus G). A linear elastic model is the simplest of the models and is useful for approximate checks of more rigorous models. Most of the algorithms used to implement more rigorous constitutive models (Mohr-Coulomb or critical state soil mechanics) include an elastic component.

Concrete behaves as a linear elastic material within most of its performance range. Only when it is in the early stages of curing, or when cracking or other degradation occurs, does it not behave elastically. For most repository sealing conditions, the mechanical properties of

concrete would be in a linear elastic state. When modelling large masses of concrete to determine the behaviour, finite element models that assume linear elastic behaviour to about 40-50% for its ultimate strength are generally employed, beyond this loading level computer codes that permit crack development may be employed (Neville 2000).

4.1.2 Mohr-Coulomb Models

The Mohr-Coulomb criterion (Terzaghi 1936) for saturated soil is usually illustrated as the net effective normal stress (σ_n') versus shear stress (τ). This yield criterion can be developed using two (2) parameters: cohesion (c') and friction angle (ϕ') (Figure 13).

Fredlund and Morgenstern (1977) proposed the Mohr-Coulomb model for unsaturated soils, shown in Figure 14. Suction (s) is added as the third orthogonal axis to describe the failure criterion for unsaturated soil. The parameter (ϕ_b), that describes the contribution of suction to shear strength, is the angle of the strength envelope in shear stress-suction space. The linear shear strength envelope for saturated soil conditions becomes a planar surface to describe the shear strength behaviour of unsaturated soil (Figure 14). The soil behaves elastically when the stress-state is located under the surface, while plastic strain occurs when the stress-state reaches the criterion (Figure 14). This Mohr-Coulomb model produces linear-perfectly plastic response with a linear response within both the elastic and plastic regions but having different slopes in both regions.

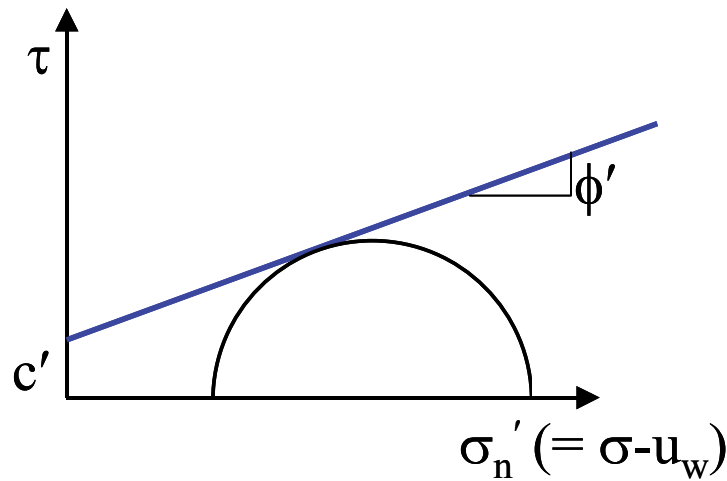


Figure 13: Mohr-Coulomb Model for Saturated Soil (after Terzaghi 1936)

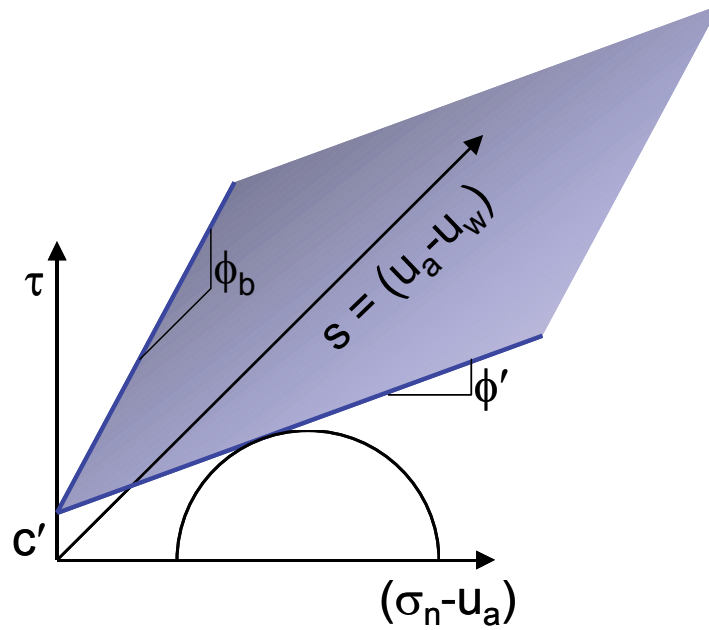


Figure 14: Mohr-Coulomb Model for Unsaturated Soil (after Fredlund and Morgenstern 1977)

4.1.3 Critical State Models

Critical state models combine a strength envelope (in p', q -space) with hardening (consolidation) behaviour (in $\ln p, V$ -space). Unique to critical state models is a region of elastic behaviour prior to yielding and the onset of non-recoverable plastic deformation. The locus of points defining this transition from elastic behaviour to the onset of plastic deformation is known as the yield locus. The Cam Clay model was the original critical state model (Roscoe et al. 1958, Shofield and Wroth 1968). It was subsequently modified (Modified Cam-Clay, MCC) to incorporate an elliptical yield locus as shown in Figure 15a (Roscoe and Burland 1968). All stress states that plot below the yield locus are considered within the elastic region of behaviour.

Critical state refers to the locus of large strain failure states where there are no further changes in deviator stress (q), mean effective stress (p'), pore water pressure (u), or specific volume (V) with continued straining. The critical state line (CSL) can be represented in p', q, V -space using the p', q -plane and the $\ln p', V$ -plane. The CSL is analogous to the Mohr-Coulomb strength envelope where the slope of the CSL, M , in p', q -space is related to the friction angle in τ, σ -space (ϕ'_{cs}) by:

$$\sin \phi' = \frac{3M}{6 + M} \quad (28)$$

The M and ϕ' values can be determined for peak strength (overconsolidated) and critical state conditions, if applicable.

Similarly, cohesion (c'_{pq}) in p', q -space can be related to cohesion (c') in τ, σ -space (ϕ') by:

$$c' = c'_{pq} \left(\frac{3 - \sin \phi'}{6 \cos \phi'} \right). \quad (29)$$

In elastic-plastic models such as MCC, the critical state line is linear in p', q -space (Figure 8a).

Figure 15b is a plot of $\ln p'$ versus V , obtained from isotropic consolidation of soil specimens in a triaxial cell. Similar information can be obtained from an oedometer test. The difference is that vertical stress is presented for oedometer tests instead of mean effective stress. Conversion of vertical stress in an oedometer test to mean effective stress requires an assumption of Poisson's ratio. The portion of the curve with slope κ is similar to the recompression or swelling portion of an oedometer test that yields the Swelling Index, C_s . It follows that the portion of the curve with slope λ , also known as the hardening law, is similar to the portion of an oedometer test that yields the Compression Index, C_c . Note that both the C_s and C_c are slopes of the compression curve in $e, \log \sigma_v$ -space. The two portions of the curve are separated by the preconsolidation pressure (which is a yield point), in terms of an oedometer test and critical state soil mechanics.

The q, p' and V axes can be visualized as mutually perpendicular, with the q axis being oriented outward from the page in Figure 15b. In $\ln p', V$ -space, the yield locus maps as a straight line with slope κ (i.e., the κ line is a "bird's-eye" view of the yield locus). If the soil is stressed beyond the preconsolidation pressure (p_c'), the yield locus expands along the hardening line with slope λ .

One-dimensional consolidation in oedometer cells provides several other useful mechanical parameters that are unique to each load increment. These parameters include the coefficient of consolidation (c_v), the coefficient of volume compressibility (m_v) or its inverse, the 1D modulus.

The c_v is the constant in the differential equation of consolidation, with suitable units being m^2/year . It is defined as:

$$c_v = \frac{k}{m_v \gamma_w} \quad (30)$$

where k = hydraulic conductivity; and
 γ_w = the unit weight of water.

The m_v value (in units of inverse pressure) represents the volume change per unit volume of soil, per unit increase in effective stress and is obtained for a given stress increment by:

$$m_v = \frac{1}{1 + e_1} \left(\frac{e_1 - e_2}{\sigma_2' - \sigma_1'} \right) \quad (31)$$

where e_1 = void ratio at the end of a load increment;
 e_2 = void ratio at the next load increment;

σ_1' = effective stress at the load increment corresponding to e_1 ; and
 σ_2' = effective stress at the next load increment corresponding to e_2 .

Alonso et al. (1987) presented a conceptual model for interpreting the mechanical behaviour of unsaturated clay within a critical state framework. The mathematical formulation for this model, known as the Basic Barcelona Model (BBM) was provided by Alonso et al. (1990). This formulation was an extension of the MCC model (Roscoe and Burland 1968) and utilized three stress-state variables including mean stress (p), deviatoric stress (q), and suction (s). The BBM includes features such as: yield surface, critical state surface, and stress-volume relationships (Figure 16). Figure 17 illustrates the yield surface of the BBM in p,q,s -space.

Figure 16b shows the yield surface in p,s -space that is limited by three lines including the LC-curve (loading collapse), the k -line (tension) and the SI-line (suction increase). The SI-line and k -line can be generated using two parameters (k and s_0), while the LC-curve is dependent on six parameters ($\lambda(0)$, κ , r , β , p_0^* , and p_1). The k parameter is the slope of k -line and s_0 is the suction limit defining the SI-line. The κ and $\lambda(0)$ parameters are the coefficients of soil compressibility corresponding with the changes in mean stress (Figure 16c). Parameter κ is the slope of $\ln(p)$ versus V within the elastic range. Parameter $\lambda(0)$ is the slope of $\ln(p)$ versus V when plastic strain occurs under saturated conditions. Parameter p_0^* is the mean stress at zero suction located on LC-line. This parameter is the same as the preconsolidation pressure in the Modified Cam-Clay model for saturated clay (Roscoe and Burland 1968). The parameter p_1 is the reference mean stress that defines the LC-curve. The parameters r and β are fitting parameters that define the LC-curve. Increases in suction can also result in deformation. This is accounted for by the coefficients of compressibility κ_s and λ_s as illustrated in Figure 16c and 16d.

Gens and Alonso (1992) proposed a conceptual model for unsaturated swelling clay. The complete mathematical formulation is presented in Alonso et al. (1999). This model, called the Barcelona Expansive Model (BExM) (Alonso et al. 1999), introduced two levels of structure, including the macrostructural and microstructural levels. The macrostructural level is mainly saturated and the effective stress concept holds, while the microstructural behaviour is elastic. The BExM proposed three additional yield loci: Normal-line (NL), Suction Increase (SI), and Suction Decrease (SD) as illustrated in Figure 18. The BExM was calibrated using the results of suction controlled oedometer tests on compacted pellets of Boom clay (Alonso et al. 1995). Due to the lack of calibration data available for the sealing materials of interest, and the number of parameters required to implement the BMM and BexM models, application to the sealing materials considered in this paper to date are limited.

Laboratory testing of unsaturated BSB conducted at the University of Manitoba has resulted in two critical state based constitutive models (Tang and Graham 2002, Blatz and Graham 2003). The Blatz and Graham (2003) model (BGM) provides a simplification to the BBM model by combining the LC, SI and k lines (Figure 19) that can be approximated by two lines (Figure 20). This can be justified based on inherently similar mechanisms of plastic hardening in the soil microstructure that result in the lines (Delage and Graham 1996). The SI line is not considered significant for the applicable suction range. Based on laboratory results, a planar critical state surface (Figure 21) with slope N is utilized (Figure 22). Figure 23 illustrates the yield and critical state surfaces of the BGM. The simplifications result in a model with less parameters, therefore making the model more readily implemented in numerical modelling. Further, calibration results are available for BSB. As such, the parameters associated with the BGM will be presented.

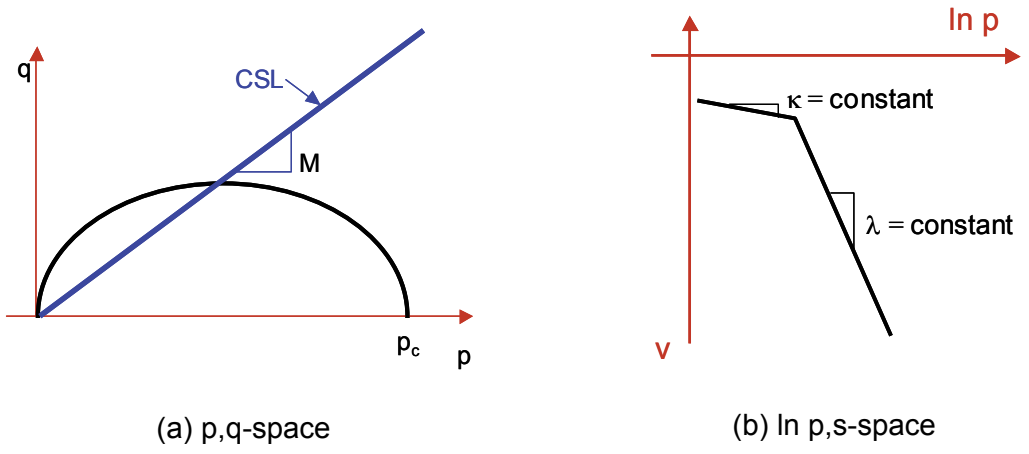


Figure 15: Modified Cam-clay Model (after Roscoe and Burland 1968; Priyanto 2007)

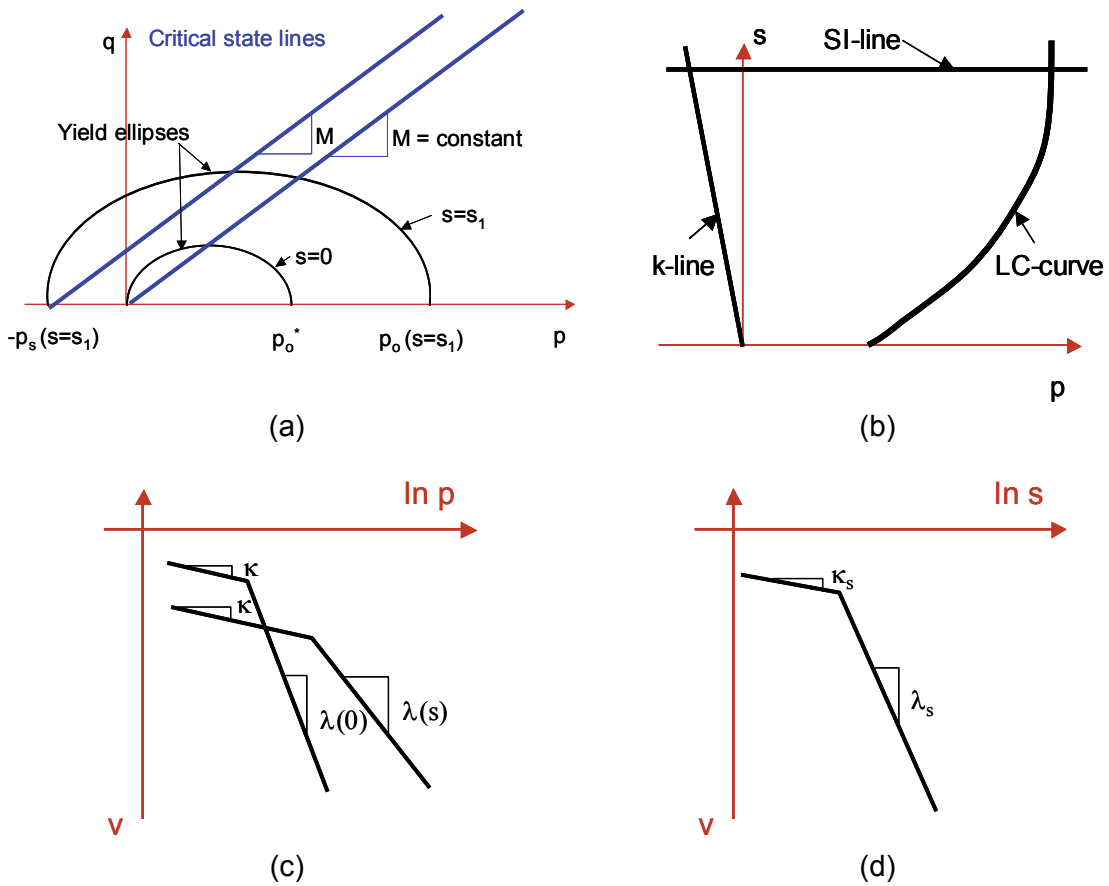


Figure 16: The Basic Barcelona Model (BBM): (a) p,q-space; (b) p,s-space; (c) v,ln p-space; and (d) v,ln s-space (after Alonso et al. 1990; Priyanto 2007)

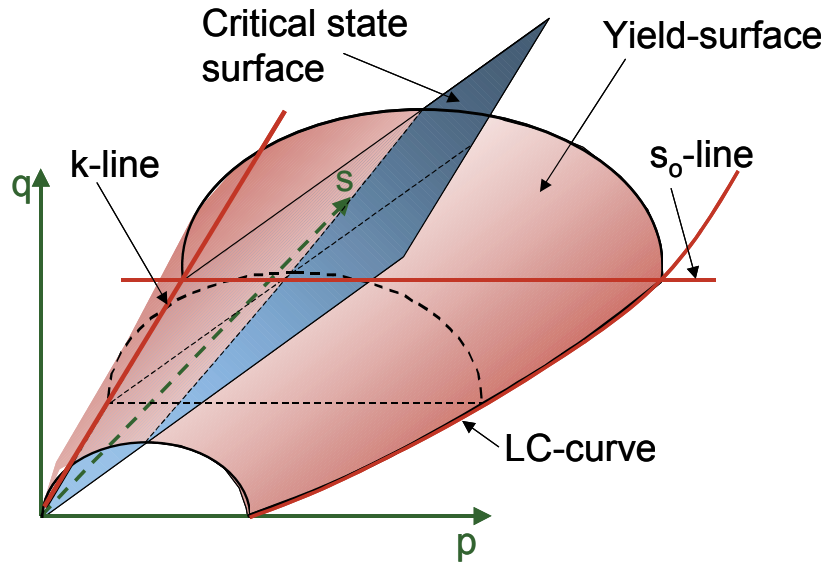


Figure 17: The Basic Barcelona Model (BBM) Yield Surface (after Alonso et al. 1990; Priyanto 2007)

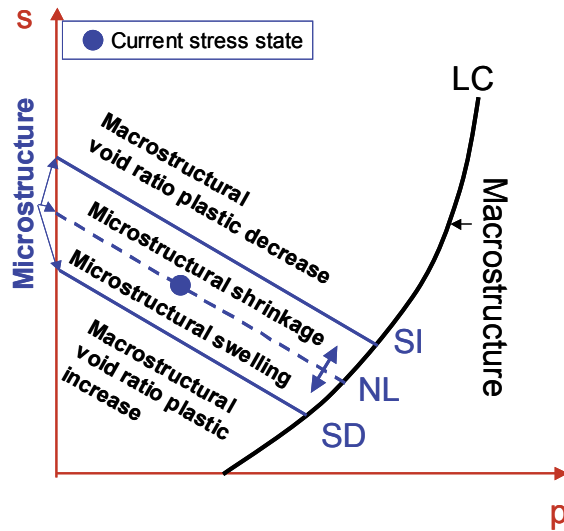


Figure 18: The Yield Surface for the BExM Model (after Alonso et al. 1990; Priyanto 2007)

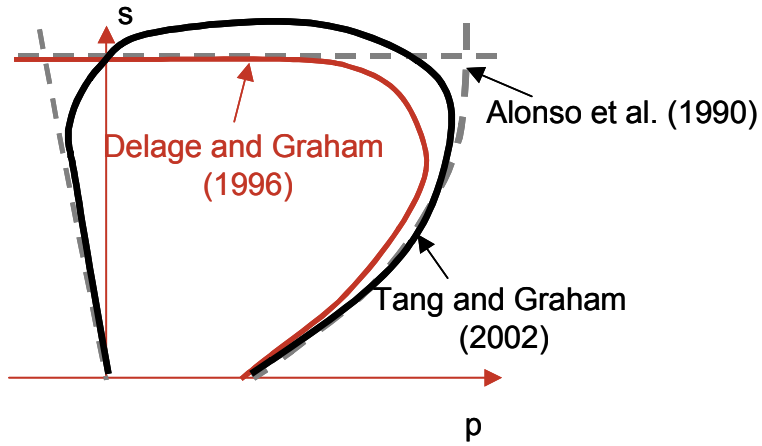


Figure 19: Coupling Yield Surfaces in p,s -Space (after Tang and Graham 2002; Delage and Graham 1996; Alonso et al. 1990; Priyanto 2007)

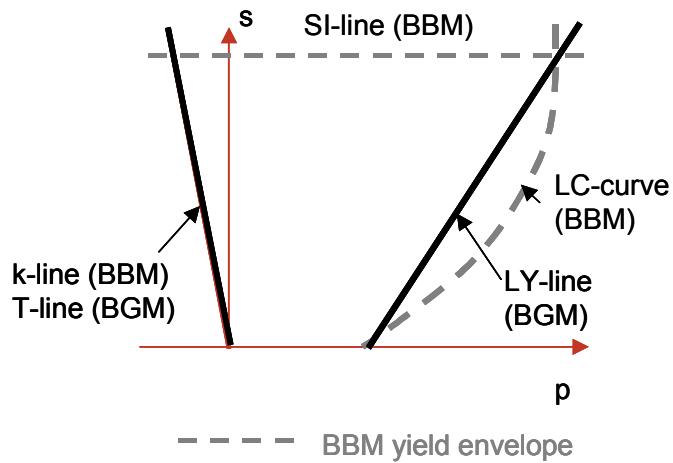
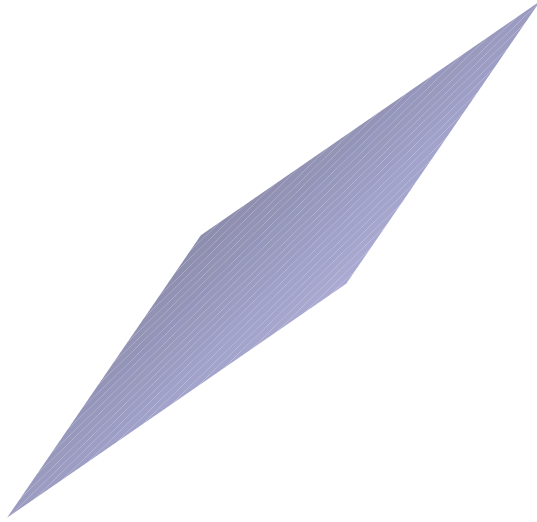


Figure 20: Yield Surfaces on p,s -Space for the BBM and the BGM (after Priyanto 2007)



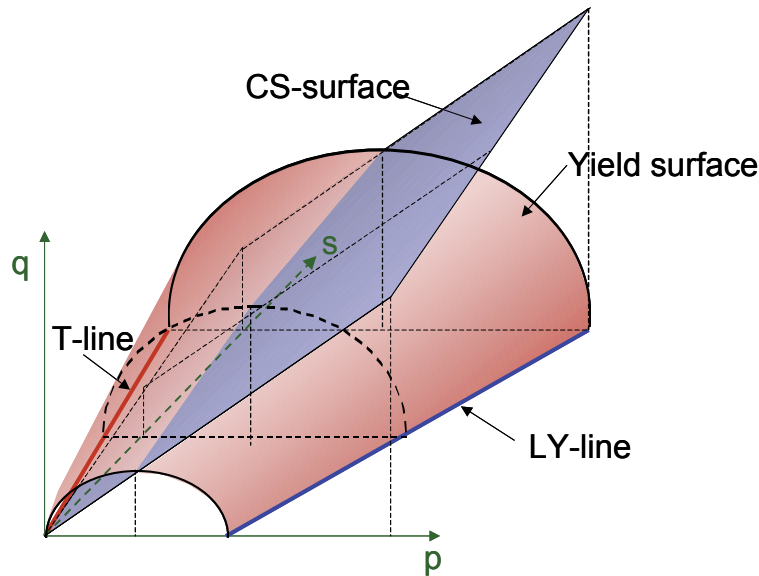


Figure 23: Critical State Slope as a Function of Suction in the BGM (after Blatz and Graham 2003; Priyanto 2007)

In summary the following is a list of parameters that will be presented where available for each material.

- Strength Envelope (peak and critical state, defined by the effective angle of internal friction, ϕ' or slope of the CSL, M , and cohesion, c' in the case of peak strength).
- Elastic Parameters (Young's Modulus E and Bulk Modulus K , or Poisson's ratio ν and Shear Modulus G).
- Hardening Behaviour (λ line and κ hardening line, 1D consolidation parameters: Compression Index, C_c , Swelling Index, C_s , the coefficient of consolidation c_v , and the coefficient of volume compressibility m_v or its inverse, the 1D Modulus).
- Yield Loci and Flow Rule.
- Unsaturated Model Parameters (e.g. BGM parameters, contribution of suction to strength, ϕ_b).

Where information is available, the effect of temperature and chemistry on the above list will be summarized.

4.2 MECHANICAL PROPERTIES OF BENTONITE-SAND BUFFER

BSB is one of the most extensively studied clay-based sealing materials, with much of the work being conducted in Canada at the University of Manitoba (U of M). Saturated compression indices and yield loci of the BSB were examined using triaxial tests at the U of M by Sun (1986), Wan (1987), Saadat (1989) and Oswell (1991). Yin (1990) examined time and strain rate effects of BSB. The effect of temperature was initially examined by Lingnau (1993). Lingnau (1994) provided a synopsis of the above work conducted at the U of M. Since then further work on temperature effects has been conducted by Yarechewski (1993). The studies showed that saturated BSB generally behaves like a stiff, normally consolidated, plastic clay, and the

effective stress concept is applicable (Graham et al. 1992) even at temperatures up to 100°C (Lingnau and Graham 1994). In general, compressibilities, stiffness, strength and pore water pressure generation in BSB are all effected by temperature, however, the changes are not great (Lingnau and Graham 1994). The data supports a conceptual model based on critical state soil mechanics for BSB (Graham et al. 1986). Details of these programs are provided in the following sections.

It is recognized that there will be an extended transient period between placement of the backfill material in an unsaturated state to complete saturation as natural groundwater potentials recover. This transient groundwater flow phase will be coupled with heat and chemical processes. Wan (1996), Wiebe (1998), Tang (1999), Blatz (2000), Anderson (2002), and Siemens (2006) examined the mechanical properties of unsaturated BSB. As such, an extensive series of laboratory tests of unsaturated BSB at the University of Manitoba (Tang 1999; Blatz 2000; Anderson 2003; Siemens 2006) has resulted in at least two critical state based constitutive models by Tang and Graham (2002) and Blatz and Graham (2003).

4.2.1 Strength Envelope

Peak and critical state strength envelopes for BSB are non-linear over stresses ranging from $p' = 0$ to 10 MPa (Lingnau 1994). Therefore, there is no unique value for c' or ϕ' , and appropriate values must be selected for the stress range being considered. However, for small stress ranges, a linear relationship is applicable. Further, the initial density and condition of swelling will affect the strength envelope (Lingnau 1994). Initial compaction of BSB imparts overconsolidated behaviour to the material. Swelling removes any preconsolidation effects that are developed during compaction of the specimens, thereby reducing c' to 0. In order to select appropriate Mohr-Coulomb values, the swelling history of the soil must be considered in q , p' , V -space. The following presents linear Mohr-Coulomb parameters for specified stress ranges and provides equations for the CSL in both q , p' -space and $V, \ln p'$ -space for the stress range examined in the testing programs.

Oswell (1991) presented a linear end-of-test strength envelope with $c' = 0.088$ MPa and $\phi' = 14^\circ$ for BSB close to its initial compacted dry density ($\gamma_d = 1,670$ kg/m³). This is applicable isotropic preconsolidation pressure in the range of 1.5 to 2.1 MPa. Since swelling was not permitted, the strength envelope is applicable to overconsolidated specimens and the peak strength envelope will correspond to the upper portion of the yield locus (i.e. for $p' \sim < p'_c/2$). Specimens compacted to a lower initial density ($\gamma_d = 1,500$ kg/m³) displayed a similar effective friction angle but had a lower cohesion of approximately 0.04 MPa (Graham et al. 1985; Sun 1986; Wan 1987).

As mentioned above, swelling tends to remove the preconsolidation effects of compaction and the soil will behave as a normally consolidated soil. For a given range of mean effective stress, the strength envelope will consist of a straight line, defined by the friction angle or M , passing through the origin (i.e. $c' = 0$). Normally consolidated friction angles have been found to range from $\phi' = 13^\circ$ to 16° (i.e. $M = 0.49$ to 0.61) for BSB that has undergone swelling to a dry density of $1,500$ kg/m³. These values are appropriate for isotropic consolidation pressures up to 3.0 MPa (Graham et al. 1985, Sun 1986, Graham et al. 1986, Graham et al. 1989, Oswell 1991, Wan 1987). The higher end of this range (i.e. 16°) is only valid for a low stress range of approximately $p' = 0$ to 250 kPa (Wan 1987).

For larger stress ranges, a power law relationship provides the best fit to the data. Saadat (1989) provided a number relationships for different densities and a stress range of $p' = 0$ to 10,000 kPa. Saadat's (1989) work was conducted at a temperature of 26°C. For BSB in its initial compaction density ($\gamma_d = 1,670 \text{ kg/m}^3$), Saadat (1989) provided the following relationship (with p' in kPa):

$$q = 2.64(p')^{0.79} . \quad (32)$$

For lower density material ($\gamma_d = 1,500 \text{ kg/m}^3$), Saadat (1989) provided the following relationship:

$$q = 2.29(p')^{0.79} \quad (33)$$

which is applicable to BSB that has undergone some swelling.

The critical state line can be mapped into V_c , $\ln p'$ -space. Saadat (1989) provided the corresponding equation to Equation 33 or BSB in its initial compacted density ($\gamma_d = 1,670 \text{ kg/m}^3$):

$$V_c^{26^\circ C} = 4.363 - 0.279 \ln p' . \quad (34)$$

Where V_c is the specific volume of the clay component, i.e. $V_c = (1 + V_{\text{voids}}) / V_{\text{clay}}$. For this case, the conversion is $V_c = 2.037V$.

The corresponding CSL for lower density BSB is as follows (Saadat 1989):

$$\ln V_c = 1.763 - 0.126 \ln p' . \quad (35)$$

The strength envelope for BSB is not sensitive to temperature changes in the 26°C to 65°C range (Lingnau 1993). However, the strength envelope increases for temperatures in the order of 100°C. Power law relationships have been used to describe the effect of temperature on the critical state strength envelope. The following equations for the CSL were provided by Lingnau (1993) and Graham et al. (1989):

$$q^{26^\circ C} = 2.640(p')^{0.79} \quad (36)$$

$$q^{65^\circ C} = 4.147(p')^{0.733} \quad (37)$$

$$q^{100^\circ C} = 8.142(p')^{0.674} \quad (38)$$

Figure 24 illustrates these CSLs and also shows peak strength envelopes at the tested temperatures. Figure 25 compares the strength envelopes obtained by Saadat (1989), Lingnau (1993) and Yarechewski (1993). It should be noted that specimens were sheared in undrained conditions, and did not reach the critical state strengths described by these

equations (36 to 38). This is due to the generation of large pore water pressures at elevated temperature that caused early failure.

The corresponding equations for the CSL at different temperatures in $V, \ln p'$ -space are as follows (Lingnau 1993):

$$V_c^{26^\circ C} = 3.102 - 0.121 \ln p'. \quad (39)$$

$$V_c^{65^\circ C} = 3.020 - 0.121 \ln p'. \quad (40)$$

$$V_c^{100^\circ C} = 2.930 - 0.121 \ln p'. \quad (41)$$

These CSLs are illustrated in $V, \log p'$ -space in Figure 26. Yarechewski (1993) observed a similar trend in $V, \log p'$ -space and provided the following equations for the CSL:

$$V_c^{26^\circ C} = 3.527 - 0.160 \ln p'. \quad (42)$$

$$V_c^{65^\circ C} = 3.369 - 0.153 \ln p'. \quad (43)$$

$$V_c^{100^\circ C} = 3.335 - 0.160 \ln p'. \quad (44)$$

Figure 27 compares the CSLs obtained by Saadat (1989), Lingnau (1993) and Yarechewski (1993) in $V, \ln p'$ -space.

Tang (1999) examined the effect of chemistry on the strength of BSB. His program involved testing of unsaturated BSB, up to a degree of saturation of 98%. These results are presented in Section 4.2.5.

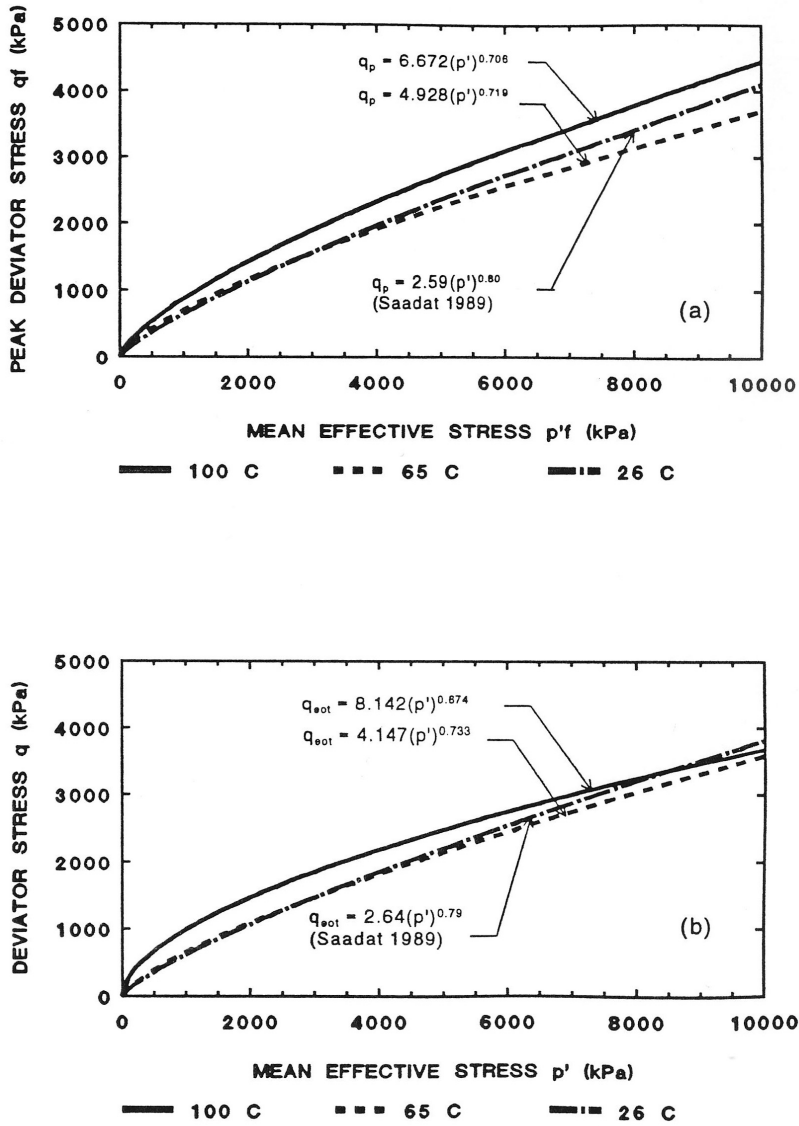


Figure 24: Summary of Strength Envelopes at Various Temperatures. Note: top = peak, bottom = end-of-test (after Lingnau 1993)

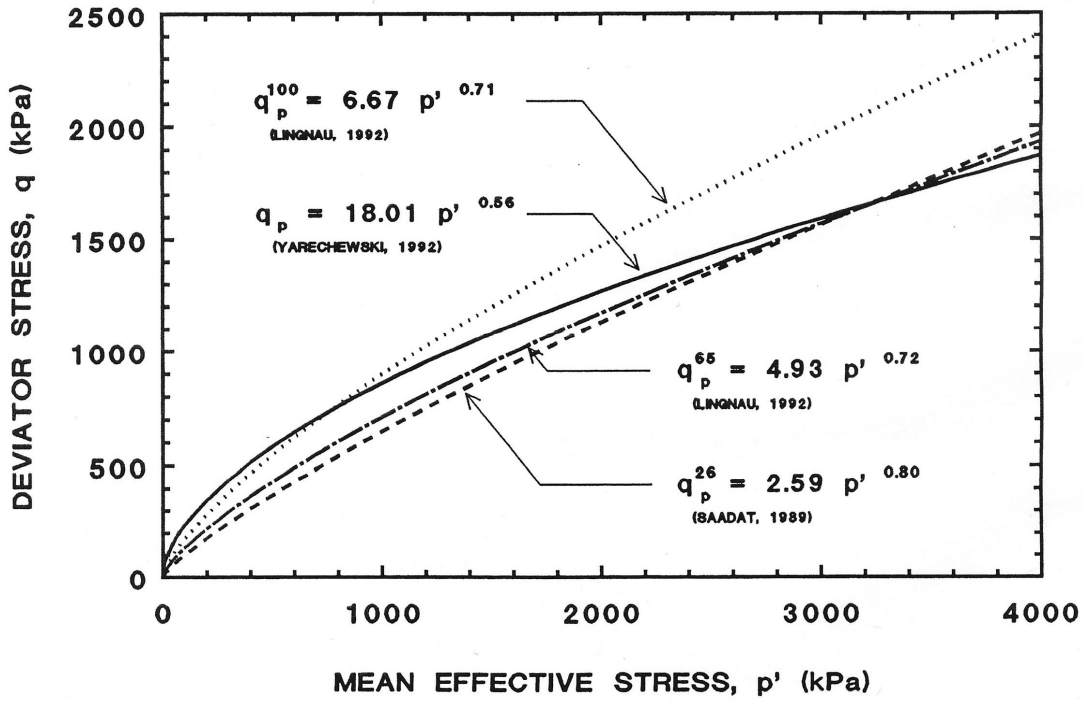


Figure 25: Summary of Shear Strength Results (after Yarechewski 1993)

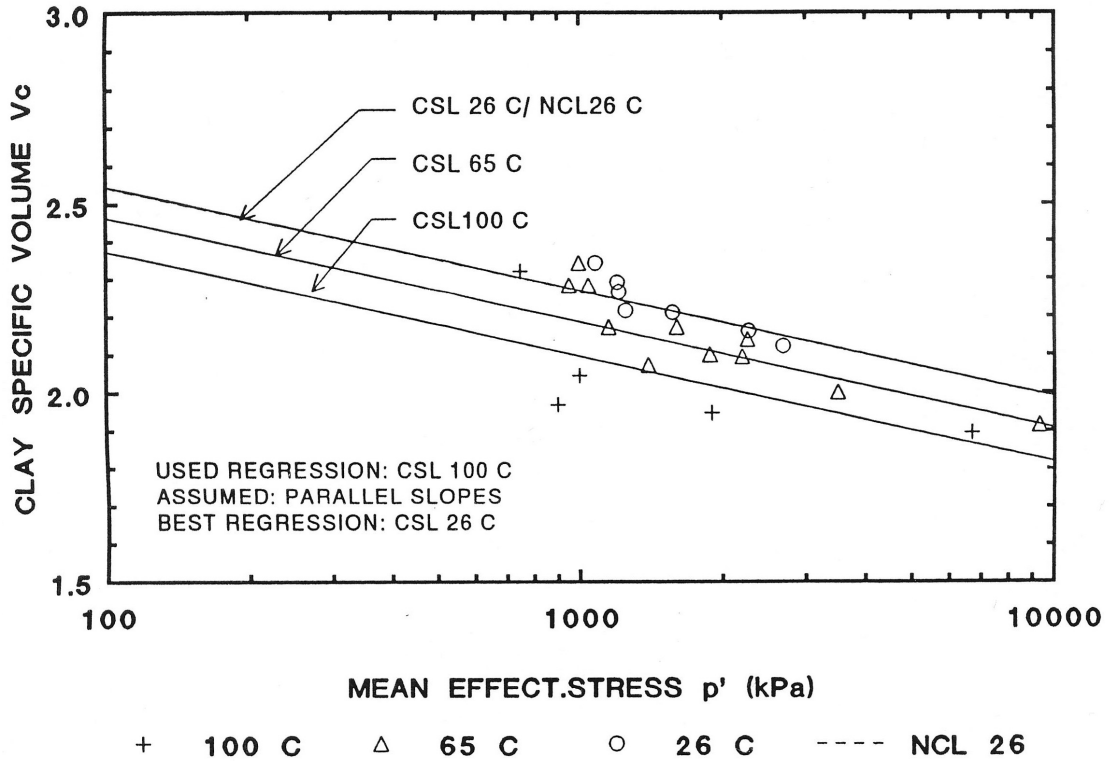


Figure 26: Summary of Critical State Lines in V_c vs. $\log p'$ -Space (after Lingnau 1993)

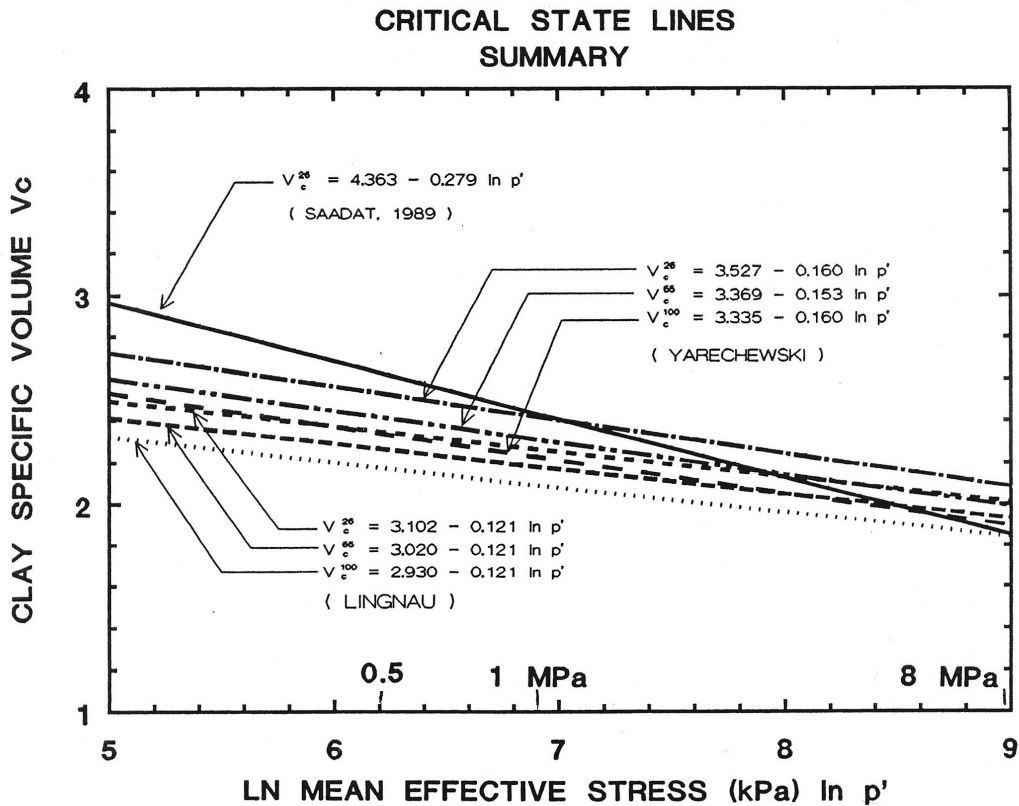


Figure 27: Summary of Critical State Lines in V_c vs. in p' -Space (after Yarechewski 1993)

4.2.2 Elastic Parameters

As expected, the compaction of triaxial specimens in a rigid mould imparts some degree of anisotropy (Saadat 1989). Oswell (1991) determined both isotropic and anisotropic elastic moduli for BSB. The anisotropic coupling modulus was found to be positive, indicating that the soil fabric is stiffer vertically than horizontally. This contradicts Saadat (1989) and Graham et al. (1989), and may be the result of swelling reducing the strong anisotropy induced during the compaction of a specimen. However, when the anisotropy is weak, especially if some swelling occurs, and BSB can be modelled with isotropic elastic moduli (Oswell 1991). The following discussion presents isotropic elastic moduli.

Soil stiffness can be related to consolidation pressure and specific volume. As such, the elastic moduli presented below have been normalized with respect to the isotropic consolidation pressure. In addition, actual values are presented for the specific testing conditions to allow for easy comparison. It should be noted that the stiffness parameters are also time dependent for bentonite based materials, especially at lower stresses. The values presented are for three days of consolidation per increment, at which time the normalized moduli appeared independent of consolidation pressure.

Sun (1986) initially presented elastic parameters for BSB initially compacted to $\gamma_d = 1,500 \text{ kg/m}^3$ over an isotropic consolidation pressure range of 0.2 to 0.6 MPa. The normalized Young's Modulus determined by Sun (1986) was found to range from E/σ_{cons} of 18.4 to 19.4 (corresponding to $E = 3.7$ to 11.6 MPa). Later work by Yarechewski (1993) on higher density specimens ($\gamma_d = 1,670 \text{ kg/m}^3$) indicated higher stiffness with a Young's Modulus value of $141 \pm 47 \text{ MPa}$.

The normalized Bulk Modulus determined by Sun (1986) ranged from a K/σ_{cons} of 28.9 to 68.4, corresponding to $K = 5.7$ to 41 MPa for the dry density ($\gamma_d = 1,500 \text{ kg/m}^3$) and consolidation pressures examined. This range of values is consistent with the values determined by Saadat (1988) and Oswell (1991) on higher density ($\gamma_d = 1,670 \text{ kg/m}^3$) specimens, who determined $K/\sigma_{\text{cons}} = 20$ to 30 , and $K/\sigma_{\text{cons}} = 31.5$, respectively (Graham et al. 1989). This gives a range of values from $K = 4.6$ to 65.5 MPa .

The normalized Shear Modulus determined by Sun (1986) ranged from a $G_{50}/\sigma_{\text{cons}}$ of 6.7 to 7.0, corresponding to $G = 1.3$ to 4.0 MPa for the dry density ($\gamma_d = 1,500 \text{ kg/m}^3$) and consolidation pressures examined (determined at a deviator stress of $q_{\text{max}}/2$). Similar values were determined by Saadat (1989) ($G_{50}/\sigma_{\text{cons}} = 9.7$ average), and Oswell (1991) ($G_{50}/\sigma_{\text{cons}} = 7.3$) on higher density ($\gamma_d = 1,670 \text{ kg/m}^3$) specimens. Yarecheski (1993) presented a slightly higher value of $G = 43 \pm 14 \text{ MPa}$ ($\gamma_d = 1,670 \text{ kg/m}^3$).

The above information is sufficient to calculate Poisson's Ratio for a given set of conditions. For example, Sun (1986) calculated Poisson's Ratio to be in the range of 0.38 to 0.45. Early modelling work assumed a Poisson's ratio of 0.4 for BSB compacted to an initial dry density of $1,670 \text{ kg/m}^3$ (Dixon et al. 1986).

4.2.3 Hardening Behaviour

Hardening behaviour can be determined through isotropic consolidation of triaxial specimens or one-dimensional consolidation of oedometer specimens. Both tests produce normal consolidation lines (NCL) in $V, \ln p'$ -space, but the different tests often produce lines that do not overlap. The isotropic NCL (from triaxial testing) will plot below the 1-D NCL (from oedometer testing) in $V, \ln p'$ -space. This is due to some (indeterminate) amount of deviator stress generated within an oedometer specimen due to the application of only a vertical load. The NCL is considered a locus of yielding states and therefore contributes to the yield locus in q, p' -space. The hardening law in MCC (i.e. the equation of the NCL) describes how the yield locus changes in size and position as plastic straining occurs.

The isotropic NCL in $V, \ln p'$ -space is equivalent to the λ line (from the MCC model). The NCL with slope λ represents total volume strain. For specimens that have been unloaded from an initial isotropic consolidation pressure, p_c' , the specific volume V of the soil will plot on the κ line at specific volumes below the NCL for a given p' . Here, κ is the slope of the unload-reload line, representing pure elastic volume strain.

The isotropic NCL will coincide with the Swelling Equilibrium Line (SEL) at pressures greater than the isotropic preconsolidation pressure, p_c' (Wan 1987). The SEL defines the equilibrium state of BSB for a given mean effective stress p' and EMDD. Depending on compaction, initial water content, chemistry, temperature and time, V can approach (creep toward) the SEL at a V

higher than the κ line. The line will be referred to as the NCL in the remainder of the report. Further discussion on swelling behaviour is provided in Volume 1 (Baumgartner 2006e) and Lingnau (1994). The interested reader is referred to Yin (1990), Yin and Graham (1989), and Yin and Graham (1994) for more complex modelling that includes a time-pressure-volume continuum. Yin's (1990) work is mathematically complex and beyond the scope of this document. Yin (1990) does provide information on elastic properties, such as G and K, and a coupling modulus between the shear and volume response. However, these parameters are dependent upon other quantities and not easily reapplied to other modelling uses.

The following is a summary of NCLs available for BSB. It should be noted that swelling would also affect the NCL. Specimens that undergo large amounts of swelling prior to recompression and definition of the NCL will follow a different NCL than a specimen that has undergone only small amounts of strain prior to compression increments. Figure 28 is provided for reference. Also note that the equations, and therefore the associated parameters, are presented in terms of V_c .

Saadat (1989) provided corresponding relationships of hardening behaviour for BSB in its initial compacted density ($\gamma_d = 1,670 \text{ kg/m}^3$):

$$V_c = 3.541 - 0.171 \ln p' \quad (45)$$

For lower density BSB ($\gamma_d = 1,500 \text{ kg/m}^3$), Saadat (1989) provided the following relationship:

$$V_c = 4.331 - 0.261 \ln p' \quad (46)$$

which is applicable to BSB that has undergone some swelling.

Oswell produced a regression that summarized the results from Wan (1987), Saadat (1989), and Oswell (1991) for the pressure range of $p' = 100$ to $3,000 \text{ kPa}$:

$$V_c = 4.651 - 0.3142 \ln p' \quad (47)$$

Equations 45 to 47 apply to isotropic conditions. Equation 47 offers two advantages over the equations presented by Wan (1987) and Saadat (1989). Firstly, it covers a wider stress range, and secondly, it covers both high and low density buffer.

Lingnau (1993) examined the effect of temperature on the position of the isotropic NCL. Tests were conducted at 26°C , 65°C , and 100°C . Increased temperature results in the expulsion of water, which results in the NCLs shifting to lower values of V . The slopes of the NCLs were similar for each temperature (Figure 29) and the same as those presented for the CSLs in the previous section. This shift in position of the NCL appears to result in a reduction in the yield point (preconsolidation pressure) with increased temperature. Lingnau (1993) provided the following regressions for the isotropic NCL at different temperatures:

$$V_c^{26^\circ\text{C}} = 3.102 - 0.121 \ln p' \quad (48)$$

$$V_c^{65^\circ C} = 3.050 - 0.121 \ln p'. \quad (49)$$

$$V_c^{100^\circ C} = 2.950 - 0.121 \ln p'. \quad (50)$$

Similar results were achieved by Yarechewski (1993), who provided the following regressions for the isotropic NCL at different temperatures:

$$V^{26^\circ C} = 2.981 - 0.084 \ln p'. \quad (51)$$

$$V^{65^\circ C} = 2.818 - 0.076 \ln p'. \quad (52)$$

$$V^{100^\circ C} = 2.778 - 0.091 \ln p'. \quad (53)$$

Figure 29 compares the results obtained by Lingnau (1993) and Yarechewski (1993), and shows that although they follow the same general trendline, they do not correlate well with one-another. This is a relationship that should be more carefully examined before defining a reference relationship between V and p' . Those using this information should select the appropriate relationship for the conditions being examined.

So far the above has focused on the λ line. Less information is available for the κ line since its position is time dependent due to significant visco-plastic swelling. Saadat (1989) determined a value of $\kappa = 0.0448$ for low density BSB. A value of $\kappa = 0.022$ was determined for the higher density material ($\gamma_d = 1,670 \text{ kg/m}^3$) (Saadat 1989).

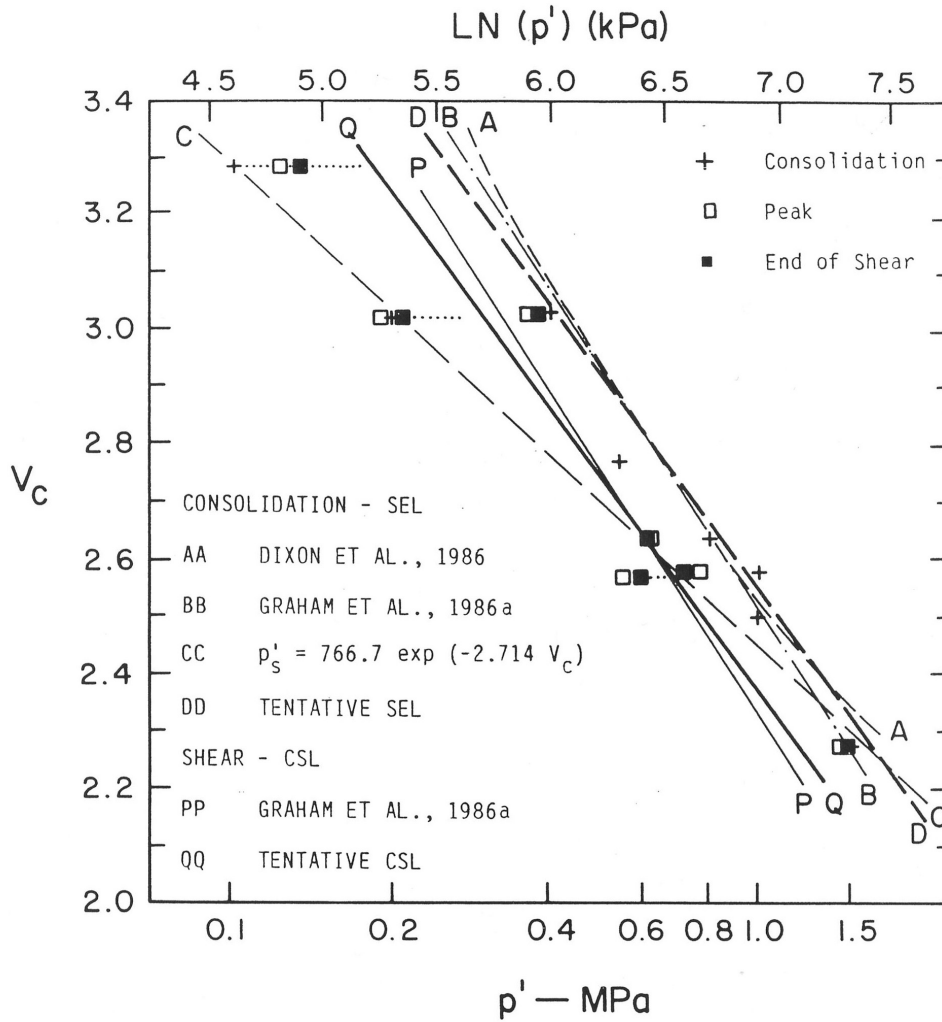


Figure 28: Summary of Hardening Behaviour of Bentonite-Sand Buffer in V_c vs. in p' -Space (after Wan 1987)

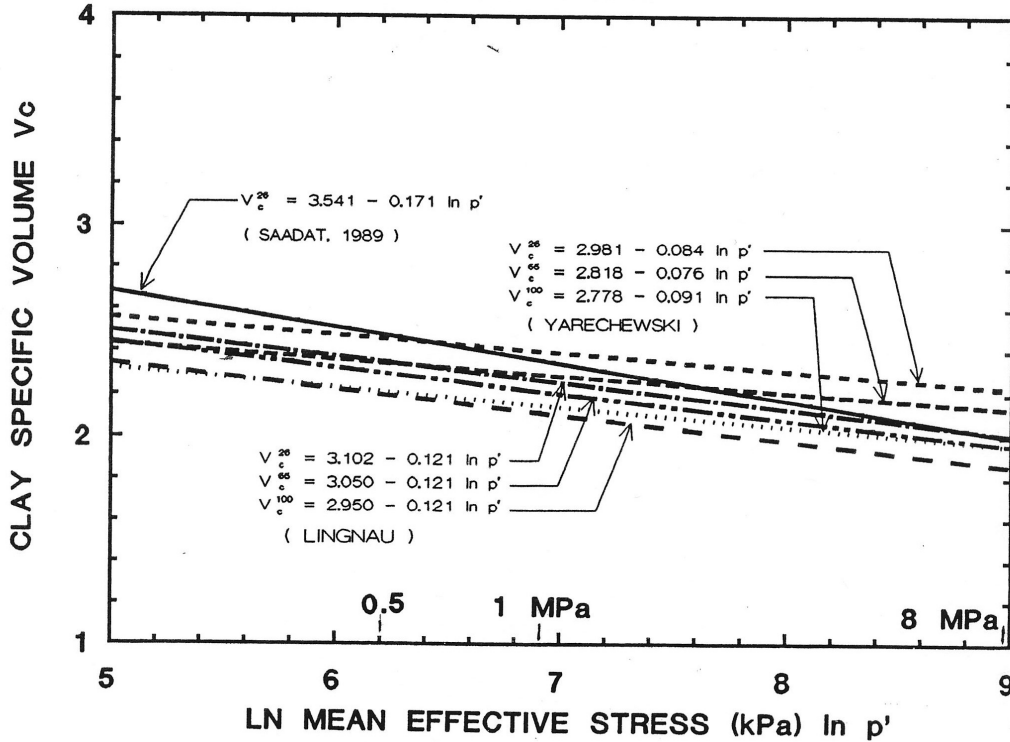


Figure 29: Summary of Normal Consolidation Lines for Bentonite-Sand Buffer (after Yarechewski 1993)

4.2.4 Yield Loci and Flow Rule

The MCC model includes a state boundary surface (SBS) that consists of the locus of points in q, p', V -space, within which the material is considered elastic. Oswell (1991) showed that a single yield locus could be used to describe yielding of high density ($\gamma_d = 1,670 \text{ kg/m}^3$) and low density ($\gamma_d = 1,500 \text{ kg/m}^3$) specimens. Figure 30 shows the yield locus for BSB, normalized with respect to the isotropic preconsolidation pressure p'_c . The capability of a single yield locus to describe BSB with different initial density and preconsolidation pressure presents significant advantages for numerical modelling. Further, it implies that the yield locus may be extended for use with LBF.

The flow rule describes the relationship between plastic volume strain and plastic shear strain. A function, known as the plastic potential, can be determined from a curve oriented such that it is perpendicular to the plastic strain increment vectors (defined by plastic volume strain and plastic shear strain). If the plastic potential coincides with the yield locus, the flow rule is termed associated. When they do not coincide (i.e. separate functions are required for description of each curve), the flow rule is termed non-associated. Based on Figure 31, the flow rule for BSB can be considered to be associated. The resulting plastic potential was similar in shape to the yield locus, however with a flatter top (Oswell 1991).

The shift in position of the NCL to lower V with increasing temperature, as noted in Section 4.2.2, implies a reduction in size of the yield locus.

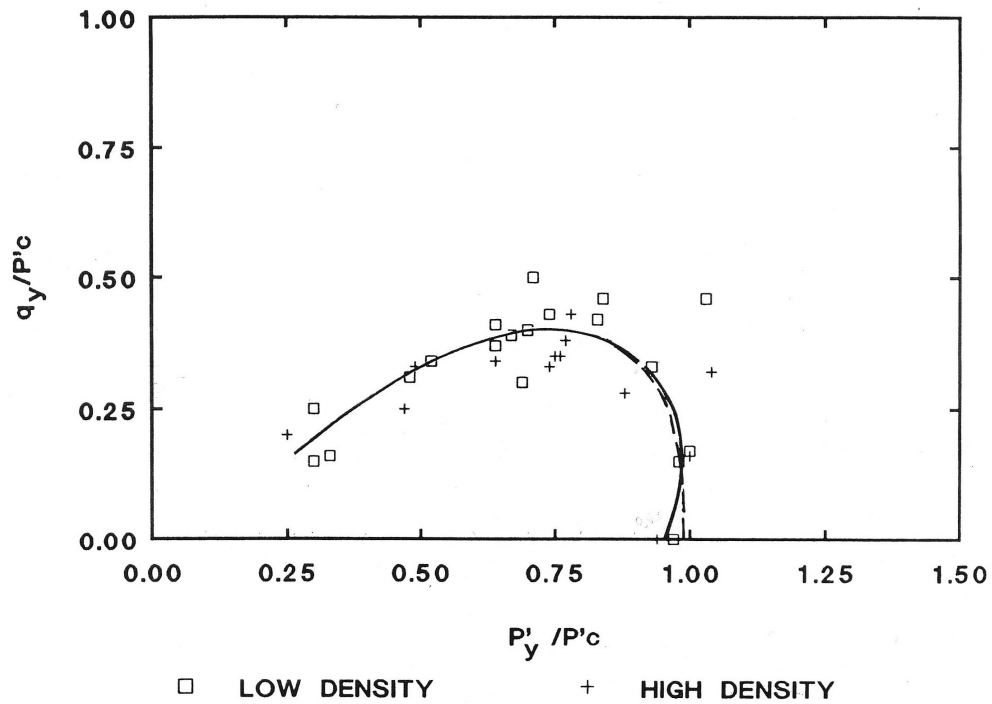


Figure 30: Yield Data, Normalized with Respect to p'_c , for Low ($\rho_d = 1.49 \text{ Mg/m}^3$) and High Density ($\rho_d = 1.67 \text{ Mg/m}^3$) Bentonite-Sand Buffer (after Oswell 1991)

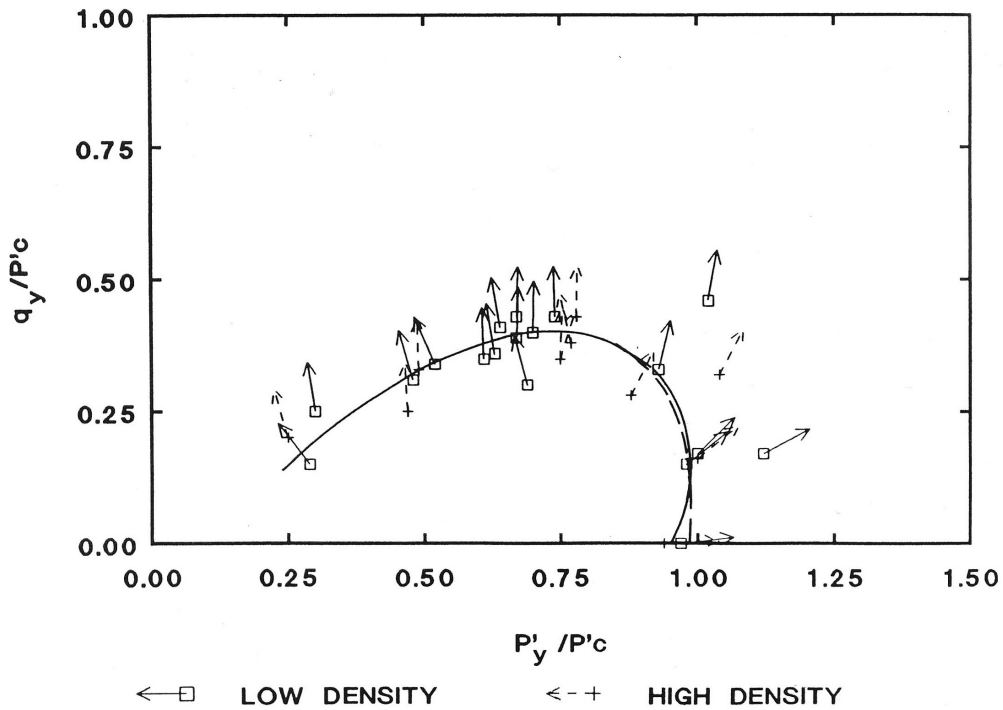


Figure 31: Plastic Strain Increment Vectors for Low ($\rho_D = 1.49 \text{ Mg/m}^3$) and High Density ($\rho_D = 1.67 \text{ Mg/m}^3$) Bentonite-Sand Buffer Indicating Non-Associated Flow (after Oswell 1991)

4.2.5 Unsaturated Conditions

Triaxial testing of unsaturated BSB has been conducted by Wan (1996), Wiebe (1998), Tang (1999), Blatz (2000), Anderson (2003) and Siemens (2006). Wan (1996) introduced a conceptual model for the behaviour of BSB in $q, p',$ suction (S)-space using the results of suction measurements taken during triaxial tests. Tang (1999) developed an elastic-plastic based model for describing the stress-strain behaviour of BSB and produced data for developing a state boundary surface in p, q, S -space. The model was subsequently refined by further quantitative development and definition of the associated parameters (Blatz 2000; Blatz and Graham 2003). Available parameters for unsaturated BSB are presented below.

It should be noted that due to the considerable amount of research conducted on BSB in Canada, this section is disproportionately longer than that for other materials. This section highlights that unsaturated soil mechanics is considerably more complex than saturated soil mechanics, and that the efforts made to develop constitutive models and define their parameters are state-of-the-art. The other materials included in this document have not undergone such rigorous testing. Current research is directed at similar programs for the other proposed sealing materials aimed at determining well-defined material properties for use in designs using unsaturated swelling clay.

4.2.5.1 Strength Envelope

In general, the results have indicated that strength increases with decreasing degree of saturation ($50\% \leq S_r \leq 100\%$), with increasing confining pressure, and with decreasing temperature. Wiebe et al. (1998) presented the results of 97 quick-undrained triaxial tests on unsaturated BSB. Saturation was varied from 50% to 98% (i.e. suction ranged from 10 MPa to 0 MPa) and confining pressure was varied from 0.2 MPa to 3.0 MPa. Specimens with varying suction were prepared by varying the amount of moisture initially mixed with dry buffer material. The study showed how the strength and stiffness of BSB varies with cell pressure, suction and temperature. The results of the extreme cases are shown in Figure 32. Shear strength was observed to increase with decreasing saturation. Stress-strain behaviour was generally ductile except for low saturation and confining pressure where some strain softening was observed.

Increases in temperature slightly reduced strength, but the reduction was small compared to the effect of degree of saturation. Overall, peak deviator strengths decreased at a uniform rate of $-6 \text{ kPa}/^\circ\text{C}$ (Wiebe 1996). However, at higher saturation values (98%), undrained strength was largely independent of temperature and confining pressure. The same effect occurred at higher confining pressures where pore air was forced into solution and $\phi_u = 0$ behaviour was observed. The combined effects of saturation, temperature and confining pressure are illustrated in Figure 33. Unsaturated parameters M^b and ϕ^b (i.e. slope of the strength envelope in deviator stress or shear stress versus suction-space) presented by Wiebe et al. (1998) are listed in Table 6 for a range of temperatures and net mean effective stresses. Values of ϕ^b decrease linearly with increasing temperature at a rate of $0.04/^\circ\text{C}$ (Wiebe, 1996).

Table 6: Values of M^b and ϕ^b for Bentonite-Sand Buffer (after Wiebe et al. 1998)

	Net Mean Stress ($p-u_a$) (MPa)			
	1.0	2.0	3.0	4.0
T = 26°C				
M^b	0.42	0.60	0.59	0.57
ϕ^b	12.3	17.5	17.2	16.7
T = 65°C				
M^b	0.32	0.52	0.51	0.58
ϕ^b	9.6	15.3	15.0	16.9
T = 100°C				
M^b	0.30	0.46	0.52	0.48
ϕ^b	8.9	13.7	15.2	14.0

Note: u_a = pore-air pressure

M^b = slope of the strength envelope in deviator stress, suction-space

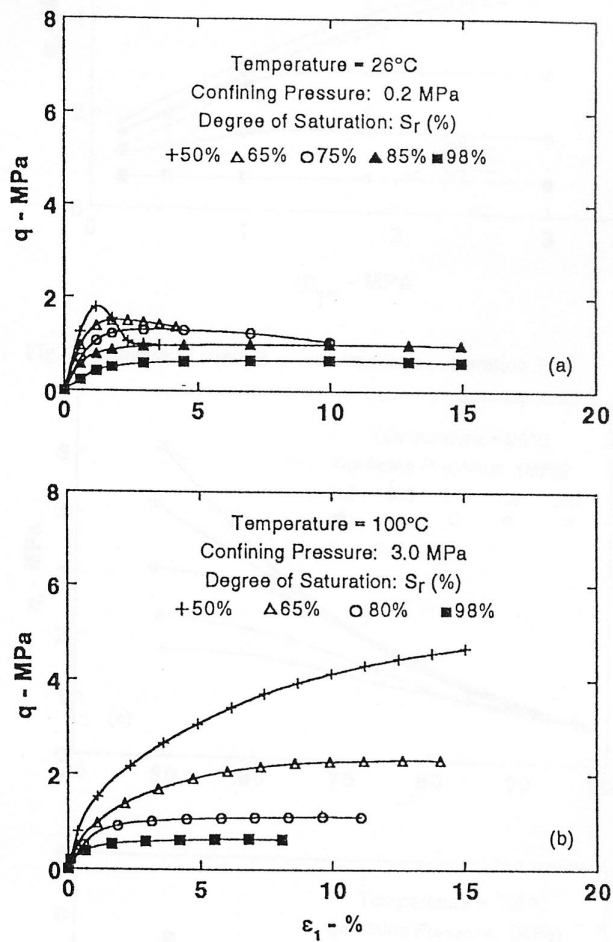


Figure 32: Typical Stress-Strain Curves for Low Temperature and Pressure (Top) and High Temperature and Pressure (Bottom) (after Wiebe et al. 1998)

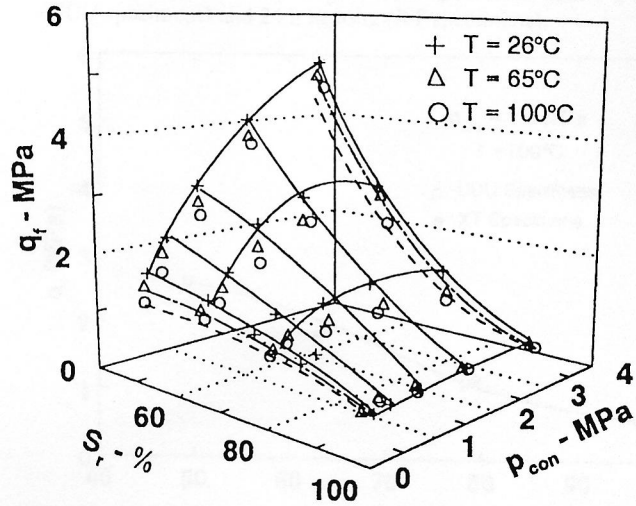


Figure 33: Boundary Surface for the Peak Strength of Unsaturated Bentonite-Sand Buffer (after Wiebe et al. 1998)

Blatz (2000) and Blatz et al. (2002) expanded on the study conducted by Wiebe et al. (1998) by testing specimens that were initially compacted with the target dry density and moisture content for BSB, and then changing the suction conditions in desiccators. This sequence is more representative of repository conditions and allowed testing at greater suction, but results in relatively long specimen preparation times (i.e. >30 days per specimen). General failure mode was consistent between the programs conducted by Wiebe et al. (1998) and Blatz et al. (2002) where behaviour was primarily ductile, with brittle, strain-softening behaviour only occurring at low confining pressures. The testing program indicated that suction had a greater influence on peak strength than confining pressure, which is consistent with the results of Wiebe et al. (1998). The peak strength envelopes determined by Blatz (2000) at varying suctions are provided in Figure 34 and peak strength envelopes at varying cell pressures are provided in Figure 35. Large strain strengths at varying suctions are provided in Figure 36. A summary of critical state M values for varying suction by Blatz (2000) is provided in Figure 37. Anderson (2003) provided a similar summary, including higher suctions (Figure 38). Note that the parameter has been renamed 'N' in Figure 38 since the slope of the CSL in p,suction-space can be viewed as different from the M value in p-q space (Graham and Blatz 2003). Figure 39 provides critical state M values for a lower range of suctions (Tang 1999).

Good agreement was observed between undrained peak strengths determined from laboratory-prepared triaxial specimens (Wiebe, 1996), and triaxial specimens obtained from full-scale field tests (Blatz 2002) including the Isothermal Test (ITT) and the Buffer-Container Experiment (BCE) conducted at AECL's Underground Research Laboratory (Dixon et al. 2002, 2005). Figure 40 compares the triaxial testing results between the two programs.

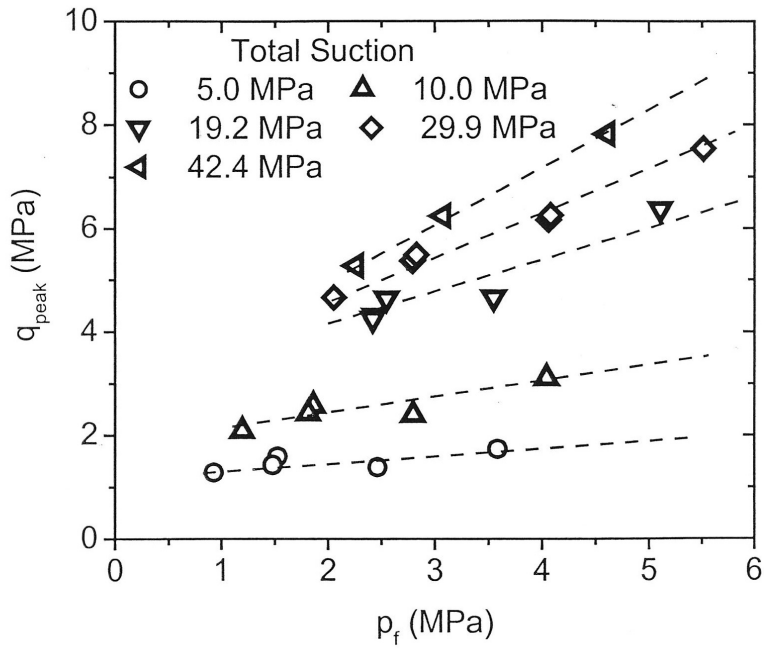


Figure 34: Peak Strength Envelopes at Various Suctions (after Blatz 2000)

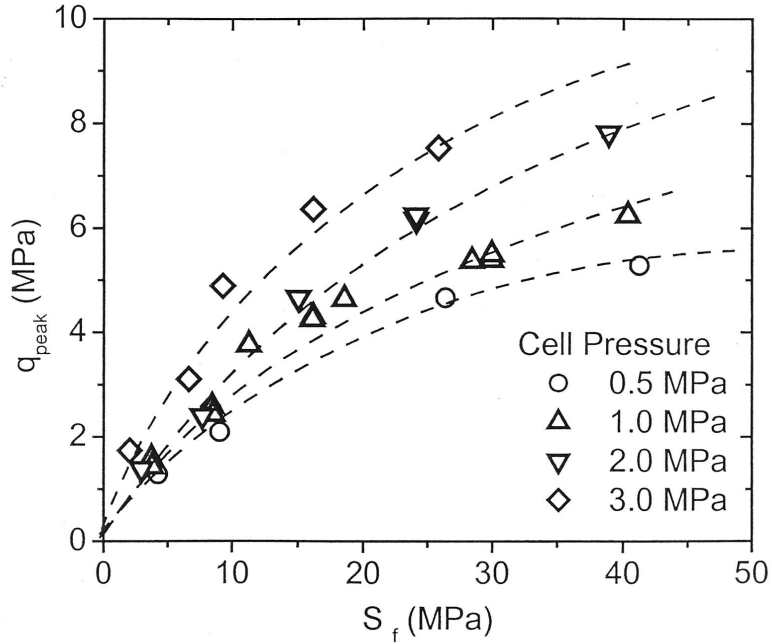


Figure 35: Peak Strength Envelopes at Various Cell Pressures (after Blatz 2000)

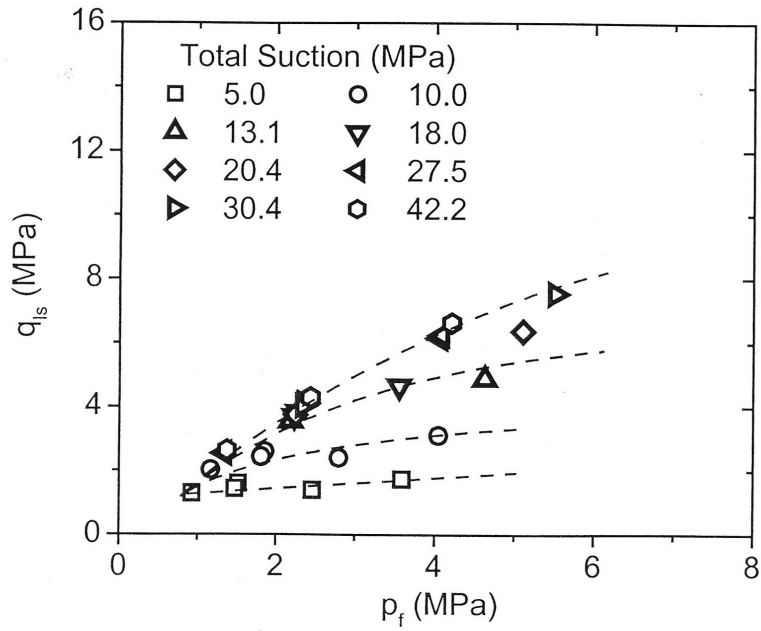


Figure 36: Large Strain Strengths at Varying Suction (after Blatz 2000)

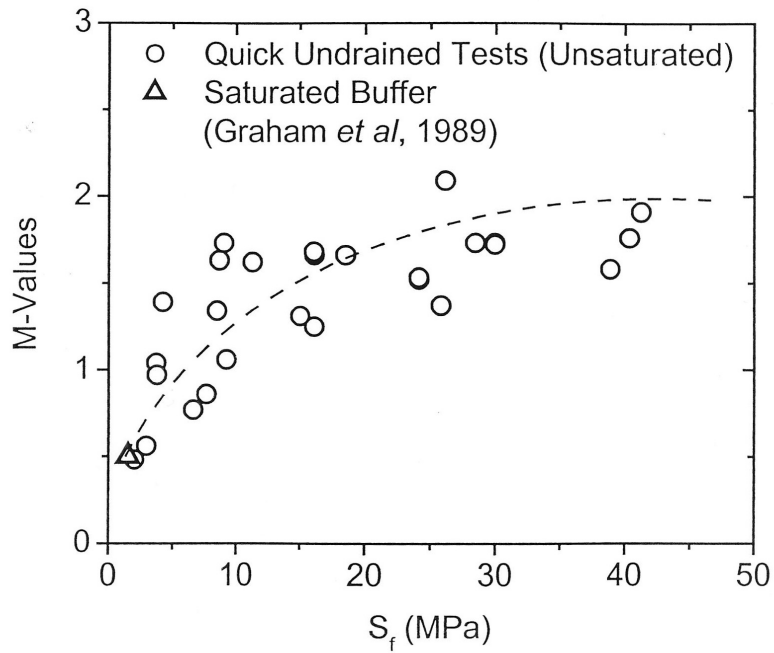


Figure 37: Summary of Critical State M Values for Varying Suction (after Blatz 2000)

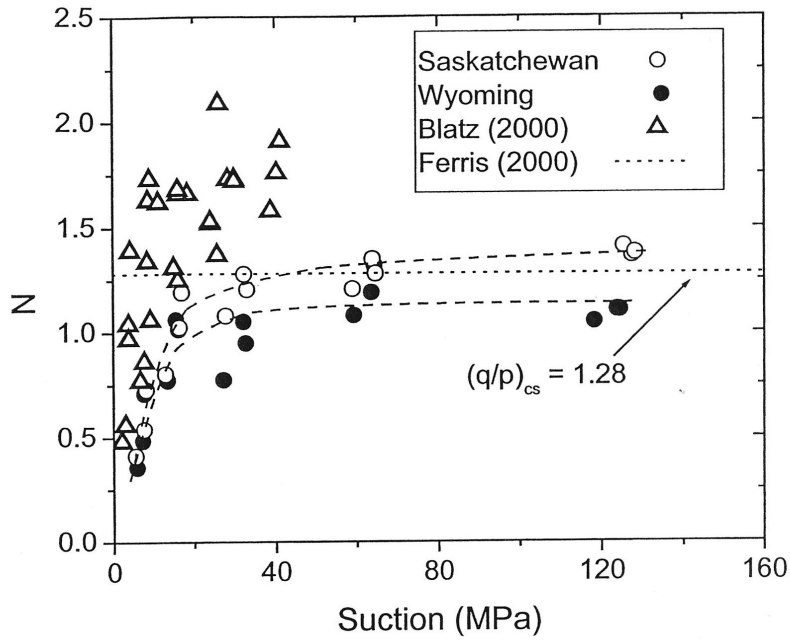


Figure 38: N Values for Bentonite-Sand Buffer Made with Wyoming and Saskatchewan Bentonite at Varying Suctions (after Anderson 2003 which referenced Ferris 2000 and Blatz 2000)

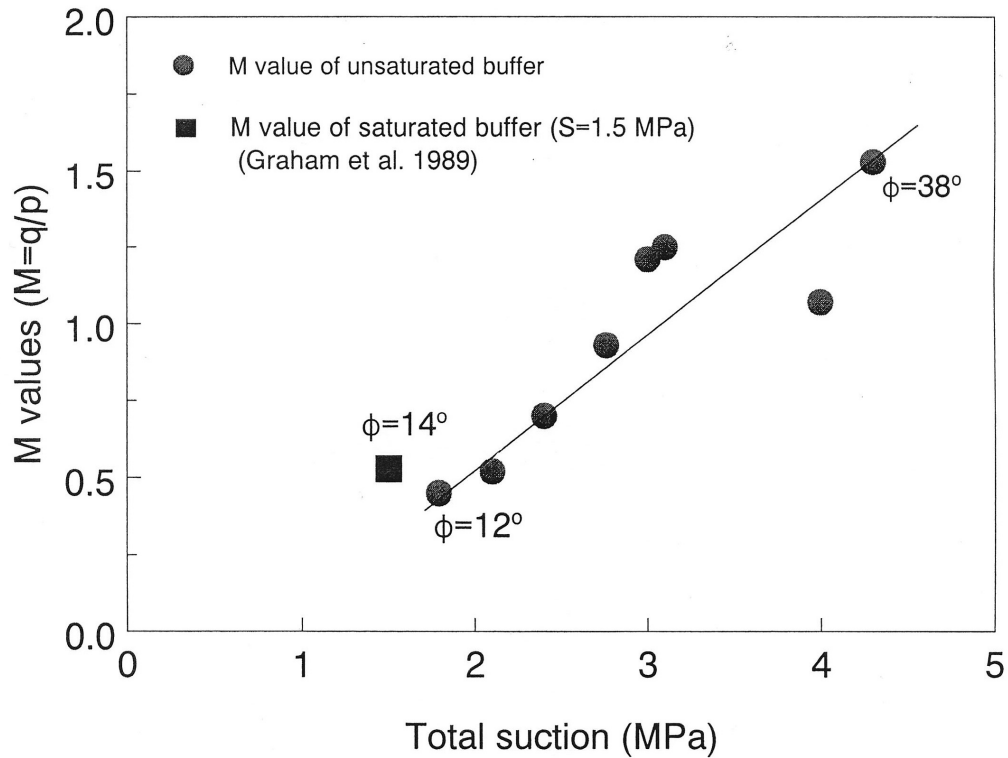


Figure 39: Summary of Critical State M Values for Varying Suction (after Tang 1999)

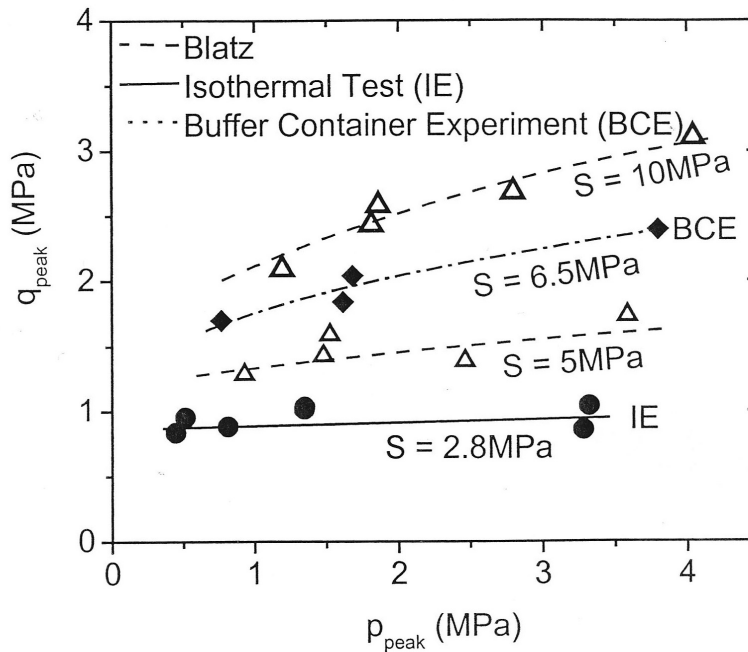


Figure 40: Comparison of Triaxial Testing Results Conducted on Specimens prepared by Blatz (2000) and on Specimens from a Large Scale in Situ Experiment (after Blatz 2000)

Tang et al. (1998), Tang (1999) and Tang et al. (2002) provide the change in peak strength with degree of saturation for concentrations of NaCl in the pore fluid (Figure 41). As per the above-mentioned studies, peak strength increases as the degree of saturation decreases. Increased salt concentration had little effect on peak strength at higher degrees of saturation. Contrary to what is predicted by diffuse double layer theory, a slight decrease in strength was noted for higher salt concentrations and a degree of saturation of 65%. This decrease was small and there are few data points, therefore more testing is required to more clearly define the effect of salinity on strength at low saturation. It should be noted that triaxial tests on saturated LBF with different pore fluid chemistry displayed the expected trend, where increases in salt concentration resulted in increased strength (Section 4.3.1).

Tang (1999) also conducted tensile strength tests on unsaturated BSB. A new method for testing the tensile strength of unsaturated soils was developed (Tang and Graham 2000). As expected, the results show an increase in tensile strength with increasing suction (Figure 45).

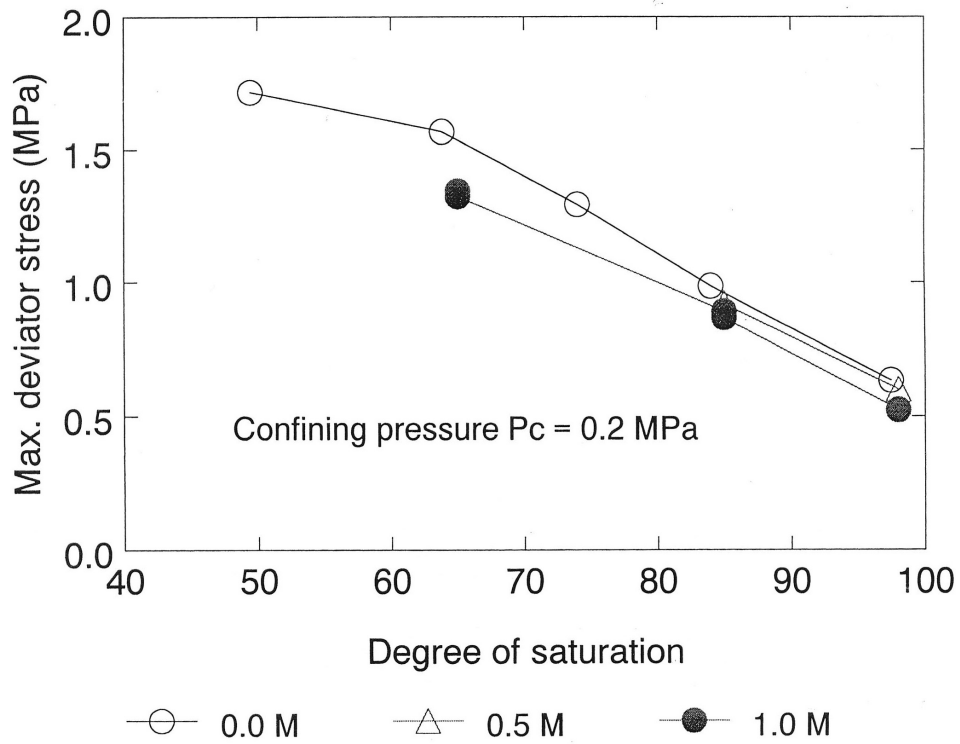


Figure 41: Peak Strength vs. Suction for a Range of Salt Concentrations in the Pore Fluid (after Tang 1999)

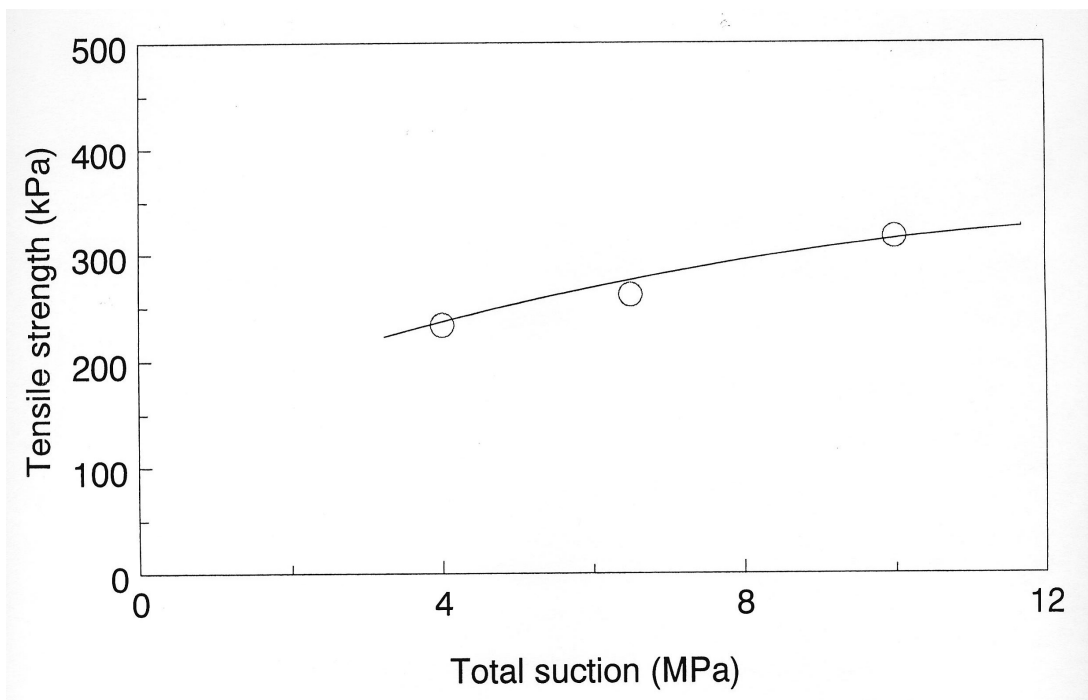


Figure 42: Tensile Strength of Bentonite-Sand Buffer as a Function of Total Suction (after Tang 1999)

4.2.5.2 Elastic Parameters

Wiebe (1998) determined Young's modulus for a range of water contents, confining pressures and three different temperatures (26°C, 65°C and 100°C). The results obtained by Wiebe (1998) are summarized in Figure 43. As expected, increased suction results in a stiffer material. For a given saturation and confining pressure, stiffness generally decreases with increasing temperature.

Tang (1999) determined the elastic modulus as a function of degree of saturation for BSB. Consistent with the results obtained by Wiebe (1998), stiffness increases as the degree of saturation decreases (Figure 44). Tang (1999) also examined the effect of salt concentration in the pore fluid on the elastic modulus. The elastic modulus was observed to decrease slightly with an increase in salt concentration (Figure 45). This trend is not consistent with diffuse double layer (DDL) theory as described in Section 4.3.1.

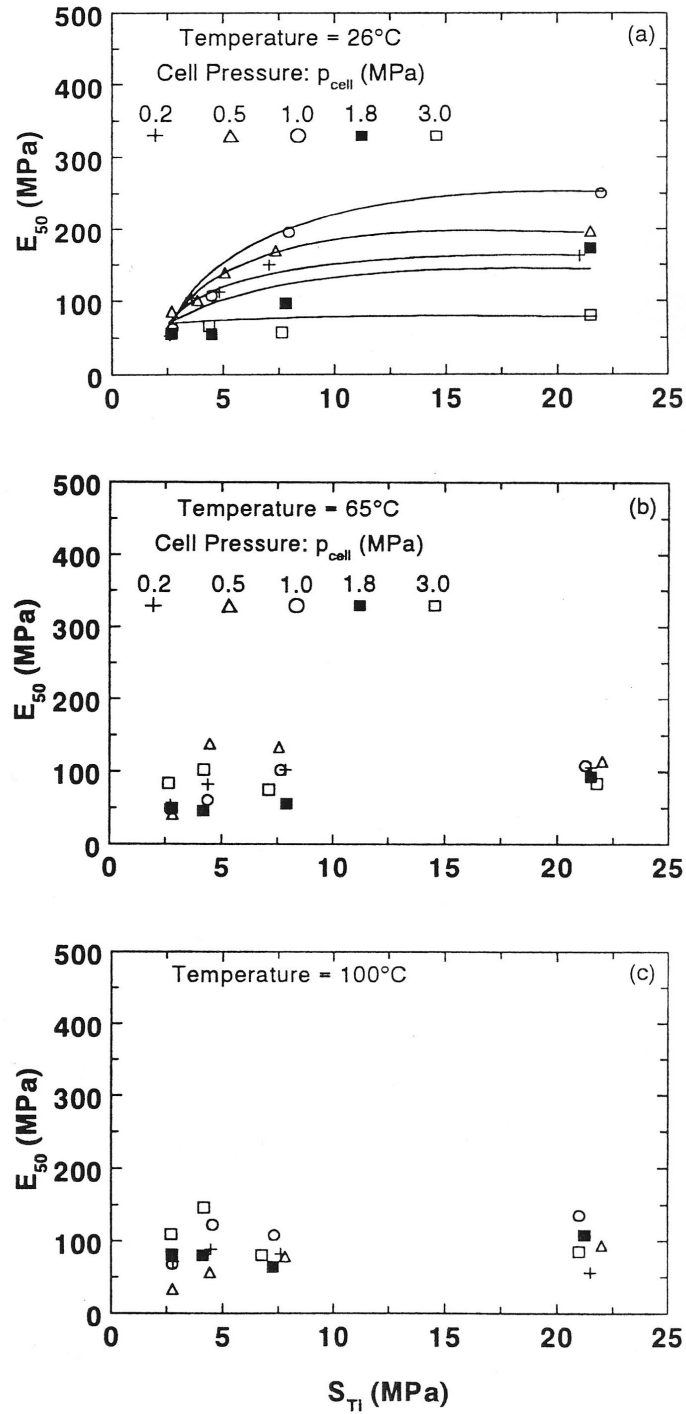


Figure 43: Effect of Total Suction and Confining Pressure on Young's Modulus at 26°C, 65°C and 100°C (after Wiebe 1998)

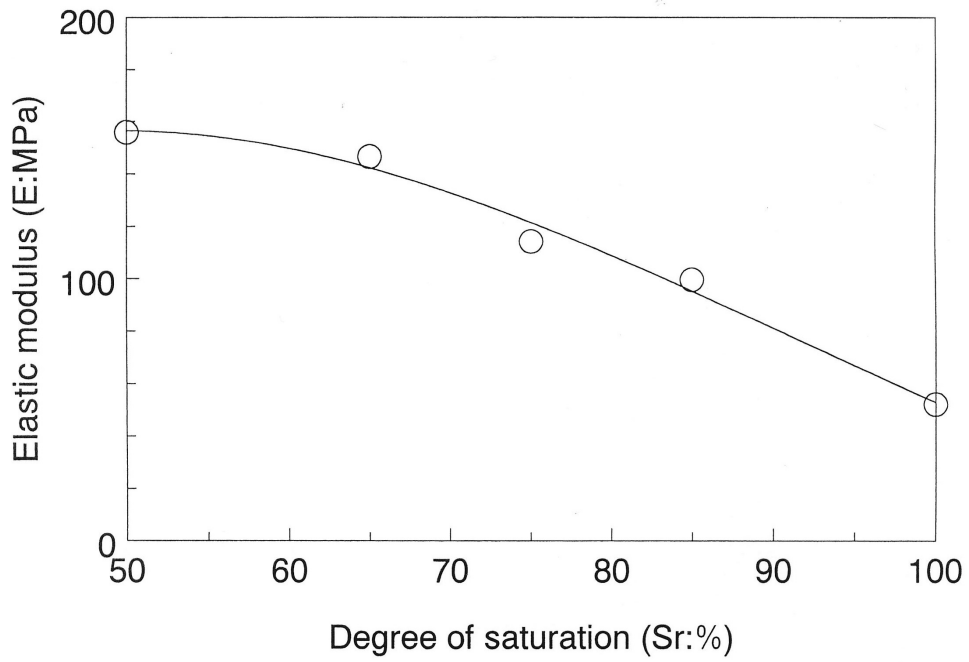


Figure 44: Young's Modulus vs. Degree of Saturation (after Tang 1999)

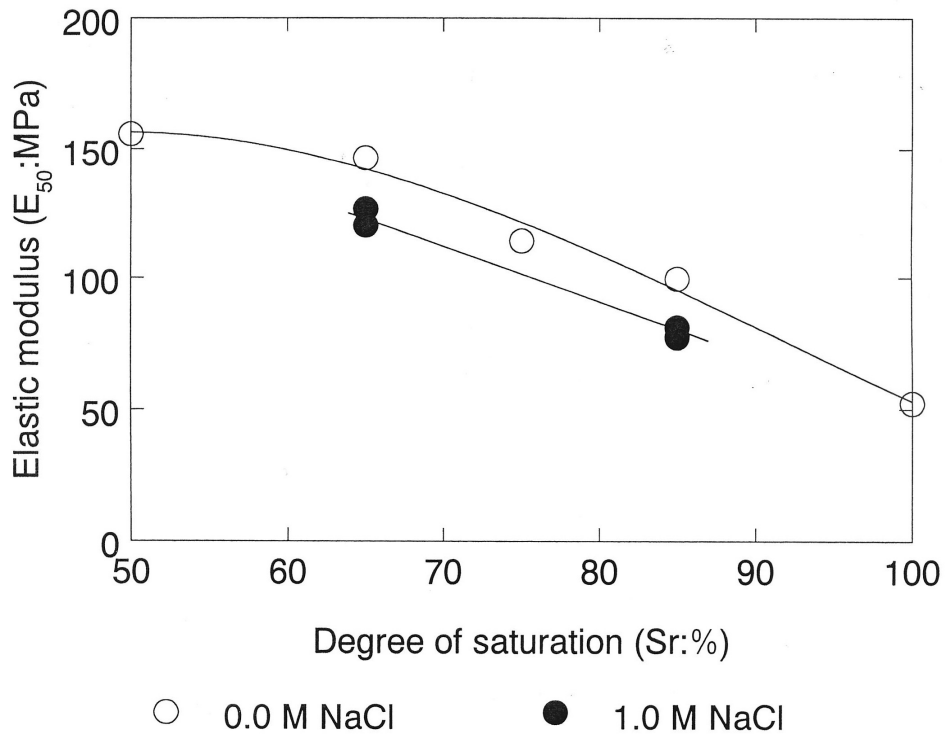


Figure 45: Young's Modulus vs. Degree of Saturation for Two Different Concentrations of NaCl in the Pore Fluid (after Tang 1999)

Blatz (2000) evaluated the effect of suction on soil stiffness. As expected, increased stiffness was observed with increasing suction up to some potential threshold (Figure 46). The results show that increases in dry density associated with shrinkage due to increased suction had a greater impact on stiffness than confining pressure. In fact, stiffness was largely independent of confining pressure. At high suctions (30-40 MPa), stiffness becomes approximately constant, corresponding to the limit of volumetric shrinkage (Blatz et al. 2002). The data in Figure 46 represent E values taken at 1% strain (i.e. $E_{1\%}$). These values are compared to E values taken at 50% of q_{\max} (i.e. E_{50}) in Figure 47. The E_{50} values are generally lower than the $E_{1\%}$ values, but they tend to converge at higher suctions near the limit of volume shrinkage.

The shear modulus determined by Blatz (2000) for BSB ranged from 111 MPa at a suction of 6 MPa to 276 MPa at a suction of 7 MPa. This is a very large range in values for this parameter for tests done with relatively small differences in the suction. This type of behaviour should be confirmed by additional testing before any behavioural generalizations are made.

Blatz (2000) presented an elastic volume change modulus for unsaturated BSB in its initial, as compacted state (representing the same portion of the curve as κ) in terms of volume strain (i.e. $C_r/(1+e_0)$). The slopes of the initial elastic portions of the curves and the unload-reload lines were consistent with an average recompression coefficient value of $C_r/(1+e_0) = 0.006$. The κ values determined by Anderson (2003) are provided in Figure 48 for BSB made with Saskatchewan bentonite. At lower suctions (less than 40 MPa) κ ranged from 0.003 to 0.015 and at higher suctions (greater than 40 MPa), κ ranged from 0.004 to 0.012.

Blatz and Graham (2003) interpreted an average suction coefficient of $C_s/(1+e_0) = 0.005$ (where C_s is the swelling index from the unloading curve of an oedometer test) for elastic suction induced volume change for tests that were monitored for volume strain versus increases in total suction.

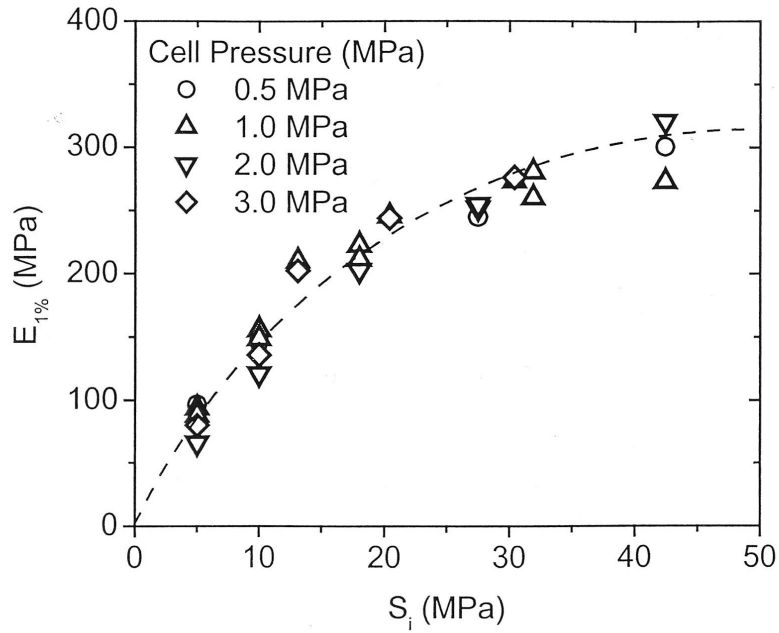


Figure 46: Bentonite-Sand Buffer Stiffness for Varying Cell Pressure and Suction (after Blatz 2000)

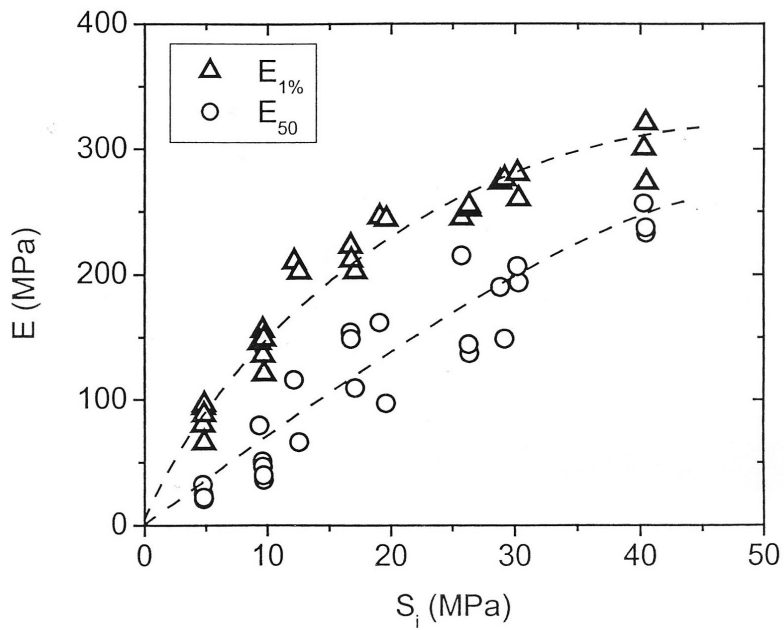


Figure 47: Comparison of Interpreted E Values (after Blatz 2000)

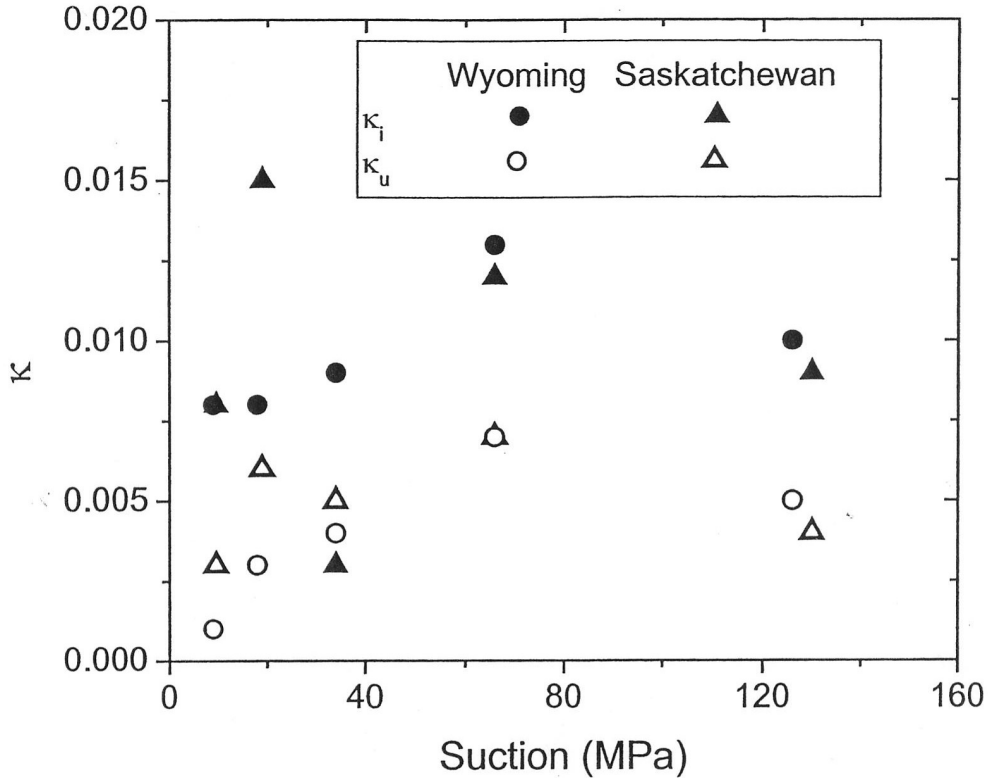


Figure 48: κ Values for Bentonite-Sand Buffer at Varying Suction (after Anderson 2003)

4.2.5.3 Hardening Behaviour

Hardening of unsaturated soils can occur by both increases in mean stress as well as increases in suction. Specific volume can therefore be plotted against mean stress (with slopes κ and λ), as for saturated soils, and suction (with slopes κ_s and λ_s). Plotting these three variables on mutually perpendicular axes, results in a three-dimensional volume state surface as shown in Figure 49. Blatz (2000), did not conclusively observe yielding due to suction in (V , suction-space) and therefore a hardening parameter was not determined that would describe the transition from elastic behaviour to plastic strain hardening behaviour. This was identified as a fundamental feature that required further investigation. Anderson (2003) examined a higher range of suctions and in doing so, observed suction induced yielding (Section 4.2.5.4).

Blatz (2000) and Blatz and Graham (2003) presented a hardening law for unsaturated BSB in its initial as compacted state (representing the same portion of the curve as λ) in terms of volume strain (i.e. $C_v/(1+e_0)$). The slopes of the volumetric hardening law were consistent with an average compression coefficient value of $C_v/(1+e_0) = 0.140$. This applies at suctions up to 3.7 MPa which is representative of BSB in its initial compacted state. After further drying of the specimens (to suction values in the range of 4.5 to 7.5 MPa), the material became stiffer with an average compression coefficient of 0.090.

The λ values determined by Anderson (2003) are provided in Figure 50 for BSB. At lower suctions (less than 40 MPa) λ ranged from 0.07 to 0.08 and at higher suctions (greater than 40 MPa), λ is approximately 0.03, which is representative of the sand used in making the BSB.

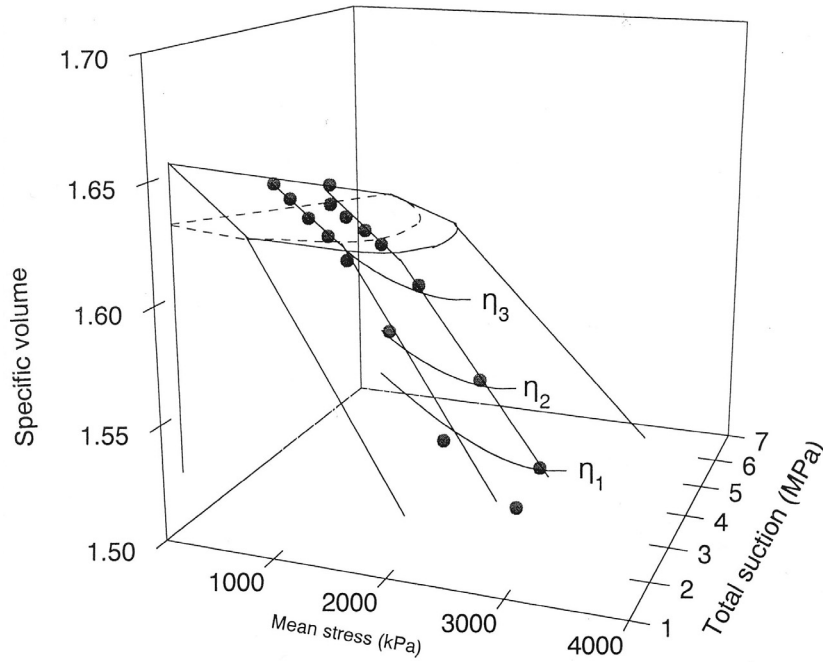


Figure 49: Volume Change with Mean Stress and Total Suction (after Tang 1999)

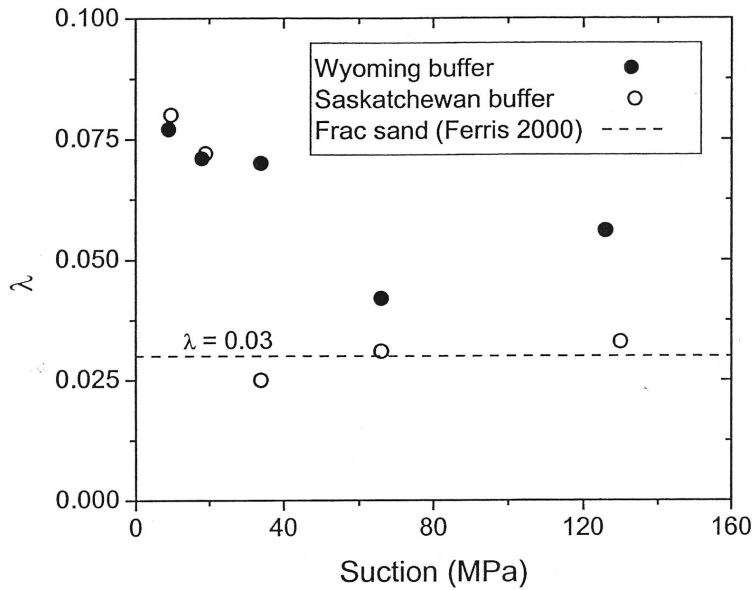


Figure 50: Hardening Line (λ) Parameters for Bentonite-Sand Buffer at Varying Suctions (after Anderson 2003)

4.2.5.4 Yield Loci and Flow Rule

Tang and Graham (2002) developed a “stress-ratio model” to describe a state boundary surface in p, q, s -space for unsaturated soils. Their model is shown conceptually in Figure 51. In this model, the state boundary surface is constructed by considering radially divergent planes, each with constant $\eta_s = s/p$ in s - p space. The planes extend vertically in the q direction. Two series of triaxial tests, shown in Figure 52, were conducted to examine the conceptual model. One series was conducted from “as compacted” conditions (Series 1), while the other series was first dried (to 6 MPa suction) in a desiccator to place them on a different η -line (Series 2). Three stress paths with different q/p ratios were then followed for each series from an over-consolidated state ($OCR = 2$ to 3). The normalized yield locus for the tests are shown in Figure 53 along with the results obtained by Oswell (1991) on saturated BSB specimens (i.e. zero matric suction and ~ 1.5 MPa osmotic suction for BSB). The shapes are broadly similar, however, the constant-stress ratio model is required to establish a single relationship for the yield locus.

Tang and Graham’s (2002) series of tests also allowed definition of a portion of what is called the LSY (Load, Suction, Yield) yield locus in p, s -space (recall Figure 19), which is labelled as II’ in Figure 54. This portion of the LSY was approximated as a straight line with slope α :

$$\alpha = \frac{p_{02} - p_{01}}{s_{02} - s_{01}} = 0.33 \quad (54)$$

Where p_{01} , s_{01} and p_{02} , s_{02} are the mean and total suction at yielding for the two series of specimens, respectively. This is valid for the stress range of approximately 800 to 1,300 kPa. Below this range, the saturated yield locus is approached. Expansion of the yield locus is represented by g_1 and g_2 as a result of increased mean stress. Line II’ represents the yield locus imparted by compaction of the specimens. This assumes that the LSY are parallel and can be approximated using a straight line.

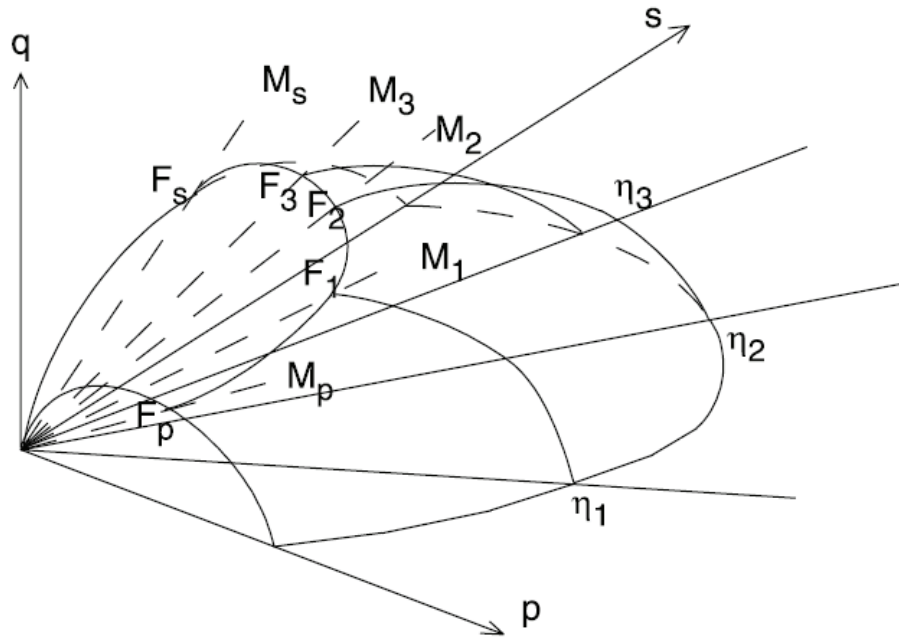


Figure 51: Conceptual Elastic-Plastic Model for Unsaturated Soils showing the State Boundary Surface in p, q, s -Space (after Tang and Graham 2002)

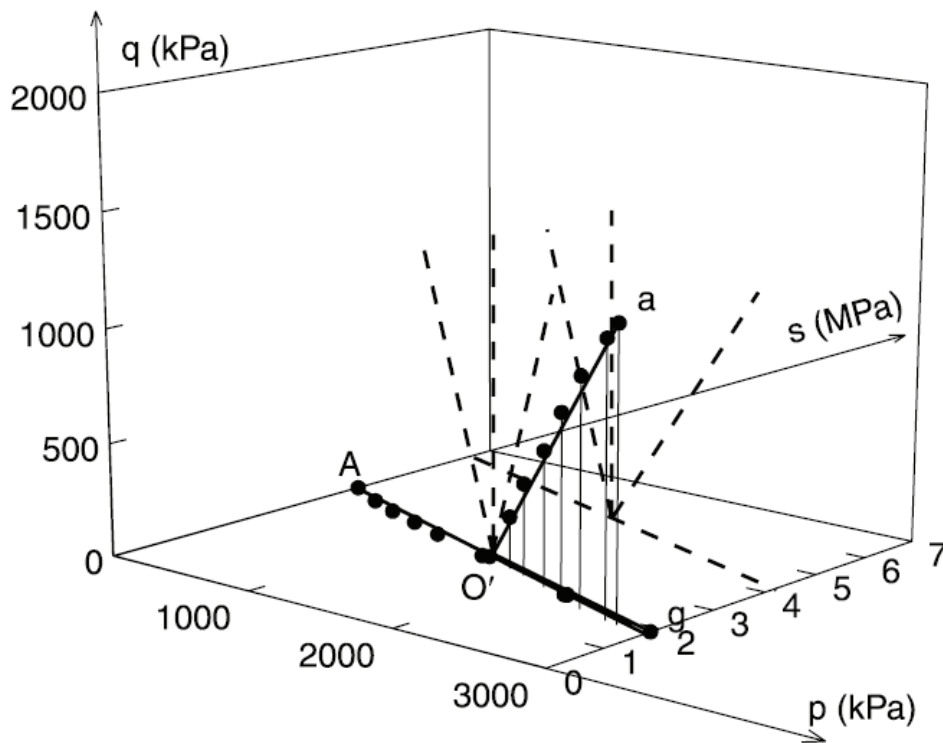


Figure 52: Two Series of Tests Examined by Tang and Graham (2002) in p, q, s -Space. Note: for clarity, data points from only one test are shown (after Tang and Graham 2002)

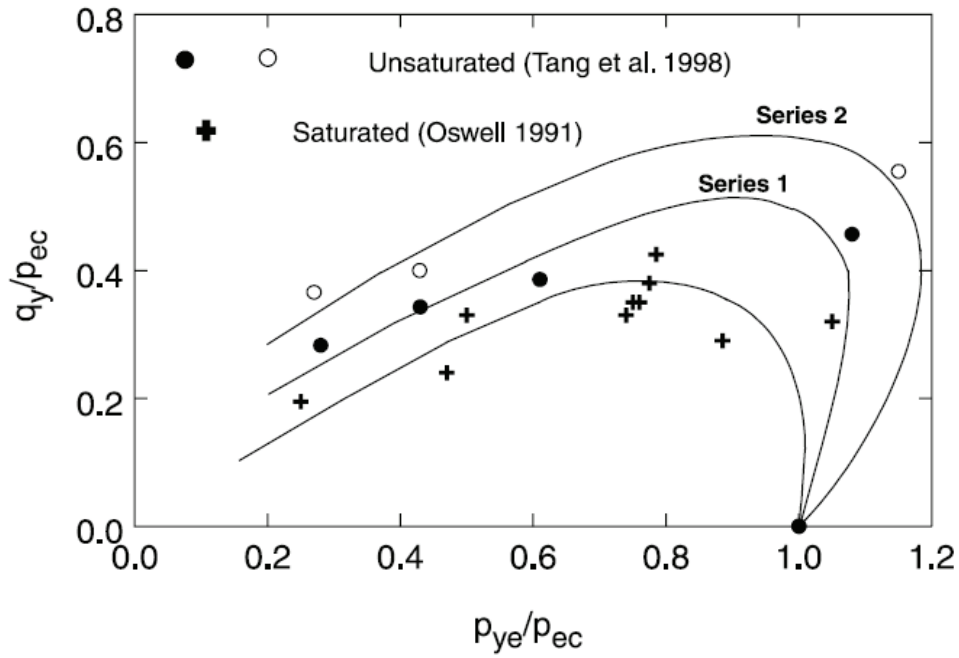


Figure 53: Normalized Yield Data for Bentonite-Sand Buffer. Series 1 was prepared with an initial suction of 4 MPa (as-compacted), and Series 2 was prepared with an initial suction of 6 MPa (after Tang and Graham 2002)

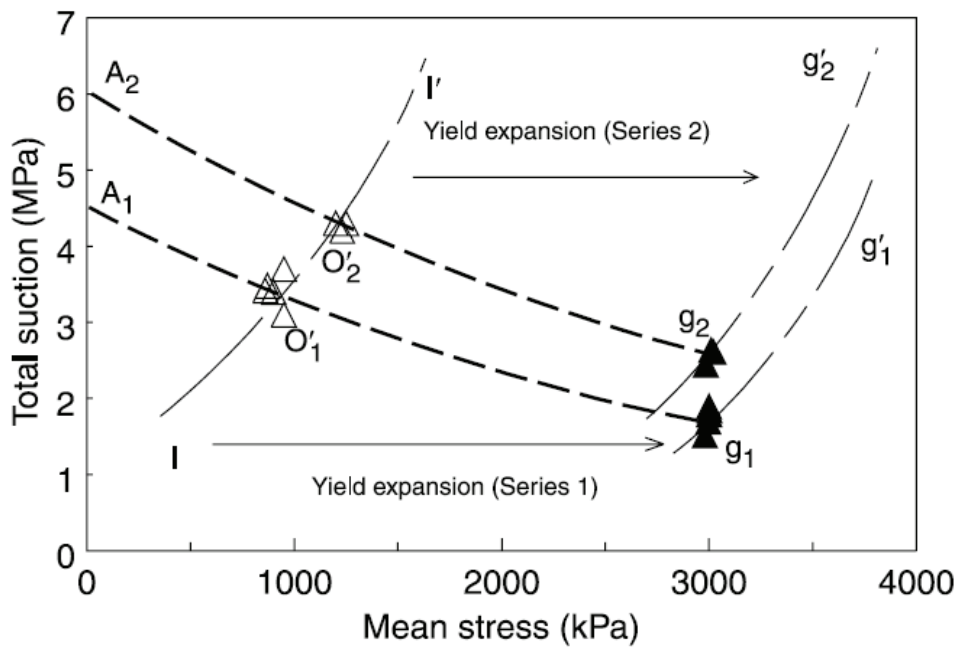


Figure 54: Expansion of the Yield Locus in p,s -Space (after Tang and Graham 2002)

Blatz (2000) conducted a series of tests to move towards a constitutive model that relates mean stress, deviator stress, suction and volume strain. The primary advancement provided by Blatz's (2000) work was the development of a method to control suctions of a specimen while it is under load in a triaxial cell. This allowed further examination of the model presented by Tang and Graham (2002). Details of the resulting model, known as the Blatz-Graham Model (BGM) are provided in Blatz and Graham (2003).

Blatz and Graham (2003) presented results for further development of the load-yield (LY) line as shown in Figure 55. The tension, or T-line, is from the relationship determined by Tang and Graham (2000). Figure 55 shows the bounds for the base of the yield loci in the p-s plane using a linear approximation. Line LY_1 represents the outer edge of the yield loci for BSB in its initial, as-compacted state, and line LY_2 represents the outer edge of the yield loci after being loaded to 2 MPa. Adding deviator stress to Figure 55 yields Figure 56, which shows approximations of the yield loci in the three dimensions.

Figure 57 shows the three-dimensional volume state surface for BSB in p,s,V-space. Six parameters are required to define this surface including: 1) the slope of the unload-reload line, 2) the plastic hardening line at constant suction, 3) the slope of volume decrease as suction increases, 4) a reference specific volume at unit suction and unit mean stress, 5) slope of the LY_i curve, and 6) the intercept of the LY_i curve at zero suction (Blatz and Graham, 2003). Figure 56 and Figure 57 provide a simplified constitutive model for unsaturated BSB in q,p,s-space and p,s,volume-space respectively. Simplifying assumptions incorporated into the model include elliptical yield loci, neglect of increased stiffness when volume strains from suction or pressure loading are beyond approximately 8-10%, and the assumption that suction loading is elastic.

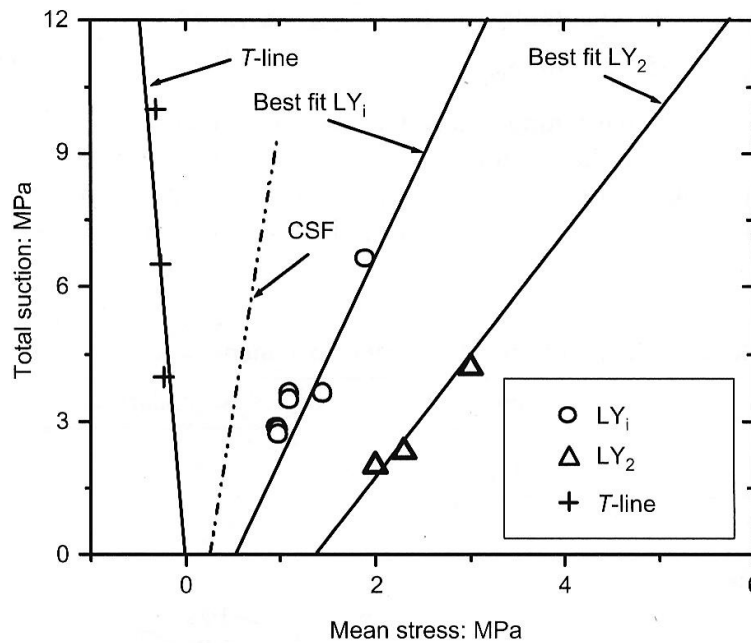


Figure 55: Modelled LY and T-line Based on Experimental Results. Note: CSF represents Critical State Failure (after Blatz and Graham 2003)

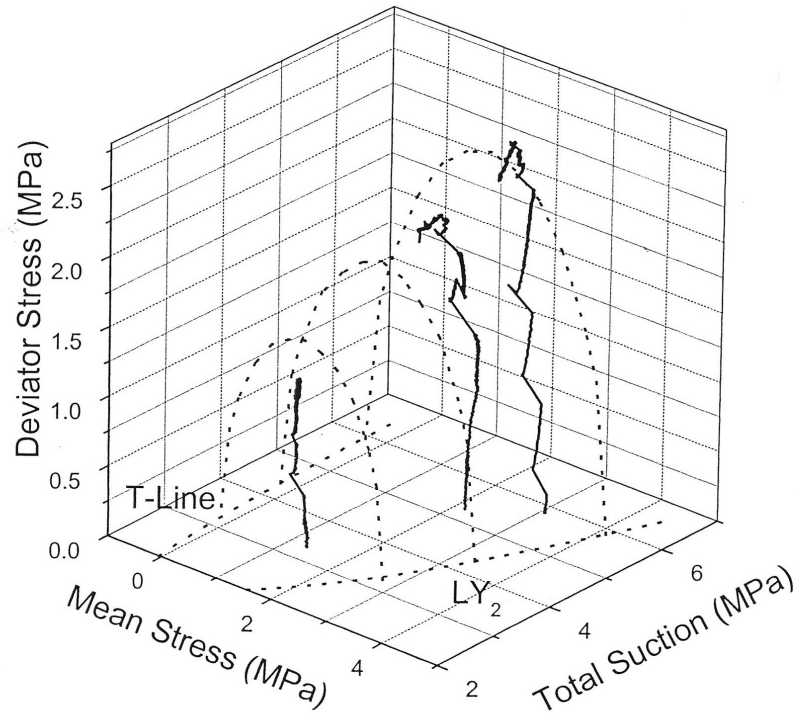


Figure 56: Three-Dimensional p,q,s Model (after Blatz and Graham 2003)

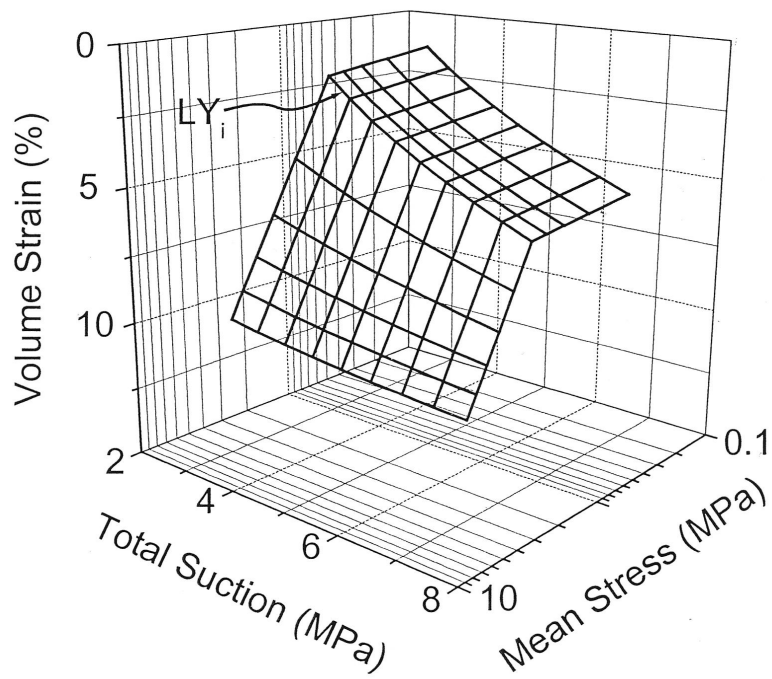


Figure 57: Three-dimensional Volume State Surface for Bentonite-Sand Buffer in p,s,V-Space (after Blatz and Graham 2003)

Due to long testing times, Blatz (2000) focused his program on specific features of the elastic-plastic modelling. Specifically, the shear portions of his tests were limited to isotropic loading and shearing with constant p (i.e. a vertical stress path upwards from the p - s plane). Anderson (2003) conducted additional tests that examined a higher suction range and other stress paths to further define the yield locus in p, q, s -space.

As mentioned earlier, Anderson (2003) examined suction induced yielding that was not conclusively observed in the suction range examined by Blatz (2000). Anderson tested BSB made with Wyoming and Saskatchewan bentonites to suctions greater than 120 MPa. For this range, suction induced yielding was observed at approximately 35 MPa suction. These results are shown on Figure 58 along with the projected line established by Blatz (2000). Testing at higher suctions allowed Anderson (2003) to extend the LY line established by Blatz (2000) as shown in Figure 59. Further, the additional stress paths examined by Anderson (2003) provided support to the shape of the yield loci in p, q -space that was established by earlier studies (Figure 60).

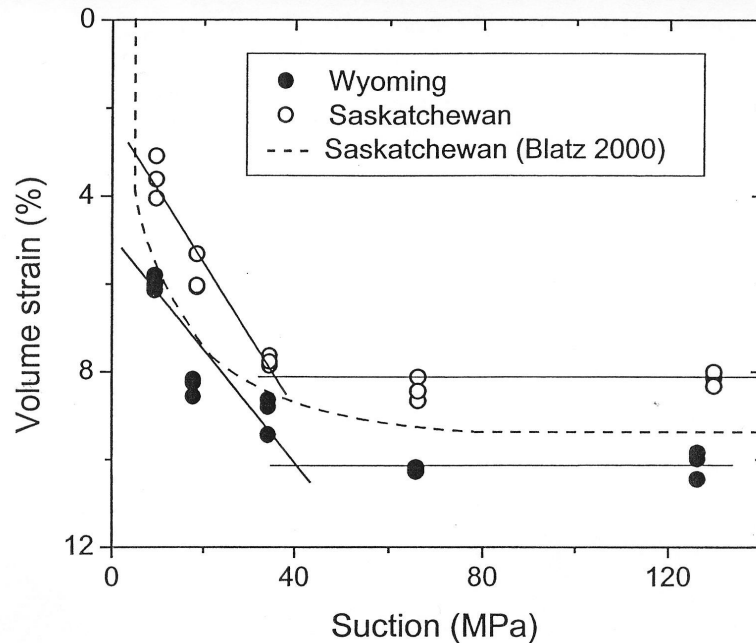


Figure 58: Shrinkage Curves Showing Suction Induced Yielding for Bentonite-Sand Buffer made with Wyoming and Saskatchewan Bentonite (after Anderson 2003)

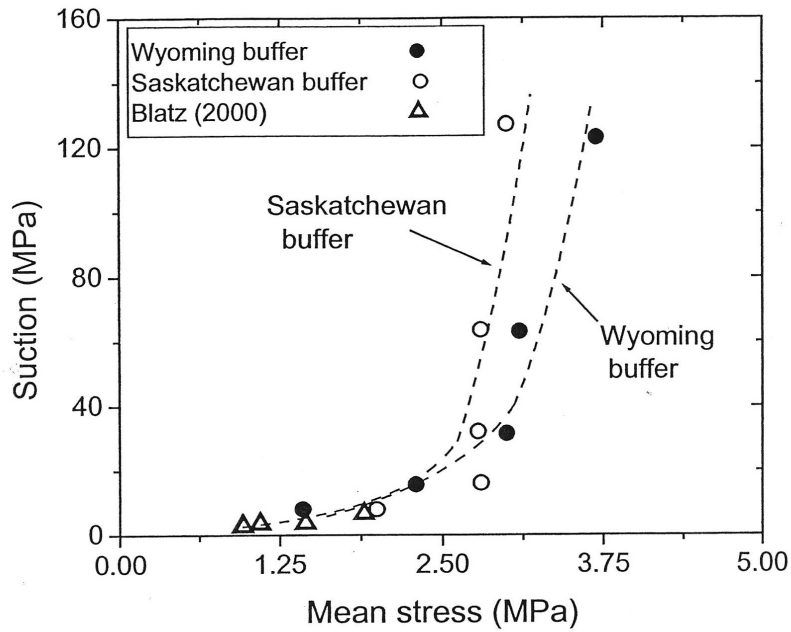


Figure 59: Load-Yield (LY) Lines for Bentonite-Sand Buffer made with Wyoming and Saskatchewan Bentonite (after Anderson 2003)

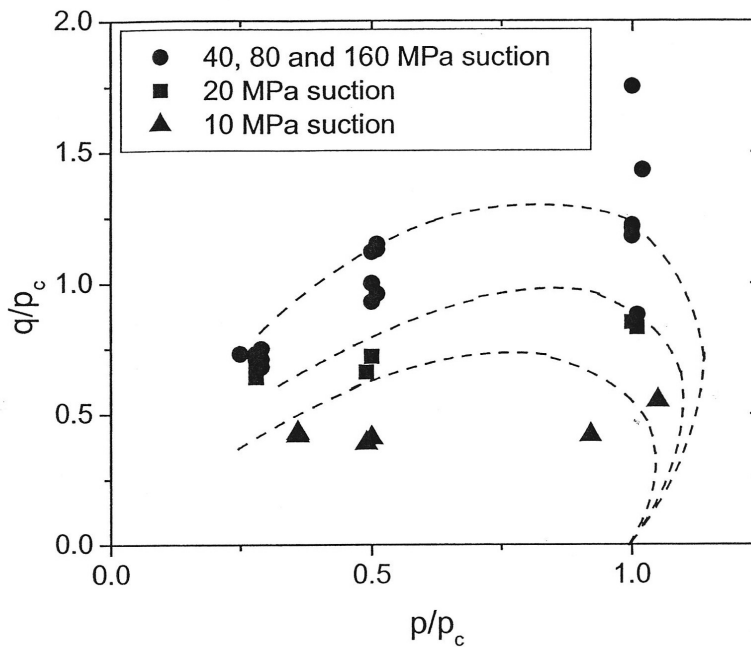


Figure 60: Normalized Peak Strengths for Bentonite-Sand Buffer made with Wyoming and Saskatchewan Bentonite, defining Yield Loci for Varying Suction (after Anderson 2003)

Siemens (2006) modified the triaxial equipments (Blatz and Graham 1999) to investigate the effect of the boundary conditions on the hydraulic-mechanical behaviour of unsaturated BSB during the infiltration process (i.e., wetting). His tests were unique compared to previous tests (i.e., drying process) and representative to the early stage (saturation process) in a Deep Geological Repository (DGR). The 50-mm-diameter and 100-mm-height BSB specimens were compacted at similar properties (i.e., 1.67 dry density and 19.4 gravimetric water content). The specimens are subjected to water uptake with various boundary conditions: constant mean stress-drained, constant mean stress-undrained, constant volume, constant stiffness of $X=25\%$ and 75% , where X was the linear slope of total mean stress and volume strain. Four levels of total isotropic mean stress were considered including 0.25, 0.50, 1.0, and 1.5 MPa. Volumes of water uptake, suction, radial and vertical displacements were measured during the tests. The radial distributions of gravimetric water content (w) and dry density (ρ_{dry}) were measured at the end of each test showing variation of w and ρ_{dry} along the radial and vertical direction. At the end of most tests, w at the perimeter was greater than that at the centre, and ρ_{dry} at the perimeter was less than that at the centre. These measurements allowed determination of both hydraulic and mechanical constitutive relationship during tests, including: matric suction (s) versus gravimetric water content (w) and the p - s - V relationship.

Figure 61 shows plots of the p - w - V relationship of the infiltration tests by Siemens (2006). Despite the various boundary conditions applied during tests, the unique p, q, V relationship at the end of test can be defined (shown as a solid line with the "Fitted Limit" label in Figure 61). Siemens (2006) also showed that this "Fitted Limit" line was analogous to the EMDD-swelling pressure relationships (e.g., Dixon 2002).

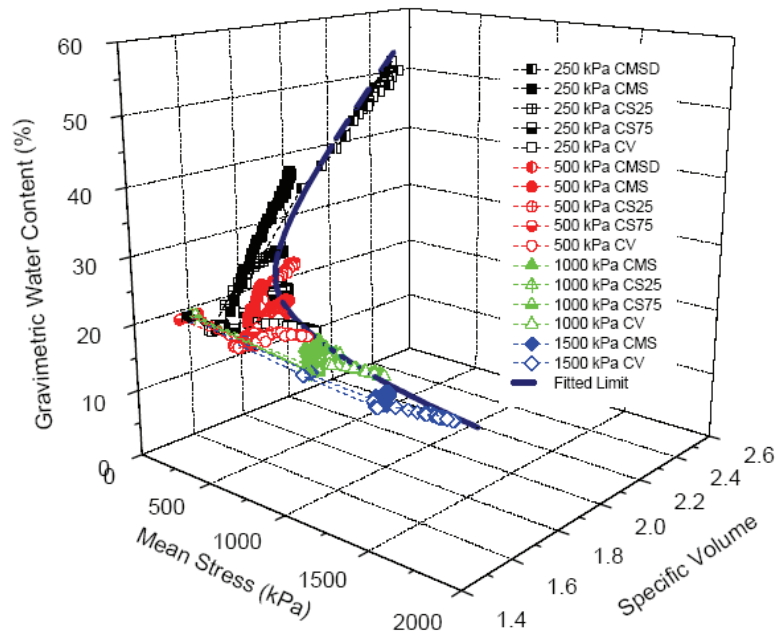


Figure 61: Results of Infiltration Test on Compacted Bentonite-Sand-Buffer on p, w, V -Space (after Siemens 2006)

Priyanto (2007) provides a summary of BGM Parameters used to model the behaviour of AECL's Tunnel Sealing Experiment (TSX). It should be noted that the parameters presented by Priyanto (2007) were obtained from the same sources presented here, and were then converted to appropriate stress state variables utilized by the FLAC modeling software. The parameters were interpreted from the experimental programs of Graham et al. (1997), Blatz (2000), Anderson (2003), Blatz and Graham (2003) and Siemens (2006), but only part of the data were considered. Priyanto (2007) also identified the limitations of the existing constitutive models (e.g., BBM and BGM). Further back-analyses using all laboratory test data for BSB (e.g., Graham et al. 1997; Blatz 2000; Anderson 2003; Blatz and Graham 2003; Siemens 2006) may result in different values of parameters or even lead to the modification of the existing constitutive models. An algorithm, called the "Parameter Estimation Method" (Priyanto 2007) can be used as an alternative to refine these parameters.

4.2.6 Swelling Behaviour

The swelling properties of BSB have been extensively investigated (Dixon 2000; Dixon et al. 2002). These studies led to the development of normalizing parameters such as ECDD and EMDD, which allows for materials of various proportioning to be described and their behaviour predicted. Swelling pressure can be inferred from the testing conducted on bentonite over a range of EMDD (Sections 4.2 and 4.4.6).

4.3 MECHANICAL PROPERTIES OF LIGHT BACKFILL

LBF has the same composition as BSB (i.e. 50% bentonite and 50% sand by mass). The difference between the two materials is that LBF is not compacted to as high a density as BSB. LBF will be installed in areas of a repository where the specified compacted density of BSB will be difficult to achieve. Maximum practical compaction effort will be applied to LBF, but slightly lower densities than BSB are anticipated. The target EMDD for LBF is 660 kg/m³, whereas the target EMDD for BSB is 1,150 kg/m³. The target dry density for LBF is 1,240 kg/m³ with a water content of 15%. This corresponds to an initial saturation of 33% for as-placed LBF.

The evaluation of mechanical properties of LBF within an elastic-plastic framework is currently the subject of ongoing laboratory testing. To date, triaxial tests have been conducted on LBF specimens made with fresh water as the pore fluid (Blatz et al. 2008). The matrix of triaxial tests performed to date on LBF made with fresh water is provided in Table 7. This testing was conducted at the University of Manitoba (U of M) using the same high temperature and pressure triaxial cells (HITEP cells) that were constructed for the testing of BSB. The same testing matrix is being repeated on LBF made with saline pore fluid (227 g/L CaCl₂). This testing program is currently in progress at the Royal Military College of Canada (RMC) in Kingston, ON (Table 8) using two of the HITEP cells from the U of M.

Oedometer testing of LBF has been completed for a more extensive range of pore fluid chemical conditions (Baumgartner et al. 2008, Priyanto et al. 2008a, Priyanto et al. 2008b). This testing program has included work performed at Lakehead University and the RMC. Ongoing work is being performed at the RMC. Details are provided in the original reports and are summarized in Section 4.3.3 below.

Table 7: Matrix of Triaxial Tests Completed on Light Backfill made with Fresh Water as the Pore Fluid (after Blatz et al. 2008)

Type of Test	Isotropic Compression Level (kPa)		
	400	800	1,200
Undrained Tests	GS-LB06 GS-LB15	GS-LB09	GS-LB10 JB-LB17
Drained Tests	GS-LB11	GS-LB14	GS-LB12 JB-LB16

Table 8: Matrix of Triaxial Tests being Completed on Light Backfill with Saline Water (227 g/L CaCl₂) as the Pore Fluid

Type of Test	Isotropic Compression Level (kPa)		
	400	800	1,200
Undrained Tests	LBF_1004	TBI	TBI
Drained Tests	LBF_1008*	LBF_1006	LBF_1007*

Notes: TBI: To be initiated in 2009
* : on-going test

4.3.1 Strength Envelope

Table 9 provides a summary of strength parameters for LBF prepared with fresh water as the pore fluid. Strength parameters include the critical state strength envelope (M) and the corresponding friction angle at critical state (ϕ'_{cs}). The average M value for all of all tests is 0.51, which is close to the value obtained from the slope of the CSL (0.47) shown in Figure 62. The corresponding critical state friction angle is 13° . This value indicates that, as expected, the strength of the LBF is similar to that of BSB.

Since the LBF material displays marked strain softening, the peak strength envelope is also included in Figure 62 and in Table 9. The average peak M value is the same as for the critical state strength envelope with $M = 0.47$ and $\phi' = 13^\circ$. The cohesion in p',q -space is c'_{pq} 125 kPa. This value is equivalent to a Mohr-Coulomb cohesion value of $c' = 60$ kPa (Section 4.1).

Preliminary unpublished triaxial testing results on LBF made with saline pore fluid (227 g/L CaCl₂) and from a limited number of tests are included in Table 9. The results of the available tests are shown in p',q -space in Figure 63a, compared to the results for LBF made with fresh water. The specimens made with saline pore fluid were significantly stronger than the corresponding tests conducted at the same pressure with fresh water. For comparison, the undrained tests conducted at 400 kPa resulted in a peak strength of 347 kPa and $M = 0.66$

using fresh water as the pore fluid (GS-LB15); and a peak strength of 431 kPa and $M = 1.1$ using saline pore fluid (LBF_1004). Similarly, the drained tests conducted at 800 kPa resulted in a peak strength of 638 kPa and $M = 0.5$ using fresh water as the pore fluid (GS-LB14); and a peak strength of 1013 kPa and $M = 0.8$ using saline pore fluid (LBF_1006). This is consistent with diffuse double layer theory and the effective stress concept described in the following equation (Graham et al. 1992):

$$\{\sigma'\} = \{\sigma^*\} + \{R - A\}. \quad (55)$$

In this equation, effective stress σ' (left hand side of the equation), is held by two components in clay including: 1) actual physical contacts between particles σ^* and 2) the stress held by face to face repulsion of some of the clay particles represented by the $R-A$ term. Increases in pore fluid salinity result in a decrease in DDL thickness (Yong 1992, Mitchell 1993). This causes a shift from stresses that were previously carried by $R-A$ to now be carried by the soil skeleton σ^* . The specimen that now has more of the original effective stress σ' held by true interparticle contacts σ^* can be expected to have greater internal friction due to more interparticle contacts. This increase in interparticle contacts results in an increase in internal friction of the material and therefore a higher strength.

A number of researchers have reported relationships between ionic concentration and soil strength through triaxial testing (Barbour and Yang 1993; Di Maio and Fenelli 1994; Di Maio and Onorati 1999; Ho 1985; Hueckel 1997; Loret et al. 2001; Olson 1974; Man 2005). Similarly, increases in shear strength with increasing electrolyte concentration and valence have been attributed to decreases in the net long-range electrostatic repulsive stress due to decreased DDL thickness. In contrast, Tang (1999) observed a slight decrease in peak strength of BSB with increased salt concentration. The reason for this disagreement is unknown.

Differences in where the critical state lines plot in p',V -space are also noted between the fresh water and saline pore fluid cases (Figure 63b). The specimens prepared with saline pore fluid have significantly lower specific volumes than the specimens prepared with deionized water. This indicates that the saline specimen had a less open structure after isotropic consolidation and during shearing. Any reductions in DDL thickness are counteracted and taken up by the cell pressure, resulting in osmotic consolidation (Barbour and Yang 1993). This is consistent with the increase in strength with increased salinity

The shape of the peak strength envelopes for LBF, combined with the strain softening behaviour, suggests that an anisotropic elastic-plastic constitutive model can describe the material behaviour. As such, a complete analysis using an elastic-plastic framework is required.

Table 9: Strength Parameters for Light Backfill

Pore Fluid	Source	Critical State		Cohesion c'_{pq} (kPa)	Peak M	Cohesion (Mohr-Coulomb) c' (kPa)	Peak Friction Angle ϕ' (degrees)
		Critical State M_{cs}	Friction Angle ϕ'_{cs} (degrees)				
Fresh ¹	(Blatz et al. 2008)	0.47	13	125	0.47	60	13
Saline ² (227 g/L)	N/A	0.86	22	150	0.76	71	20

Note: ¹ – specimens made with distilled, deionized water.
² – unpublished preliminary values based on the results of two tests.

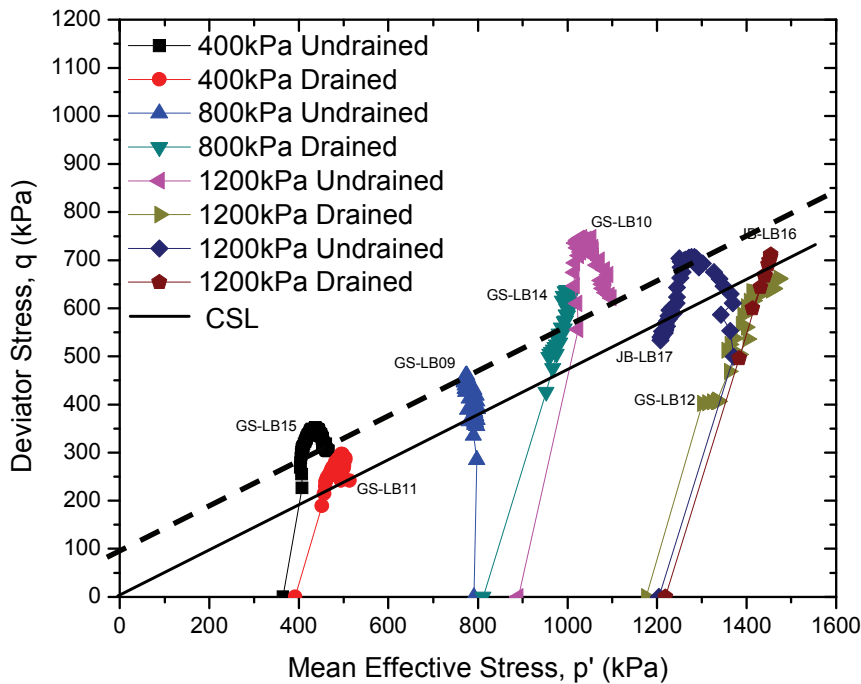


Figure 62: Critical State (Solid Line) and Peak (Dashed Line) Strength Envelopes for LBF made with Fresh (Distilled, Deionized) Water as the Pore Fluid (after Blatz et al. 2008)

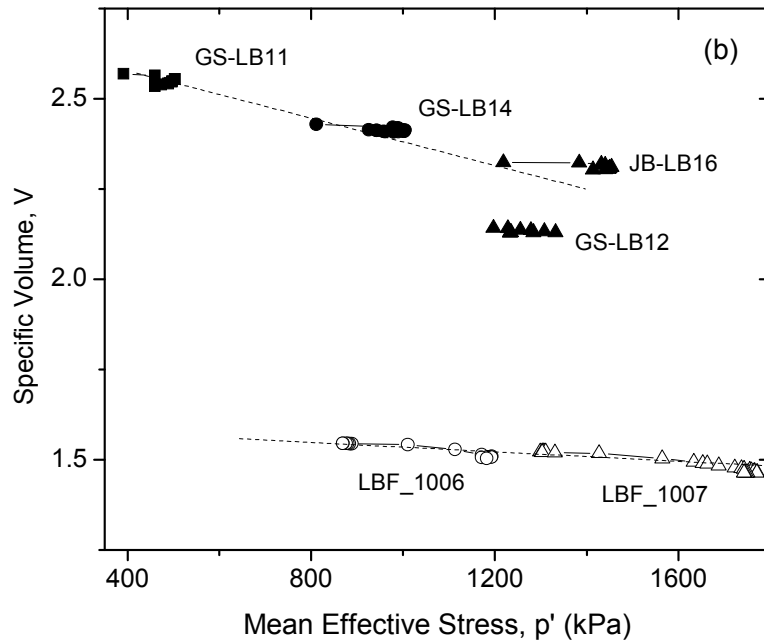
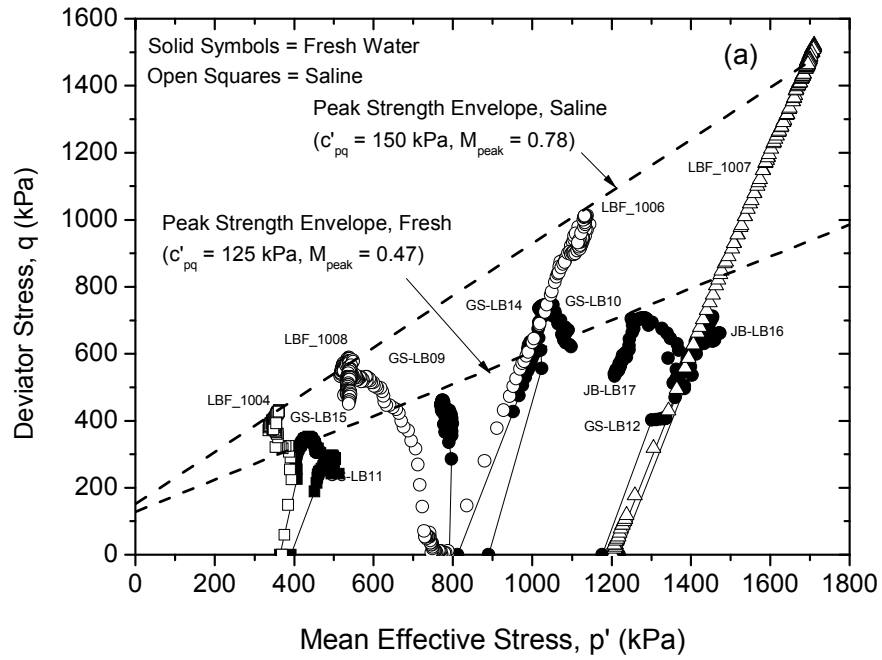


Figure 63: Strength Results for Light Backfill Made with Saline (227 g/L) Pore Fluid Compared to the Results for Light Backfill Made with Fresh Pore Water

4.3.2 Elastic Parameters

Blatz et al. (2008) indicated some inconsistencies in the elastic parameters determined on LBF prepared with fresh water. The data did not result in a reasonable Poisson's ratio, which was attributed to a low bulk modulus value. Preparation of this report allowed the re-evaluation of these parameters with comparison to the oedometer testing results. Synthesis of the oedometer and triaxial testing data provides a resolution to the noted inconsistencies and are explained below.

A review of the oedometer test data for LBF indicates that after initial compaction, this material behaves elastically for a very small range of low pressures. Plastic hardening appears to begin at vertical pressures greater than approximately 100 kPa to 200 kPa. Blatz et al. (2008) calculated the bulk modulus using combined end-of-consolidation data for several different specimens. Given that all of these triaxial specimens were consolidated to pressures larger than 200 kPa, this data is best used to calculate the hardening law rather than the elastic bulk modulus.

Instead of using end-of-consolidation data from multiple specimens, one specimen of LBF (GS-LB05) that was subjected to isotropic consolidation was used to determine the bulk modulus and the Cam Clay κ parameter (Figure 64). This specimen was initially loaded to 50 kPa, which according to the oedometer results, is in the elastic region. The next loading step for this specimen was 200 kPa, which may be close to the isotropic yield pressure (based on comparison with the oedometer results). Figure 64 yields a κ parameter of 0.004. Using the same portion of the curve indicates a bulk modulus (i.e. slope of the mean effective stress-volumetric strain curve) value of 61.6 MPa in the pressure range of 50 kPa to 200 kPa. It should be noted that a limited number of points are available in the elastic range. Further isotropic consolidation testing is required to confirm these values.

To check these values, the pre-yield oedometer test results (Baumgartner et al. 2008) for LBF made with fresh water were compared to the isotropic compression results. This was done by converting the vertical pressures used in the oedometer tests to a mean effective stress by assuming a K_o value of 0.8 (ratio of horizontal to vertical stress). This is somewhat arbitrary and may not necessarily apply (it is usually used for self-weight loads on cohesionless soil not clay materials) and is equivalent to a Poisson's ratio of 0.44. Baumgartner et al. (2008) reference the results obtained for an LBF specimen that was started at low pressures (i.e. 1 kPa to 57 kPa), thus reflecting the initial soil structure imparted by compaction. At this state the structure of the soil had not been changed by loading along the normal consolidation line and the resulting κ value was 0.006, which is consistent with the value determined by isotropic consolidation. Therefore using only pre-yield data from one-dimensional and hydrostatic consolidation tests the bulk modulus was 62 MPa. To better reflect the non-linear stress-strain response κ should be used and that this parameter is between 0.004 and 0.006.

Although oedometer tests provide the reload index (C_r) (or swelling index (C_s)), which is determined from the elastic portion of the curve, this information is presented in the following section for continuity of the oedometer test results. Further, the C_s values presented by Priyanto et al. (2008b) were determined after loading the specimens along the one-dimensional normal consolidation line (1D-NCL), which, due to changes in soil structure, may not be the same as the initial as-compacted conditions being presented in this section. As such this information is presented together in the following section (4.3.3).

The shear modulus can be determined from the results of the stress-strain curves for the CI \bar{U} tests (since $\epsilon_{axial} = \epsilon_{shear}$ when there is no volume change, as in a CI \bar{U} test). Using the results of Blatz et al. (2008), an average shear modulus value of 35.1 MPa was determined for LBF (Table 10).

Blatz et al. (2008) calculated Young's modulus, E for each CID test performed on LBF (Table 10). Since the specimens were all normally consolidated, the values should only be considered applicable to drained conditions and a narrow range of stresses around the specimen's consolidation pressure. Plastic deformation from consolidation and subsequent shearing (assuming anisotropic) will cause some stiffening and the values presented in Table 10 will therefore be higher than the initial, as-compacted state. Elastic theory equations were used to check the Young's modulus value, knowing the bulk modulus and the shear modulus. This calculation indicates that an approximate Young's modulus value for LBF is 88.7 MPa.

These elastic parameters appear larger than for BSB (Section 4.2.2). However, it must be remembered that the values presented for LBF are for a much lower and smaller range of pressures under which LBF behaves elastically.

According to elastic theory, Poisson's Ratio, ν can be determined if the bulk modulus, Young's modulus, and/or shear modulus are known. This also provides an opportunity to check the results and calculations. Using the bulk and shear modulus determined above, a Poisson's ratio of 0.26 was calculated for LBF made with fresh water.

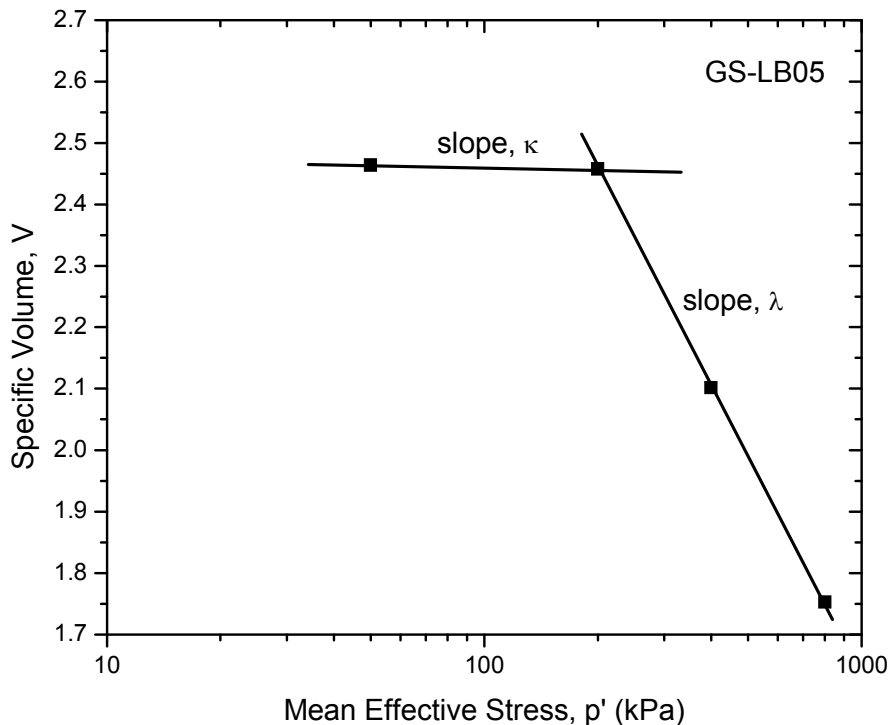


Figure 64: Light Backfill Specimen GS-LB05 (prepared with Fresh Water) used to Calculate Cam Clay Parameters κ and λ . Bulk Modulus was estimated from the same portion of the curve as κ (modified from Blatz et al. 2008)

Table 10: Deformation Parameters for Light Backfill made with Fresh Water as the Pore Fluid (after Blatz et al. 2008)

Specimen	Test Type	Bulk Modulus K (MPa)	Shear Modulus G (MPa)	Young's Modulus E (MPa)	Poisson's Ratio ν
GS-LB05	Isotropic consolidation	61.6	-	-	-
LBF Undrained Tests					
GS-LB15	CIŪ @ 400 kPa	-	37.7	-	-
GS-LB09	CIŪ @ 800 kPa	-	19.0	-	-
GS-LB10	CIŪ @ 1,200 kPa	-	40.3	-	-
JB-LB17	CIŪ @ 1,200 kPa	-	43.5	-	-
LBF Drained Tests					
GS-LB11	CID @ 400 kPa	-	-	120.3	-
GD-LB14	CID @ 800 kPa	-	-	145.8	-
GS-LB12	CID @ 1,200 kPa	-	-	175.0	-
JB-LB16	CID @ 1,200 kPa	-	-	182.4	-
Average:			35.1	155.9	
Calculated:				88.7[†]	0.26

Note: [†] – ν value calculated from elastic theory equations since results from CID tests on normally consolidated specimens are expected to be slightly high.

Bold – recommended values based on available information

It should be noted that the inconsistencies identified above required further investigation. Ongoing testing aimed at resolving these issues is being conducted.

4.3.3 Hardening Behaviour

The hardening law, also known as the Cam Clay λ parameter (obtained from the slope of the isotropic normal consolidation line), for LBF was calculated from data provided by Blatz et al. (2008). Two methods were utilized, including the results from an isotropic consolidation test on a single specimen (GS-LB05, shown in Figure 64) and from the end-of-consolidation data from a series of separate specimens (Figure 65). All of these specimens were prepared with fresh water as the pore fluid. Isotropic consolidation of specimen GS-LB05 provided a λ value of 0.5. The end-of-consolidation data was in general agreement, providing a range of λ values from 0.2 to 0.5.

As a check, the one-dimensional normal consolidation line (1D-NCL) from the oedometer test results (Baumgartner et al. 2008) for LBF made with fresh water was compared to the isotropic compression results. As above, this was done by converting the vertical pressures used in the oedometer tests to a mean effective stress by assuming a K_o value of 0.8 (ratio of horizontal to vertical stress). The resulting λ value is 0.3, which is generally consistent with the values determined by isotropic consolidation. This value is similar to that of BSB.

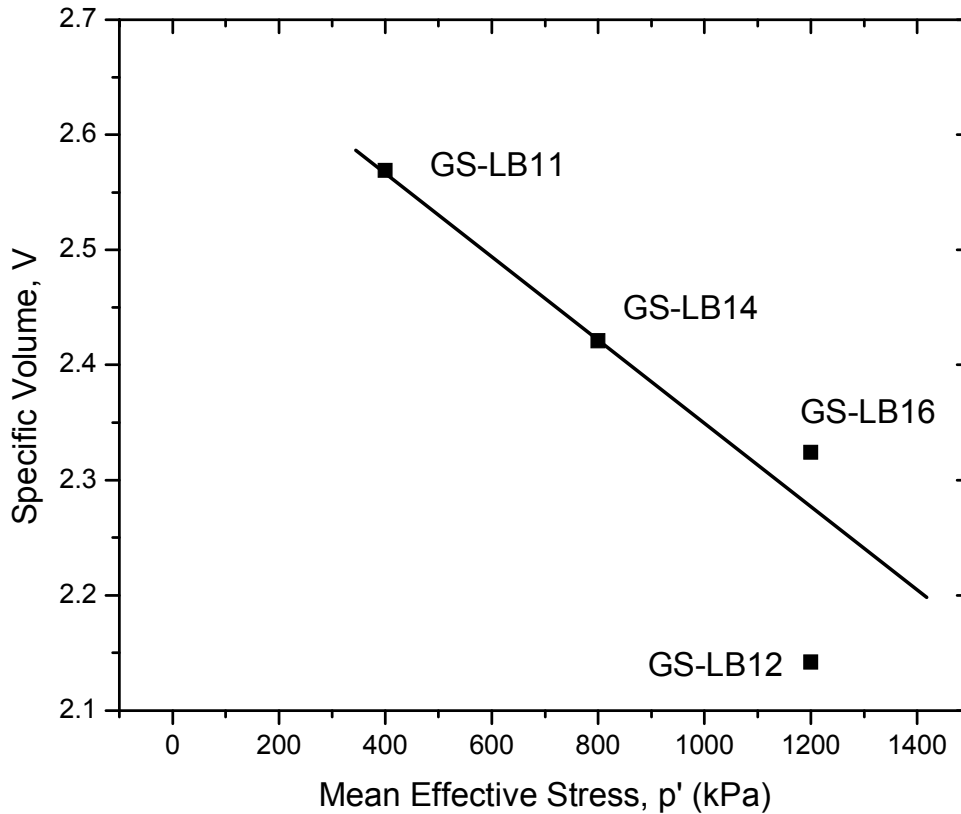


Figure 65: Isotropic Consolidation Data from Drained Tests on Light Backfill (prepared with Fresh Water) used for the determination of Cam Clay λ Parameter. Note: The plot was established by combining the end-of-consolidation data from the tests shown (from Blatz et al. 2008)

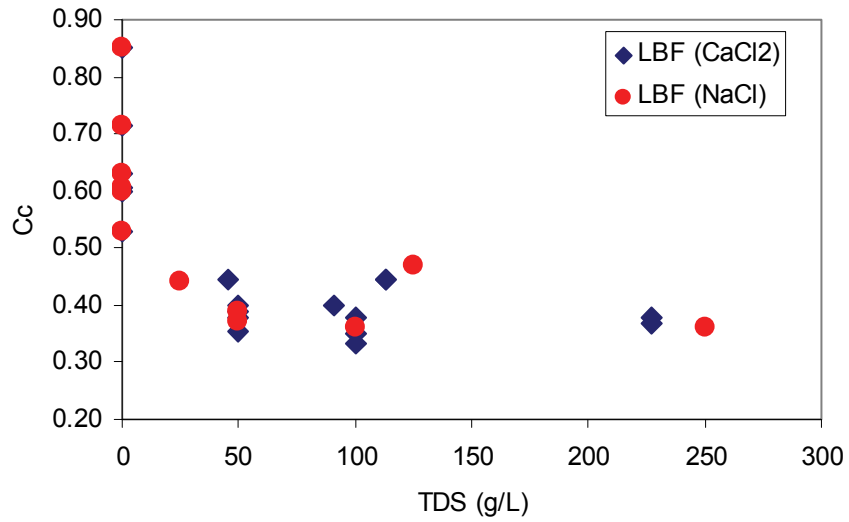
Baumgartner et al. (2008), Priyanto et al. (2008a), and Priyanto et al. (2008b) present the compression index (C_c) and the swelling index (C_s) for LBF, DBF and HCB under a range of pore fluid chemical conditions. Table 11 summarizes the C_c and C_s values for LBF. The compression and swelling indices decrease with increasing concentration of salts in the pore fluid. This is illustrated in Figure 66. The type of salt used in the experiment has little effect on the results; therefore the data can be plotted in terms of total dissolved solids (TDS) (Figure 67). A decrease in the compression index (C_c) indicates that the materials become stiffer and less compressible; while a decrease of the swelling index (C_s) indicates a reduction of the ability of the material to swell (Priyanto et al. 2008a).

The one-dimensional constrained moduli obtained from the loading portions of the oedometer tests are shown on Figure 68. Recall that these values are dependent on the stress level at any given point in a test. As such the data is presented in terms of EMDD for each material under each specific pore fluid condition. Priyanto et al. (2008b) provides tabulated values of these parameters for each load increment.

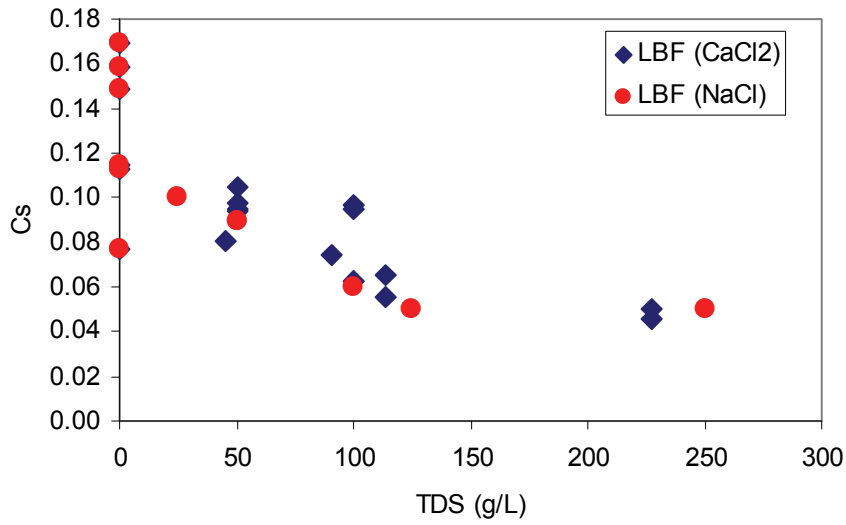
Table 11: Summary of Compression Index (C_c) and Swelling Index (C_s) for LBF under Various Pore Fluid Conditions (Priyanto et al. 2008b)

Pore Fluid Condition	C_c		C_s	
	mean	std.dev.	mean	std.dev.
Distilled, deionized water	0.638	0.112	0.130	0.035
91 g/L CaCl_2	0.423	0.032	0.077	0.005
100 g/L CaCl_2	0.367	0.025	0.097	0.004
200 g/L CaCl_2	0.380	- ¹	0.062	- ¹
227 g/L CaCl_2	0.409	0.043	0.054	0.008
50 g/L NaCl	0.415	0.035	0.095	0.007
100 g/L NaCl	0.365	0.007	0.075	0.021
250 g/L NaCl	0.415	0.078	0.050	0.000

Note: ¹ – value based on one test only.

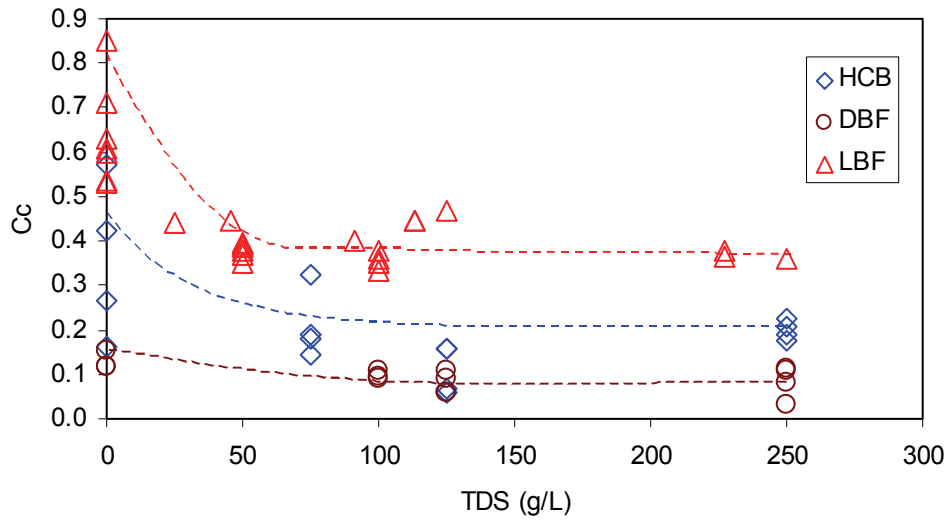


(a) Compression Index (C_c)

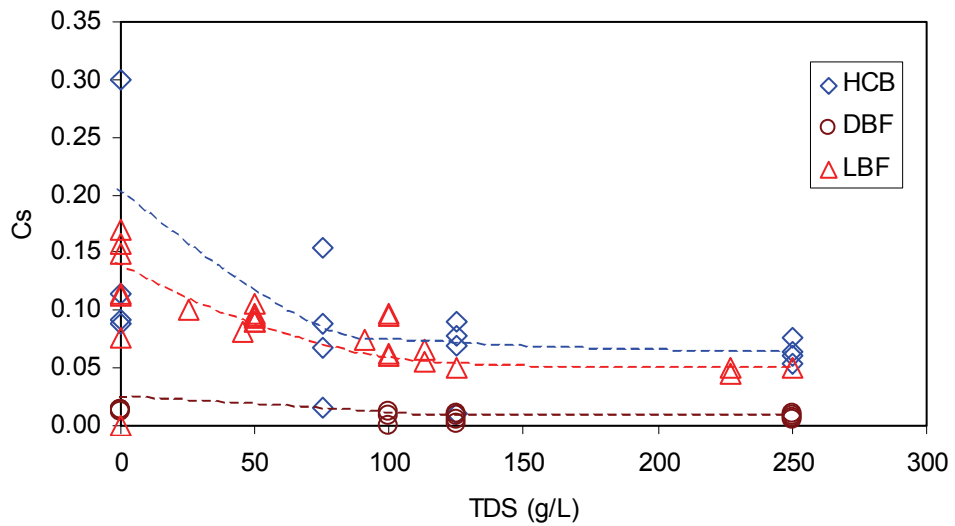


(b) Swelling Index (C_s)

Figure 66: The Effect of CaCl₂ and NaCl Solution to the Compression Index (C_c) and Swelling Index (C_s) of Light Backfill (after Priyanto et al. 2008b)



(a) Compression Index (C_c)



(b) Swelling Index (C_s)

Figure 67: Relationship of Compression Index (C_c) and Swelling Index (C_s) and TDS of Solution (after Priyanto et al. 2008b)

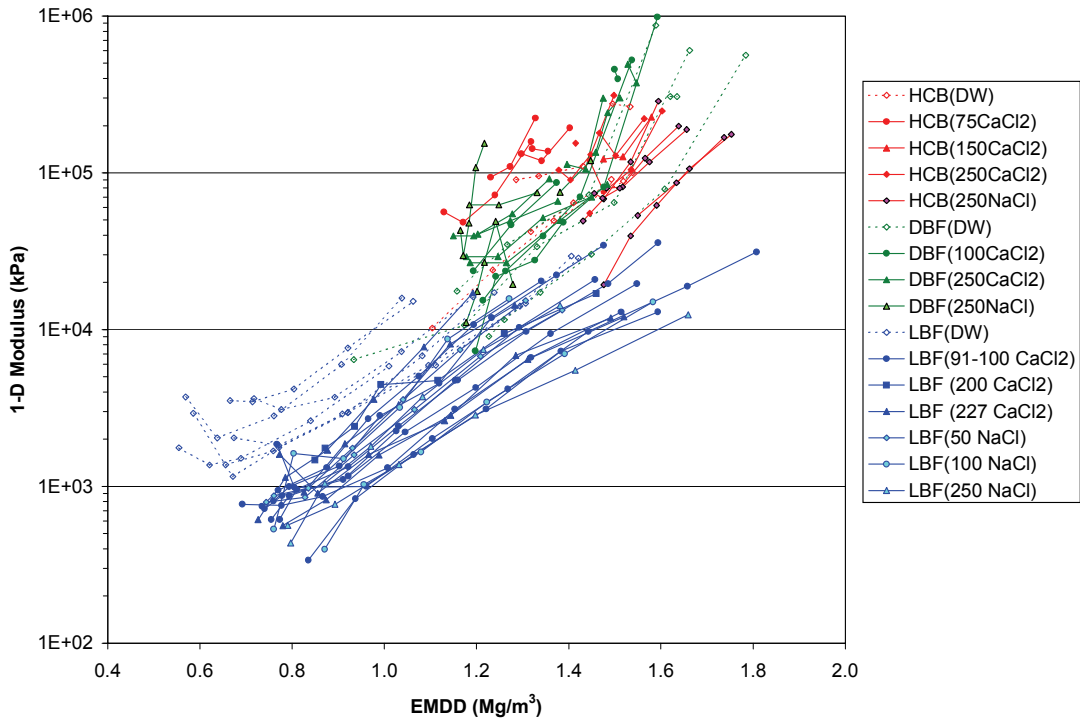


Figure 68: 1-D Constrained Moduli as a Function of Effective Montmorillonite Dry Density for Samples made with Fresh Water and Saline Water for the Loading Path (after Baumgartner et al. 2008; Priyanto et al. 2008b)

4.3.4 Yield Loci and Flow Rule

LBF in its as-placed state is a relatively soft material with a very limited domain of elasticity. As such, complete definition of the as-placed yield locus was difficult since the isotropic consolidation pressures of interest result in hardening of the material. Further, swelling would occur during unloading of a saturated specimen, thus potentially precluding the definition of an as-compacted yield locus for saturated conditions. Testing is being conducted on unsaturated specimens to define the as-compacted yield locus.

To address these issues, normalized yield points, with respect to the isotropic consolidation pressure (p'_c) were used to construct yield loci. Figure 69 shows the normalized yield loci for LBF, using unpublished data and data from Blatz et al. (2008). The shapes are similar to those presented by Oswell (1991), showing anisotropic behaviour of BSB. Using a similar normalization approach, Oswell (1991) showed that a single anisotropic yield locus could be used to describe yielding of high density ($\gamma_d = 1,670 \text{ kg/m}^3$) and low density ($\gamma_d = 1,500 \text{ kg/m}^3$) specimens of BSB.

The data for LBF indicates that the yield locus expands with increasing pore fluid salinity. This expansion of the elastic region is not the result of plastic deformation due to higher isotropic consolidation pressures. Instead, osmotically induced consolidation results in expansion of the yield locus.

The flow rule for LBF has not been investigated to date.

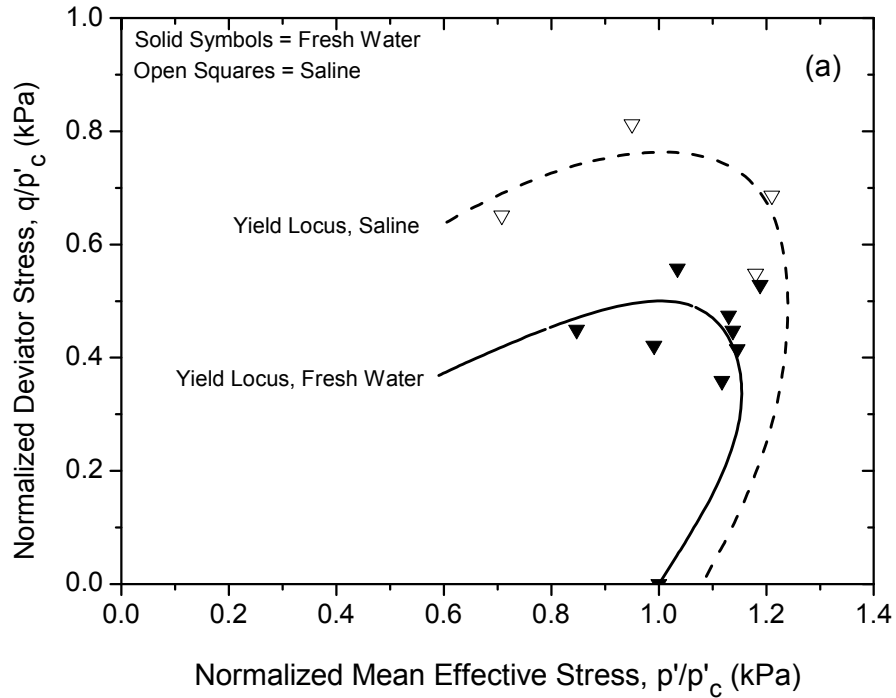


Figure 69: Normalized Yield Loci for LBF

4.3.5 Unsaturated Conditions

The properties of unsaturated LBF have not been investigated to date.

4.3.6 Swelling Behaviour

The swelling properties of LBF have not been specifically investigated to date. However, swelling pressure can be inferred from the testing conducted on bentonite over a range of EMDD (Section 4.4.6). Further testing is not required.

4.4 MECHANICAL PROPERTIES OF HIGHLY COMPACTED BENTONITE

The majority of testing for mechanical properties of HCB has been conducted using compacted blocks of 100% Wyoming bentonite supplied by the American Colloid Co. The commercial name for the material used in these tests is MX-80. The number 80 refers to the sieve size used in the material preparation. In Canada, MX-80 is being used to examine the one-dimensional mechanical behaviour of HCB (Baumgartner et al. 2008, Priyanto et al. 2008a, and Priyanto et al. 2008b), as well as in compliance tests between two different sealing materials. MX-80 is also considered the reference buffer material for the Swedish KBS-3 concept (Dueck 2004). As such, the primary focus of the following section will be on the properties of HCB

made with MX-80 bentonite. Where available, properties determined from tests conducted on HCB from other sources are provided for comparison.

4.4.1 Strength Envelope

Pusch (1983) presented the stress-strain-time properties of highly compacted MX-80 bentonite by applying a stress-controlled deviator stress to triaxial specimens for extended periods of time. The triaxial specimens were compacted and saturated with a synthetic groundwater containing 91 mg of cations and 215 mg of anions. The testing program indicated HCB displayed strain hardening behaviour with a maximum long-term shearing resistance of 2.5 MPa. This applies to a dry density of 1.9 Mg/m³ (EMDD = 1.74 Mg/m³). Pusch (1983) also presented creep curves up to and beyond 10⁵ seconds. Increasing heat from room temperature to 93°C resulted in a three- to six-fold increase in creep rates.

Further testing by Börgesson and Pusch (1987) indicated that the Mohr-Coulomb friction angle is in the order of 7° for consolidation pressures greater than 1 MPa and in the order of 13° for consolidation pressures less than 1 MPa.

The Japan Nuclear Cycle Development Institute (JNC) published mechanical properties of compacted Kunigel bentonite (JNC 2000a, JNC 2000b). The estimated EMDD for the tested material is 1.12 Mg/m³, based on a dry density of 1.60 Mg/m³, initial void ratio of 0.53 and an initial water content of 6%. Results of triaxial tests on this material indicated critical state M parameter of 0.58, which is equivalent to a critical state friction angle of 15°. Unconfined compressive strength varied from 5 MPa at a water content of 10% to 3 MPa at a water content of 18%. Tensile strength for the material is 0.56 MPa at a water content of 6.9%.

4.4.2 Elastic Parameters

Pusch (1983) presented Young's modulus values for saturated MX-80 HCB (i.e. water content = 16%). Specimens compacted to 1.9 Mg/m³ (EMDD = 1.74 Mg/m³) had Young's modulus values in the range of 31 to 46 MPa, with an average of 39 MPa. Specimens compacted to 2.0 Mg/m³ (EMDD = 1.85 Mg/m³) were significantly stiffer, having Young's modulus values in the range of 117 to 533 MPa, with an average of 340 MPa.

For comparison, HCB made from Kunigel bentonite (compacted to a dry density of 1.80 Mg/m³, EMDD = 1.34 Mg/m³) has a Young's modulus value of 500 MPa at a water content of 10% and 200 MPa at a water content of 18% (Cho et al. 2001).

Poisson's ratio for Kunigel bentonite was found to range from approximately 0.2 to 0.5 for dry densities in the range of 1.4 to 1.6 Mg/m³ (Takaji and Taniguchi 1999, Maeda et al. 1997). These values are generally consistent with those for sand-bentonite mixtures with values of 0.2 to 0.25 being applicable to unsaturated conditions and 0.5 being applicable to saturated conditions (Cho et al. 2001).

4.4.3 Hardening Behaviour

Baumgartner et al. (2008), Priyanto et al. (2008a), and Priyanto et al. (2008b) present the compression index (C_c) and the swelling index (C_s) for LBF, DBF and HCB under a range of

pore fluid chemical conditions. Table 12 summarizes the C_c and C_s values for HCB. The compression and swelling indices generally decrease with increasing concentration of salts in the pore fluid. This is illustrated in Figure 70. The type of salt used in the experiment has little effect on the results; therefore the data can be plotted in terms of total dissolved solids (TDS) (Figure 67 in Section 4.3.3). A decrease in the compression index (C_c) indicates that the materials become stiffer and less compressible; while a decrease of the swelling index (C_s) indicates a reduction of the ability of the material to swell (Priyanto et al. 2008a).

The values presented in Table 12 are consistent with the C_c and C_s values for HCB made with Kunigel bentonite. The JNC (2000a) presented a C_c value of 0.21 and a C_s value of 0.11 for HCB made with fresh water as the pore fluid.

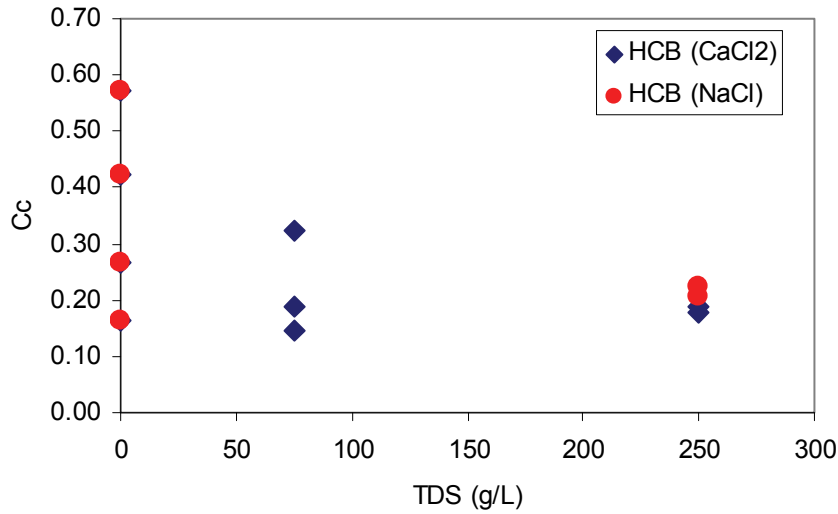
Marcial et al. 2002 separated the compression indices into low pressure (C_{c1}) and high-pressure ranges (C_{c2}) to reflect a significant decrease in these parameters at pressures greater than 2 MPa. The low pressure values of $C_{c1} = 5.22$ and $C_{s1} = 6.24$ were measured for the stress range of 0.001 MPa to 1 MPa and were higher than those presented in Table 12. This is likely due to differences in boundary conditions, where free swell results in significantly higher values. Higher pressures greater than 2 MPa yielded values of $C_{c2} = 0.42$ and $C_{s2} = 0.40$ which are in general agreement with those presented in Table 12, which include loads up to 3 MPa.

The 1-D constrained moduli obtained from the loading portions of the oedometer tests are shown on Figure 68 (in Section 4.3.3). Recall that these values are dependent on the stress level at any given point in a test. As such the data is presented in terms of EMDD for each material under each specific pore fluid condition. Priyanto et al. (2008b) provides tabulated values of these parameters for each load increment.

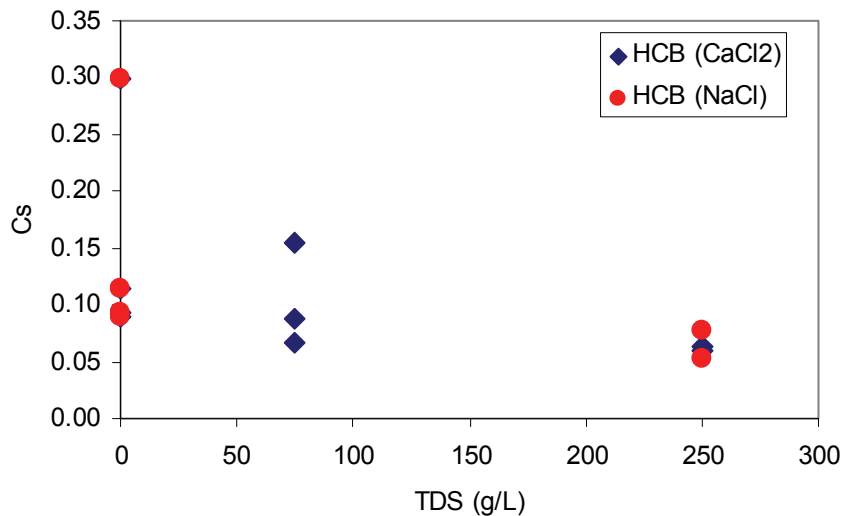
Table 12: Summary of Compression Index (C_c) and Swelling Index (C_s) for Highly Compacted Bentonite under Various Pore Fluid Conditions (Priyanto et al. 2008b)

Pore Fluid Condition	C_c		C_s	
	mean	std.dev.	mean	std.dev.
Distilled, deionized water	0.356	0.179	0.149	0.101
75 g/L CaCl_2	0.219	0.093	0.103	0.046
150 g/L CaCl_2	0.180	- ¹	0.016	- ¹
250 g/L CaCl_2	0.173	0.016	0.072	0.016
250 g/L NaCl	0.143	0.076	0.057	0.028

Note: ¹ – value based on one test only.



(a) Compression Index (C_c)



(b) Swelling Index (C_s)

Figure 70: The Effect of CaCl₂ and NaCl Solution to the Compression Index (C_c) and Swelling Index (C_s) of Highly Compacted Bentonite (after Priyanto et al. 2008b)

4.4.4 Yield Loci and Flow Rule

Although models exist for describing the elastic-plastic behaviour of bentonite, there is limited laboratory data available to calibrate the models. Further testing is required to define the yield locus for HCB. This will consist of an extensive triaxial testing program, similar to that conducted for BSB. Testing times will be lengthy due to the low hydraulic conductivity of the material.

4.4.5 Unsaturated Conditions

As mentioned above, mathematical models exist for describing the elastic-plastic behaviour of expansive clay including the BBM and BExM models (Alonso et al. 1987; Alonso et al. 1990; Gens and Alonso 1992; Alonso et al. 1999). However, there is limited laboratory data available to calibrate the models. This is especially true for behaviour of bentonites in p',q,s -space. (Experimental data for Boom clay pellets were used for comparison to the BExM predictions.) The majority of research on the mechanical behaviour of HCB has focused on its swelling behaviour. A testing program similar to that conducted on BSB to characterize its elastic-plastic behaviour is warranted for HCB.

The unconfined compressive strength (UCS) of HCB made with Kunigel bentonite has been characterized under unsaturated conditions for the Japanese and Korean programs (JNC 2000a,b, Cho et al. 2002). For a range of density conditions, the following relationships were established for UCS as a function of water content, w (Cho et al. 2002):

For dry density = 1.4 Mg/m^3 , EMDD = 0.93 Mg/m^3 :

$$\log \text{ UCS} = 5.38 \times 10^{-4} w^2 - 0.0454w + 0.3235 \quad (56)$$

For dry density = 1.6 Mg/m^3 , EMDD = 1.12 Mg/m^3 :

$$\log \text{ UCS} = -2.57 \times 10^{-4} w^2 - 0.0164w + 0.3185 \quad (57)$$

For dry density = 1.8 Mg/m^3 , EMDD = 1.34 Mg/m^3 :

$$\log \text{ UCS} = -0.0038w^2 - 0.0678w + 0.4742. \quad (58)$$

4.4.6 Swelling Behaviour

Figure 71 is a database (Dixon et al. 2002) of swelling pressures collected from the international literature and from AECL's tests on a range of North American bentonites, which is updated with recent results for MX-80 bentonite (SKI 2005; Hedin 2004). The swelling pressures generated by bentonite clays are dependent on their composition and dry densities and on the chemistry of infiltrating groundwater. The wide scatter in data is largely attributed to large variations in the $\text{Na}^+/\text{Ca}^{2+}$ cation ratios and inherent salt contents of the different-source bentonites, for which no compensation has been attempted. The swelling pressure is expressed as a function of EMDD to account for the variations in montmorillonite content of bentonites from different sources.

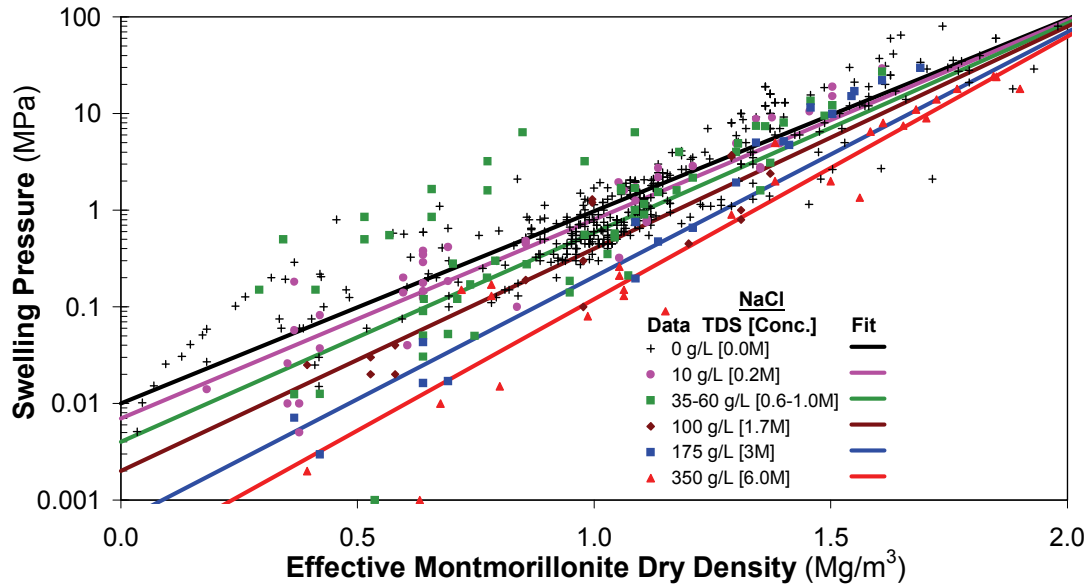


Figure 71: Swelling Pressure as a Function of Effective Montmorillonite Dry Density and Total Dissolved Solids (TDS) for Saturated Smectite-based Sealing Materials. Note: TDS is based on NaCl solutions (after Baumgartner 2006e)

The approximate swelling pressure (P_s) for a wide range of Na-bentonites in fresh water (i.e., deionized-distilled water added to natural bentonite), including the recent MX-80 bentonite data (SKI 2005) is:

$$P_s = 1 \times 10^{-2} e^{4.58EMDD} \quad (59a)$$

Increasing salinity decreases swelling pressure (Dixon et al. 2003, Dixon et al. 2002, Dixon 2000) as shown in Figure 71. Empirical exponential functions for differing salinities expressed as total dissolved solids (TDS) for NaCl solutions are as follows:

$$35\text{-}60 \text{ g/L} \quad P_s = 4 \times 10^{-3} e^{5.0EMDD} \quad (59b)$$

$$100 \text{ g/L} \quad P_s = 2 \times 10^{-3} e^{5.3EMDD} \quad (59c)$$

$$175 \text{ g/L} \quad P_s = 6 \times 10^{-4} e^{5.83EMDD} \quad (59d)$$

$$350 \text{ g/L} \quad P_s = 2.3 \times 10^{-4} e^{6.26EMDD} \quad (59e)$$

It is noted that the trends of Equations 59a-59e (Figure 77) are consistent with Swedish results for MX-80 bentonite (SKI 2005). These data and equations have been generated from a compilation of extensive literature information for Wyoming bentonite materials that have been and converted from dry density (ρ_d) to EMDD as shown in Figure 72.

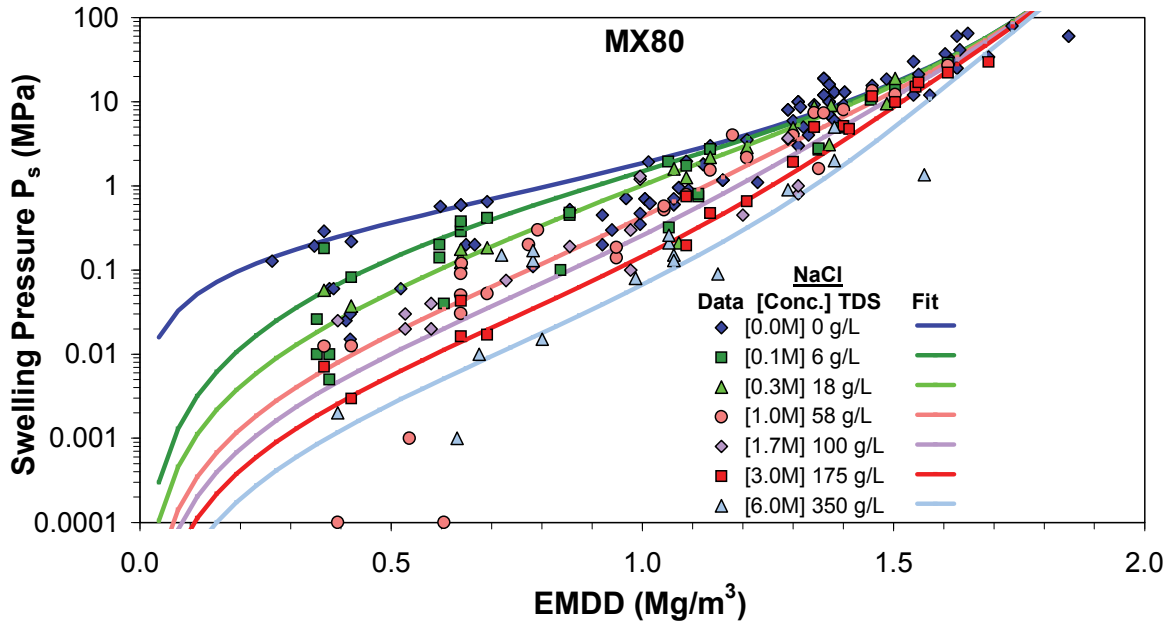


Figure 72: Swelling Pressure of MX-80 Bentonite as a Function of Effective Montmorillonite Dry Density and Total Dissolved Solids (TDS) (after SKI 2005; Hedin 2004). Note: Concentration and TDS are based on NaCl solutions

The fresh water swelling-pressure curve in Figure 72 (i.e., the blue curve labelled in the legend as [0.0M] 0 g/L) is derived from that in Hedin (2004), which has the following form:

$$P_s = AT \left\{ \exp \left[B \cdot G_s \frac{\rho_d}{(\rho_s - \rho_d)} \right] - 1 \right\} \quad (60)$$

where ρ_s = density of the solid particles (kg/m^3);
 T = absolute temperature (K);
 A = fitting parameter (e.g., 1.153×10^{-3} for MX-80); and
 B = fitting parameter (e.g., 0.896 for MX-80).

It should be noted that the A and B parameters will be unique for a given pore fluid composition. As a result of this uniqueness, there is a need to have sufficient data available to allow for prediction over a range of TDS conditions.

Substituting for dry density terms, where:

$$\rho_d = \rho_s \frac{(\rho_{\text{sat}} - \rho_w)}{(\rho_s - \rho_w)} \quad (61)$$

Substituting for EMDD terms (i.e., Equation 6 in Volume 1 (Baumgartner 2006e)), P_s becomes:

$$P_s = AT \left\{ \exp \left[B_{EMDD} \cdot G_s \frac{EMDD}{(\rho_s - EMDD)} \right] - 1 \right\} \quad (62)$$

where:

ρ_{sat} = saturated bentonite density (kg/m³);
 B_{EMDD} = fitting parameter (e.g., 1.189 for MX-80).

The role of salinity on swelling pressure (Hedin 2004) is expressed as follows:

$$P_s = \sqrt{(P_s^{fresh})^2 + (2RTC\alpha_d)} - 2RTC\alpha_d \quad (63)$$

where P_s = swelling pressure, which must be in kPa for Equation. 63;
 R = molar gas constant (J/(mol·K));
 T = absolute temperature (K);
 C = salt concentration (kmol/m³); and
 α_d = the tabulated degree of dissociation (unitless) for the external NaCl solution of concentration C (Hedin 2004) given approximately by:

$$\alpha_d \approx 10^{\frac{-0.34\sqrt{C}}{(1+1.83\sqrt{C})}} + 0.03C \quad (64)$$

The equations defining Figure 71 are for a broad range of Na-bentonite clays (i.e., Na/Ca ratios >1). The equations defining Figure 72 are for the high-quality MX-80 Na-bentonite (i.e., Na/Ca ratio ~1.8).

The results of the one-dimensional consolidation tests of the Highly Compacted Bentonite (HCB) support the above results, they show a loss of 2.5 MPa in its swelling pressure with an increase of concentration of calcium chloride (CaCl₂) solution from 0 g/L to 250 g/L (Priyanto et al. 2008a) (Figure 73).

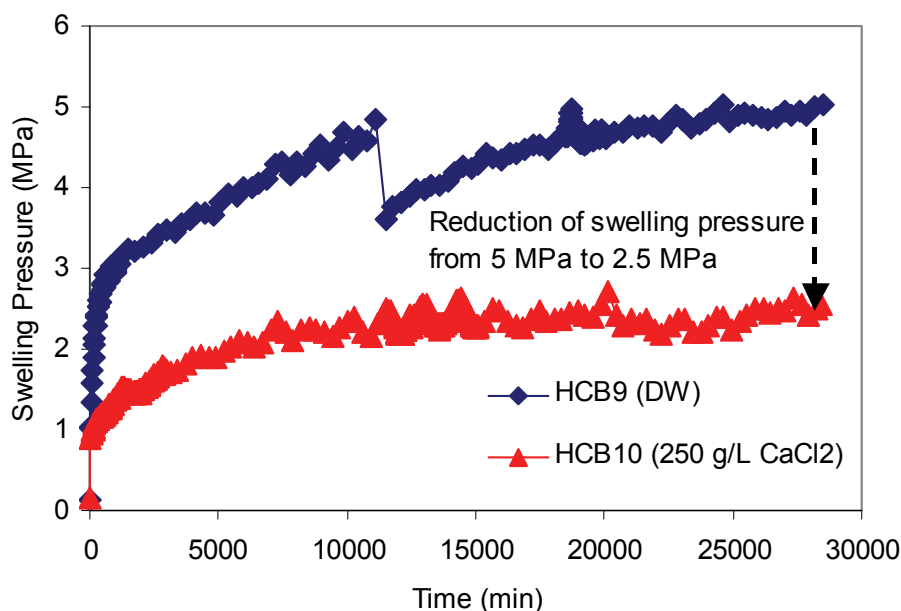


Figure 73: The Effect of CaCl₂ Concentration in Pore Liquid on the Swelling Pressure of Highly Compacted Bentonite (after Priyanto et al. 2008b)

4.5 MECHANICAL PROPERTIES OF GAP FILL

Testing for the mechanical properties and behaviour of GF is limited. Mechanical properties of GF can be inferred from the results of testing programs on HCB that has swelled to a similar EMDD as GF. Dixon et al. (2005) determined the correlation between the initial GF EMDD and the resulting average EMDD of the system upon swelling of the GF pellets. This relationship is shown in Figure 10.

This figure shows the range of averaged sealing system EMDDs for a range of HCB and GF EMDDs, assuming that the combined materials will ultimately equilibrate or homogenize after system saturation and swelling. The HCB component dominates the value of the equilibrated EMDD, but the addition of GF plays a role in minimizing the loss in HCB density.

4.5.1 Strength Envelope

Triaxial testing of GF as defined in by Russell and Simmons (2003) has not been conducted to date.

4.5.2 Elastic Parameters

Triaxial testing of GF as defined in by Russell and Simmons (2003) has not been conducted to date.

4.5.3 Hardening Behaviour

Triaxial testing of the GF defined by Russell and Simmons (2003) has not yet been undertaken, and its behaviour has been extrapolated from data produced for other materials. For example, hardening properties obtained from testing of HCB can be inferred for GF under the appropriate dry density or EMDD conditions. However, it should be noted that the evolution of GF throughout the life of a repository is complex and will influence its properties over time. Its behaviour is anticipated to change from that of an unsaturated granular material (as placed) through to a saturated but non-homogeneous material, to a saturated homogeneous material, and then undergo consolidation as the adjacent HCB swells and compresses it. Given its likely evolutionary path and as-placed condition, it is likely reasonable to expect that GF would never behave as an elastic material. This is based on the assumption that if the material swells before it is consolidated it would always be normally consolidated when saturated. Since it is 100% bentonite, C_c values for low density or low pressures obtained for HCB could potentially be applicable to GF but this should be confirmed through a limited number of scoping tests.

4.5.4 Yield Loci and Flow Rule

Triaxial testing of GF as defined in by Russell and Simmons (2003) has not been conducted to date.

4.5.5 Unsaturated Conditions

Hoffman et al. (2007) examined the hydro-mechanical behaviour of bentonite pellet mixtures within an unsaturated elastoplastic framework. The pellets were compacted to a dry density of 1.3 to 1.5 Mg/m³. The testing program was designed to provide information regarding the LC curve for the BBM model as shown in Figure 74 and Figure 75.

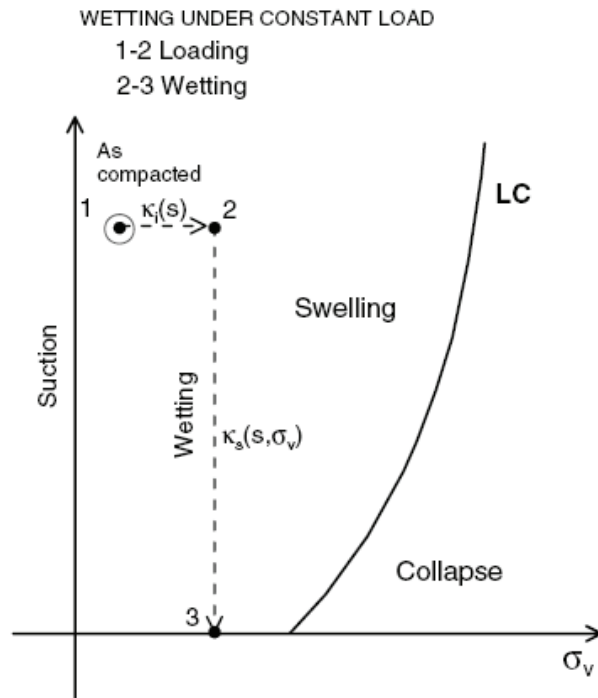


Figure 74: Stress Path Followed during Wetting of Gap fill at Constant Loading (after Hoffmann et al. 2007)

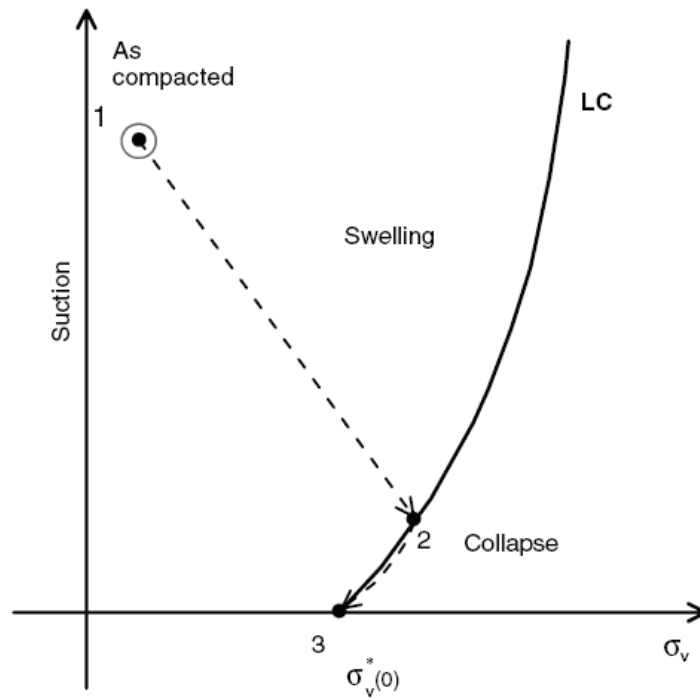


Figure 75: Stress Path Followed during Wetting of Gap fill at Constant Volume (after Hoffmann et al. 2007)

4.5.6 Swelling Behaviour

The swelling of GF has been investigated, as shown in Figure 76 to Figure 78. In an effort to assess what is needed to create conditions in the vicinity of the container that limit microbial activity, a series of tests examining microbial growth in bentonite materials have been completed. Initial testing found that limiting the water activity (a_w) to below 0.96 results in conditions that are not conducive to microbial growth. This corresponds to an EMDD of 1.4 Mg/m^3 (Dixon and Stroes-Gascoyne 2005). Since this EMDD value is higher than the specified value for GF, studies are being continued to better refine the limits of density on microbial activity and to assess what density the HCB-GF will evolve towards as saturation is achieved.

Kjartanson et al. (2005) presented the results of the free swell of a number of loosely placed bentonite materials saturated with distilled deionized water (DDW), 100 g/L NaCl or 100 g/L CaCl_2 . Maximum free swell ranged between 230% and 70% in DDW (Figure 82), between 100% and 8% in the 100 g/L NaCl solution, and 76% and 28% in 100 CaCl_2 solution (Figure 78). It was found that, in general, the free swell capacity of the bentonite materials in both NaCl or CaCl_2 solutions of 100 g/L concentration are in the same order of magnitude. Thus it is expected that bentonite products retain a reduced, but still positive, swelling capability when exposed to high salinity solutions even at relatively low emplaced density (Dixon et al. 2005). Swelling pressures measured by Kjartanson (2003) for a range of GF material in 100 g/L NaCl solution are provided in Figure 79.

Swelling pressures measured by Hoffmann et al. (2007) for GF made with MX-80 pellets saturated with 100 g/L NaCl solution are provided in Figure 80. The swelling strain depends linearly on the logarithm of the confining vertical stress. The set of results plotted in Figure 80 can be described by the following regression function:

$$\varepsilon_v = 0.094 \ln(\sigma_v) - 0.732 \rho_d + 0.416 \quad (65)$$

where ε_v is the volumetric deformation (negative means swelling), σ_v is the total confining vertical stress (kPa) and ρ_d is the dry density (Mg/m^3).

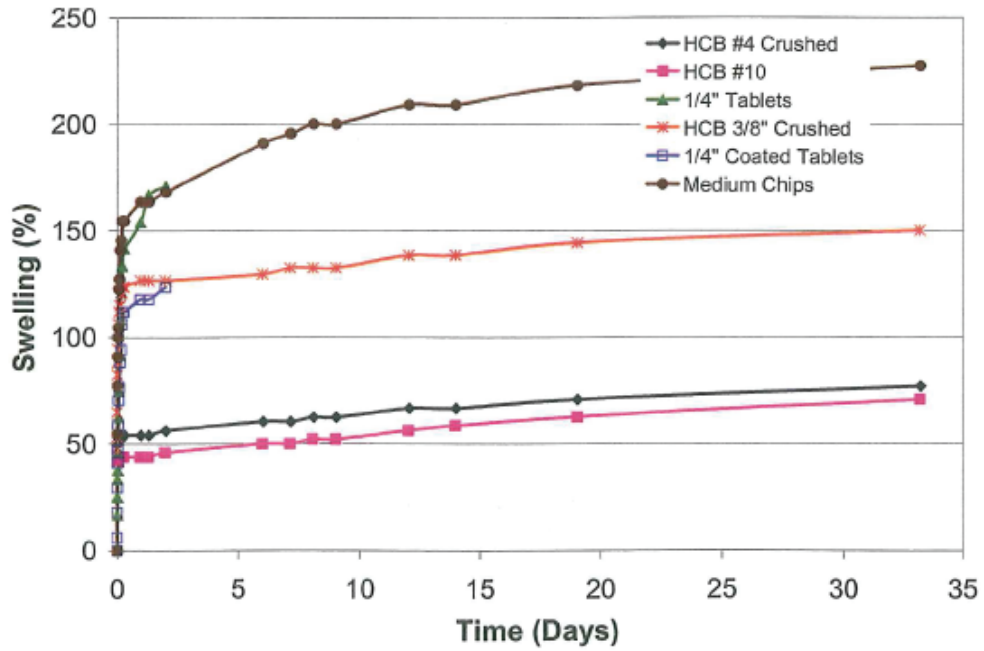


Figure 76: Pellet and Granule Free Swell Tests in Distilled Deionized Water (after Kjartanson et al. 2005)

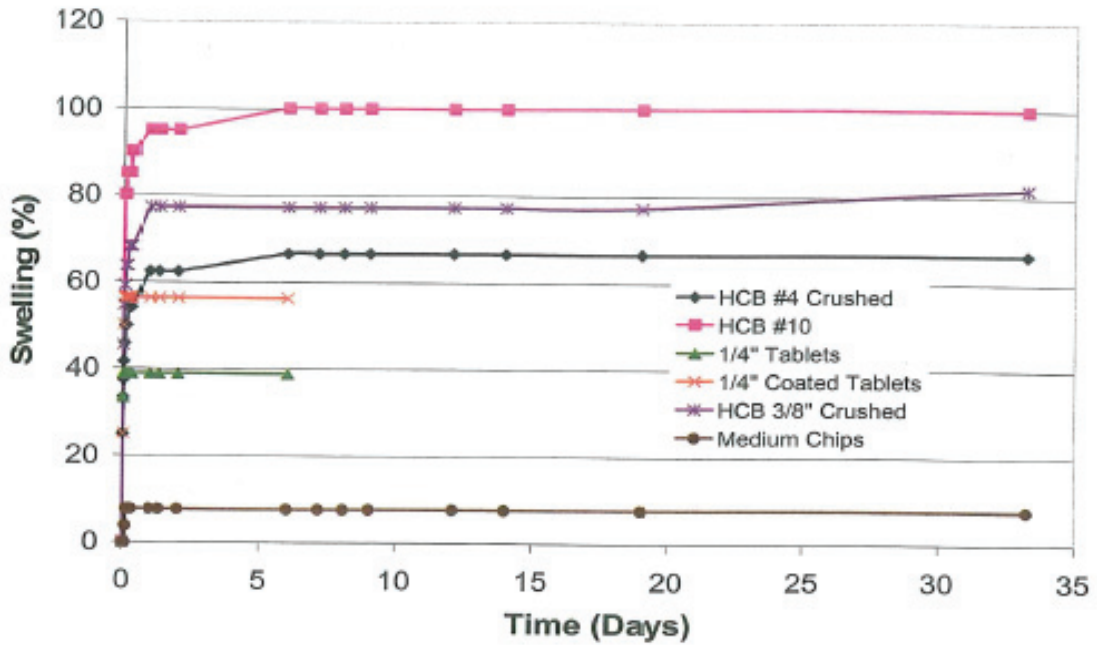


Figure 77: Pellet and Granule Free Swell Tests in 100 g/L NaCl Solution (after Kjartanson et al. 2005)

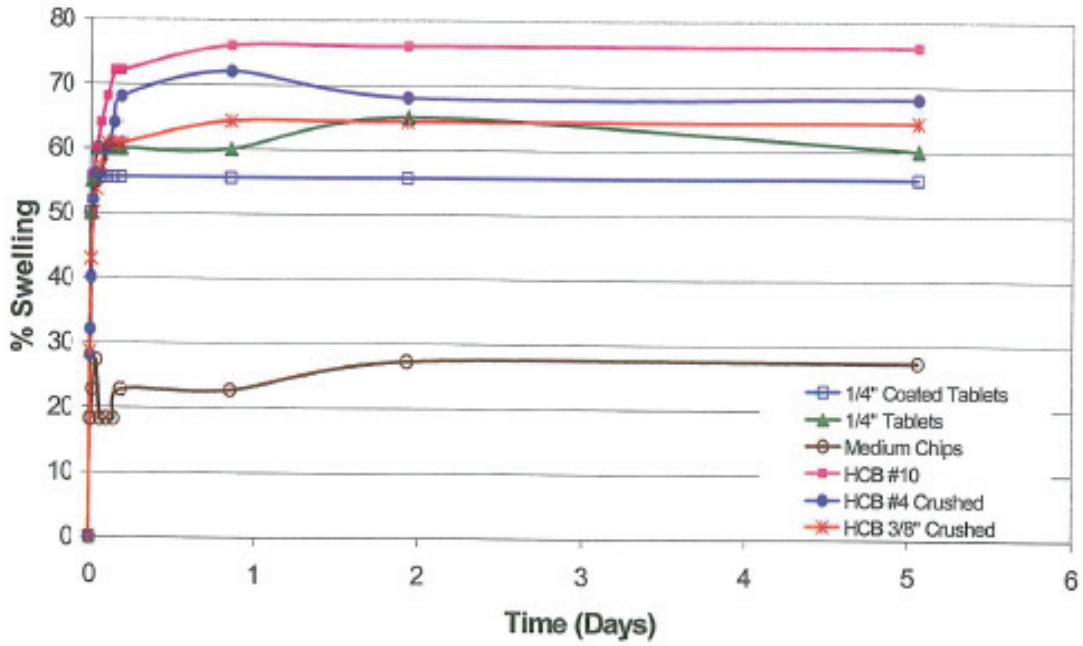


Figure 78: Pellet and Granule Free Swell Tests in 100 g/L CaCl₂ Solution (after Kjartanson et al. 2005)

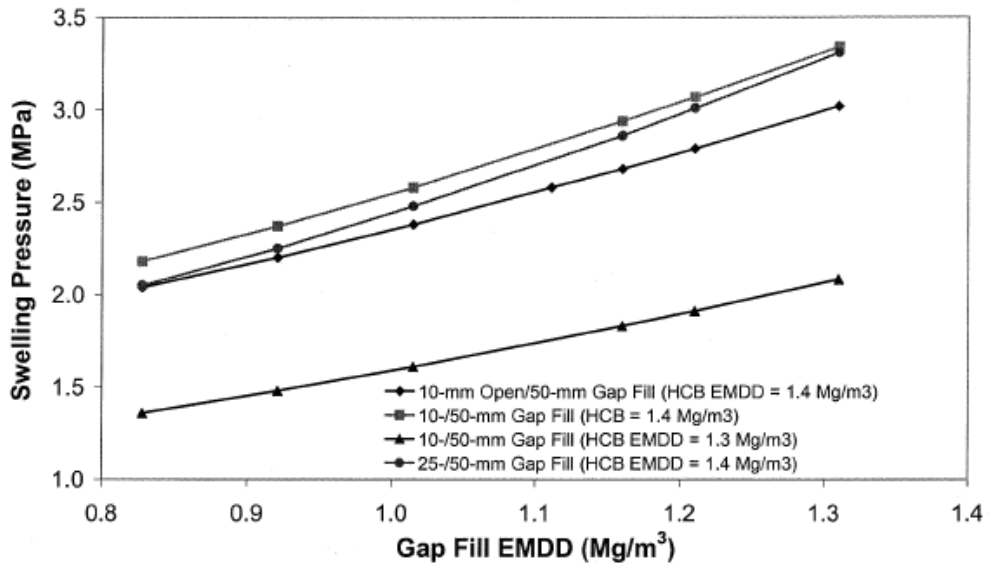


Figure 79: Swelling Pressure of Gap Fill in 100 g/L TDS Solution (after Kjartanson et al. 2003)

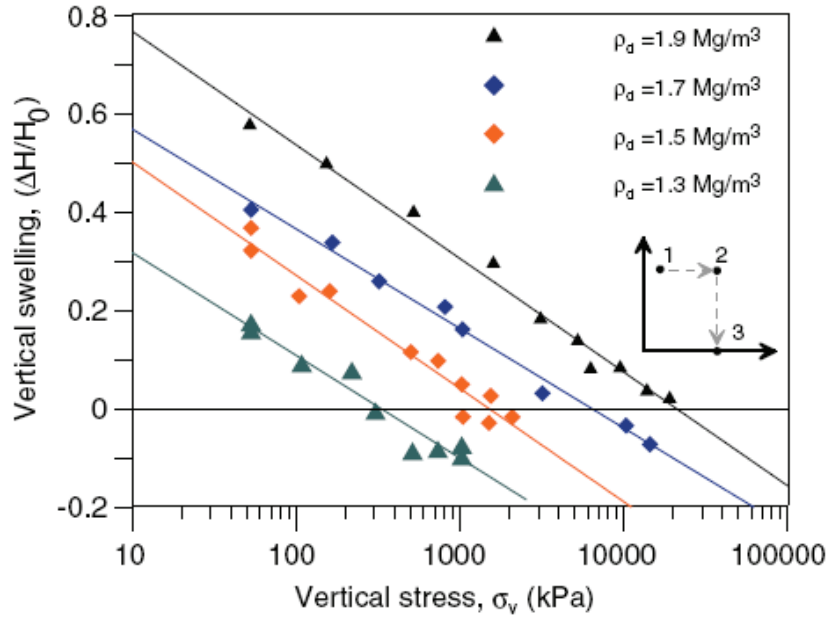


Figure 80: Swelling Strain versus Vertical Stress for Gap Fill for a Range of Dry Density (after Hoffmann et al. 2007)

Karnland et al. (2008) measured the swelling pressure of GF made with MX-80 pellets that were saturated with 0.2 mol/L NaCl solution (~11.7 g/L TDS). Figure 81 shows swelling pressure as a function of dry density for all samples tested. In this figure, squares show results from reference bentonite, diamonds show results from pelletized material, and triangles show results from the second series of pelletized material before (blue) and after heating (red). The results indicate that swelling pressure is primarily dependent on initial dry density and not on drying or compaction treatment.

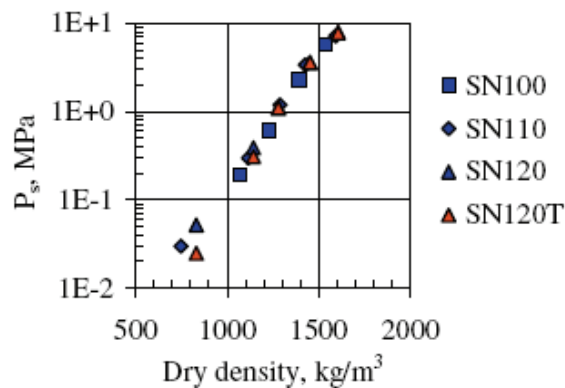


Figure 81: Swelling Pressure of Gap fill made with MX-80 Pellets Saturated with 0.2 mol/L NaCl Solution (after Karnland et al. 2008)

For comparison, the swelling pressure of pellet and powder mixture and compacted powder (FoCa) bentonite in large oedometer test cells was measured by infiltration tests (Imbert and Villar 2006). Figure 82 shows the final swelling pressure values obtained at the end of the infiltration tests are plotted as a function of the final dry density. The swelling pressure (P_s , MPa) and final dry density (ρ_d , g/cm^3) in Figure 82 are related by Equation 68.

$$P_s = 0.0061 \rho_d^{13.272} \quad (68)$$

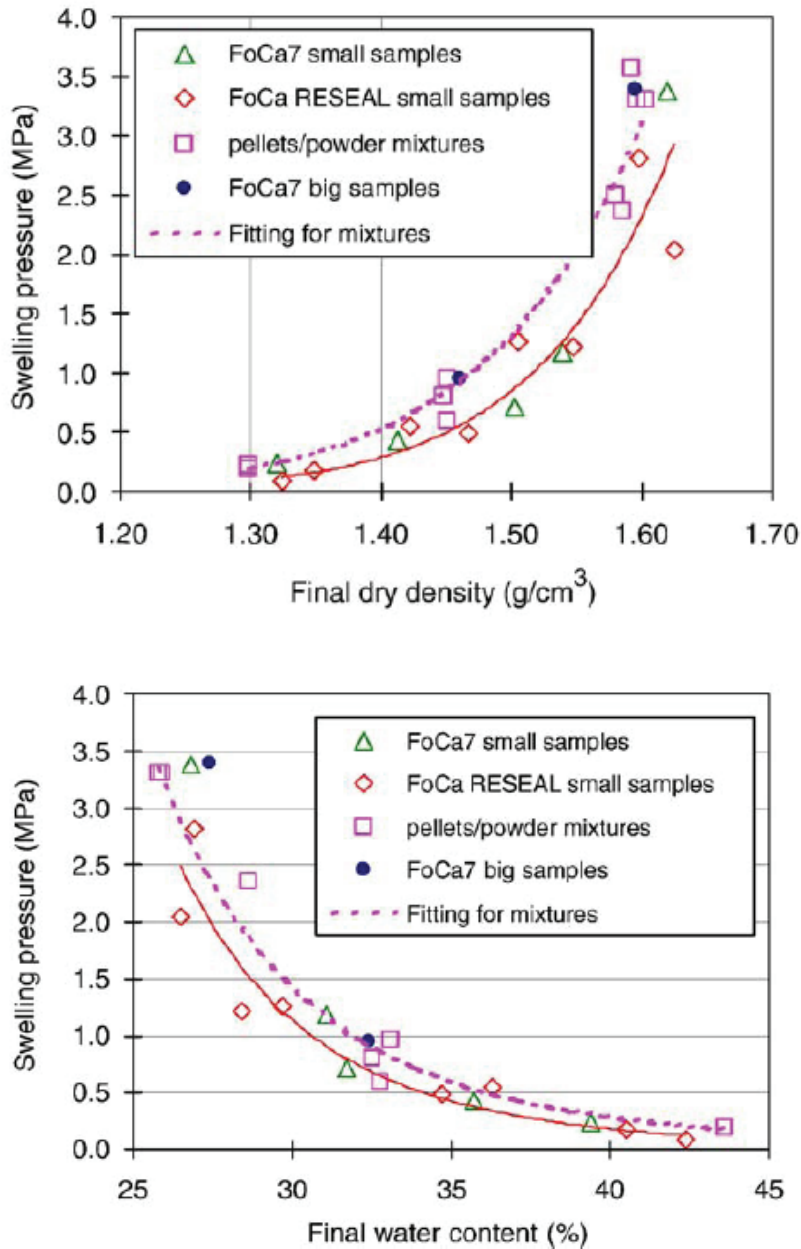


Figure 82: Swelling Pressure of Compacted FoCa Bentonite Powder and Powder/Pellet Mixtures (after Imbert and Villar 2006) (solid line shows relationship for FoCa samples)

4.6 MECHANICAL PROPERTIES OF DENSE BACKFILL

In 2006 and 2007, a number of triaxial tests were conducted on saturated DBF at the U of M (Blatz et al. 2008). The testing program only included specimens prepared with distilled, deionized water. The matrix of triaxial tests performed to date on DBF made with fresh water is provided in Table 13. This testing was conducted using the same high temperature and pressure triaxial cells (HITEP cells) that were constructed for the testing of BSB at the U of M.

The evaluation of mechanical properties of DBF within an elastic-plastic framework is currently the subject of ongoing laboratory testing. The same testing matrix will be repeated on DBF made with saline pore fluid (250 g/L CaCl₂).

Oedometer testing of DBF has been completed for a more extensive range of pore fluid chemical conditions (Baumgartner et al. 2008; Priyanto et al. 2008a; Priyanto et al. 2008b). This testing program is on-going at the U of M. Details are provided in the original reports and are summarized in Section 4.6.3 below.

Table 13: Matrix of Triaxial Tests on Dense Backfill Made With Fresh Water as the Pore Fluid (Blatz et al. 2008)

Type of Test	Isotropic Compression Level (kPa)		
	400	800	1,200
Undrained Tests	GS-DBF19	JB-DBF16	JB-DBF14 GS-DBF17
Drained Tests	GS-DBF15	GS-DBF18	GS-DBF12 GS-DBF13

4.6.1 Strength Envelope

Table 14 provides a summary of available strength parameters for DBF prepared with fresh water as the pore fluid. Strength parameters include the critical state strength envelope (M) and the corresponding friction angle at critical state (ϕ'_{cs}). The results indicate that the strength of DBF is not significantly affected by saline conditions relative to what was observed under fresh water conditions. This is expected due to the relatively low montmorillonite content and high density. The average M value for all tests is 1.12, which is close to the value obtained from the slope of the CSL ($M = 1.10$) shown in Figure 83. The corresponding critical state friction angle is 28° .

Table 14: Strength Parameters for Dense Backfill

Pore Fluid	Critical State	Critical State	Cohesion	Peak	Cohesion	Peak
	State	Friction	c'_{pq}	M	(Mohr-Coulomb)	Friction
	M_{cs}	Angle	(kPa)		c'	Angle
		(degrees)			(kPa)	(degrees)
		ϕ'_{cs}				ϕ'
Fresh & Saline (250 g/L)	1.10	28	100	1.10	48	28

Similarly, a peak strength envelope can be identified in p',q -space, as illustrated in Figure 83. The cohesion in p',q -space is $c'_{pq} = 100$ kPa, with the same slope as for the critical state strength envelope ($M = 1.10$). The corresponding Mohr-Coulomb peak strength parameters are $c' = 48$ kPa and $\phi' = 28^\circ$ (refer to Section 4.1 for conversion).

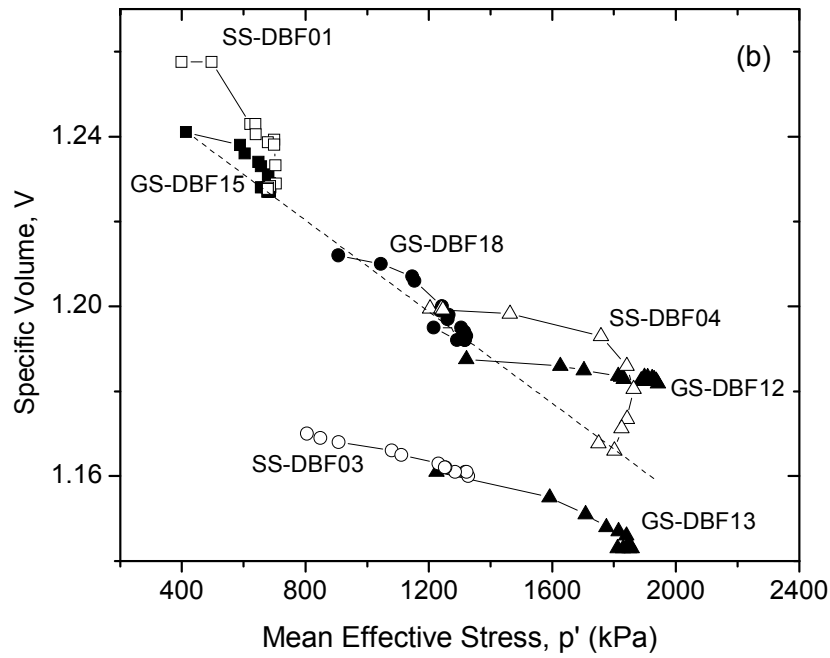
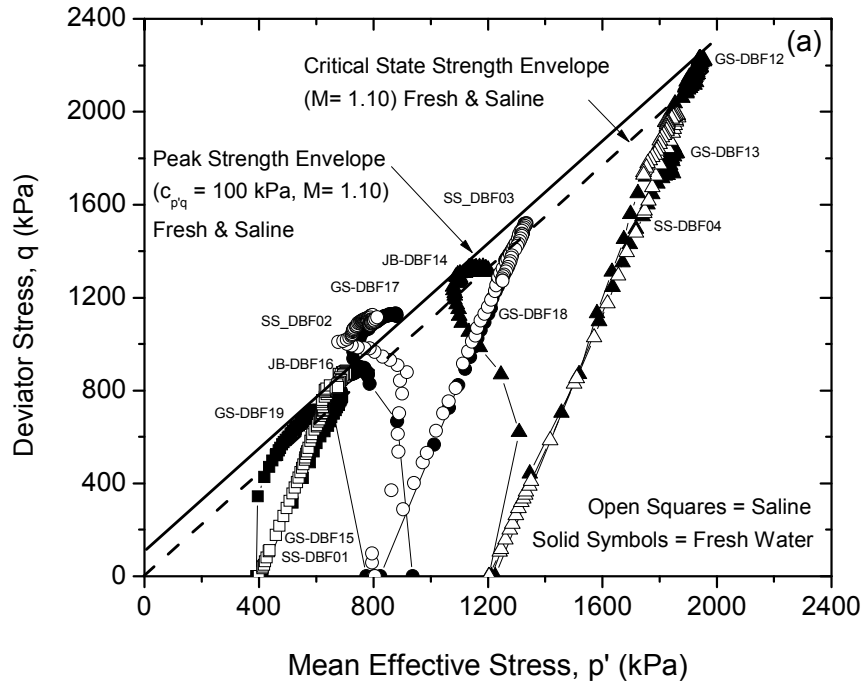


Figure 83: Critical State (Solid Line) and Peak (Dashed Line) Strength Envelopes for Dense Backfill made with Fresh (Distilled, Deionized) Water

4.6.2 Elastic Parameters

The testing conducted by Blatz et al. (2008) provided some preliminary elastic parameters for DBF made with fresh water as the pore fluid. The preliminary data are shown in Table 15. Further testing is required to confirm the appropriate values. Specifically, an isotropic consolidation test is required to confirm the bulk modulus and κ parameter. (The post-yield data from this test will be used to determine the λ parameter.)

Oedometer testing of DBF suggest that the isotropic preconsolidation pressure is in the order of 1 to 2 MPa. As such, the tests conducted at lower consolidation pressures in Table 15 are likely more representative of as-placed, saturated DBF.

Table 15: Preliminary Deformation Parameters for Dense Backfill (after Blatz et al. 2008)

Specimen ¹	Test Type	Bulk Modulus K (MPa)	Shear Modulus G (MPa)	Young's Modulus E (MPa)	Poisson's Ratio ν
DBF Undrained Tests					
GS-DBF19	CI \bar{U} @ 400 kPa	-	31.4	-	-
JB-DBF16	CI \bar{U} @ 800 kPa	-	- ²	-	-
GS-DBF17	CI \bar{U} @ 1,200 kPa	-	73.4	-	-
JB-DBF14	CI \bar{U} @ 1,200 kPa	-	67.9	-	-
DBF Drained Tests					
GS-DBF15	CID @ 400 kPa	-	-	124.7	-
GS-DBF18	CID @ 800 kPa	-	-	230.9	-
GS/JB-DBF13	CID @ 1,200 kPa	-	-	344.0	-
GS/JB-DBF12	CID @ 1,200 kPa	-	-	347.1	-
Average:		- ³	57.5	178 ⁵	- ⁴

Note: ¹ – specimens made with distilled, deionized water.

² – insufficient early time data.

³ – further isotropic consolidation testing required.

⁴ – to be confirmed upon further testing.

⁵ – for the stress range of 400 kPa to 800 kPa.

4.6.3 Hardening Behaviour

As mentioned above, further isotropic consolidation testing is required to confirm the hardening behaviour of DBF. Specifically, an isotropic consolidation test is required to pressures beyond the expected isotropic preconsolidation pressure of approximately 1 to 2 MPa, based on oedometer test results.

Blatz et al. (2008) presented some combined end-of-test consolidation test data for the drained tests (Figure 84). This preliminary data suggest a λ parameter value in the order of 0.13, based on the slope defined by the last two points. As a check, the 1D consolidation (oedometer) test

results were compared to this value by assuming a K_o value of 0.5. Data from DBF specimen DBF2(06), made with fresh water, suggest a λ value of 0.07. These numbers are in general agreement, but should be viewed as preliminary until further testing is completed.

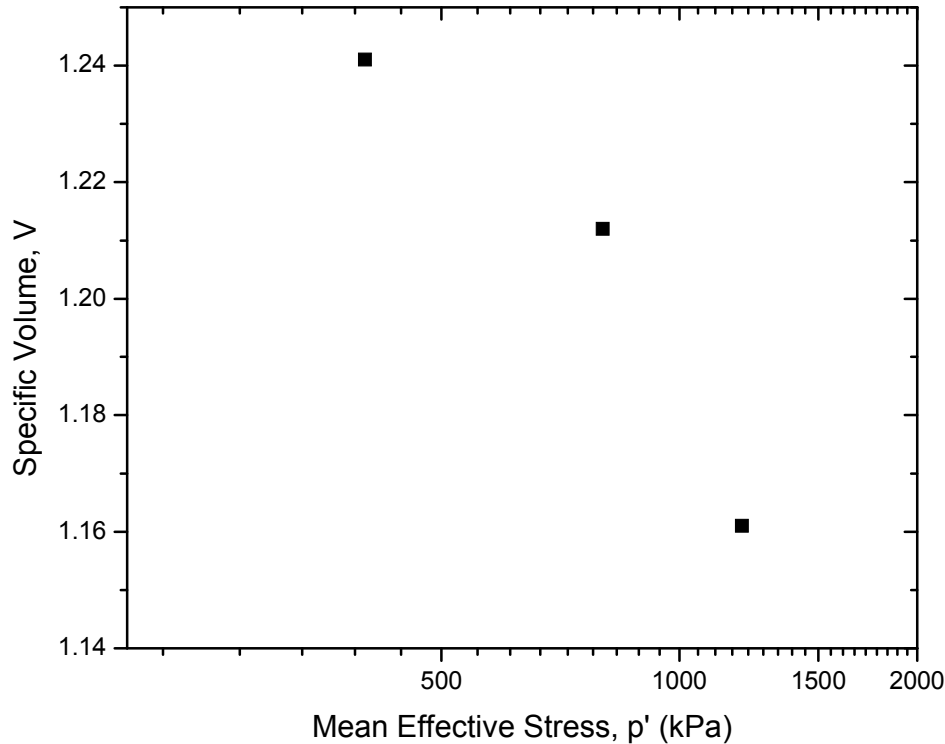


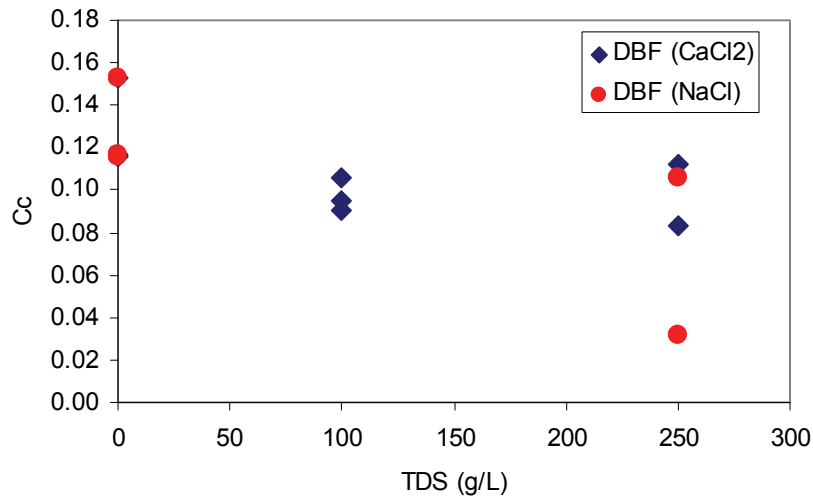
Figure 84: Combined End-of-Test Isotropic Consolidation Data for Dense Backfill (after Blatz et al. 2008)

Baumgartner et al. (2008), Priyanto et al. (2008a), and Priyanto et al. (2008b) present the compression index (C_c) and the swelling index (C_s) for LBF, DBF and HCB under a range of pore fluid chemical conditions. Table 16 summarizes the C_c and C_s values for DBF (which can be assumed to be equivalent to the Modified Cam-Clay parameters κ , λ if it is assumed that the vertical mean stress in an oedometer is the mean stress). The compression and swelling indices generally decrease with increasing concentration of salts in the pore fluid. This is illustrated in Figure 85. The type of salt used in the experiment has little effect on the results; therefore the data can be plotted in terms of total dissolved solids (TDS) (Figure 67 in Section 4.3.3). A decrease in the compression index (C_c) indicates that the materials become stiffer and less compressible; while a decrease of the swelling index (C_s) indicates a reduction of the ability of the material to swell (Priyanto et al. 2008a).

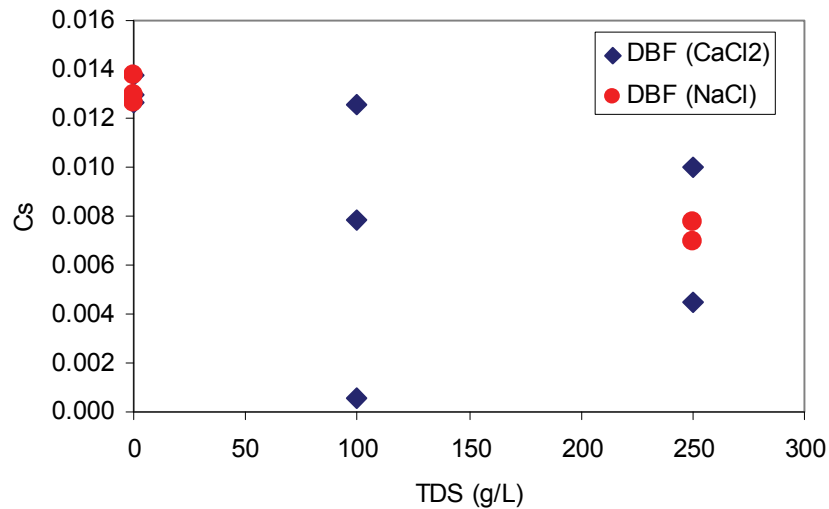
The coefficient of consolidation and 1-D constrained moduli obtained from the loading portions of the oedometer tests are shown on Figure 68 (in Section 4.3.3). Recall that these values are dependent on the stress level at any given point in a test. As such, the data is presented in terms of EMDD for each material under each specific pore fluid condition. Priyanto et al. (2008b) provides tabulated values of these parameters for each load increment.

Table 16: Summary of Compression Index (C_c) and Swelling Index (C_s) for Dense Backfill Under Various Pore Fluid Conditions (Priyanto et al. 2008b)

Pore Fluid Condition	C_c		C_s	
	mean	std.dev.	mean	std.dev.
Distilled, deionized water	0.128	0.021	0.013	0.001
100 g/L CaCl_2	0.097	0.008	0.007	0.006
250 g/L CaCl_2	0.099	0.014	0.007	0.003
250 g/L NaCl	0.064	0.031	0.006	0.003



(a) Compression Index (C_c)



(b) Swelling Index (C_s)

Figure 85: The Effect of CaCl_2 and NaCl Solution on (a) the Compression Index (C_c) and (b) Swelling Index (C_s) of Dense Backfill (after Priyanto et al. 2008b)

4.6.4 Yield Loci and Flow Rule

The estimated yield locus for as-compacted DBF is presented in Figure 86, using data from Blatz et al. (2008). Further testing is required to confirm the right-hand-side of the yield locus. The available results indicate that the yield locus for DBF is not sensitive to changes in pore fluid salinity.

The flow rule for DBF has not been specifically investigated to date.

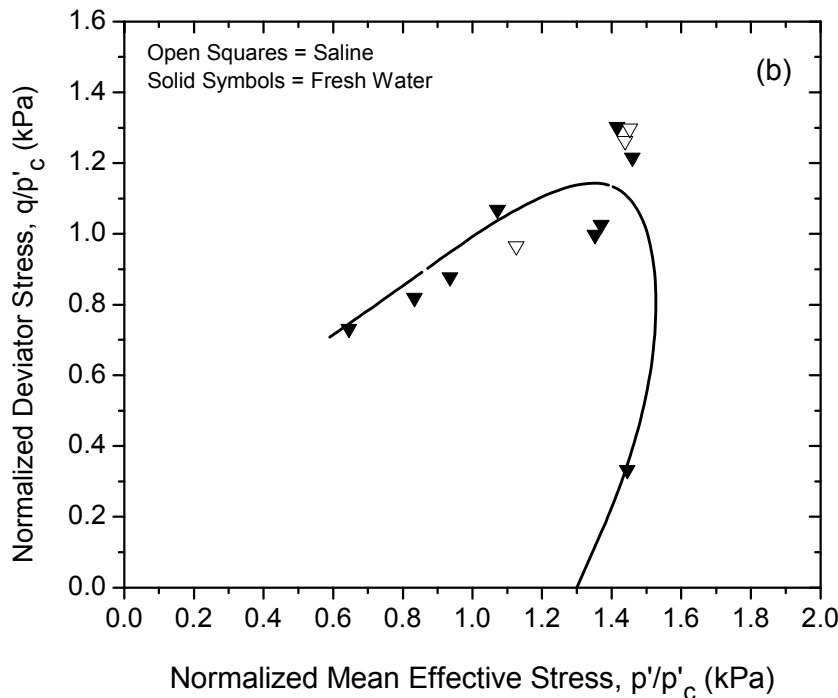


Figure 86: Normalized Yield Locus for DBF

4.6.5 Unsaturated Conditions

The properties of unsaturated DBF have not been investigated to date.

4.6.6 Swelling Behaviour

DBF is not required to develop a high swelling pressure in the reference design (Dixon et al. 2002). Its low swelling clay content (~10-15%) means that it has a very low EMDD, although it has a high dry density. Although the relationships developed between EMDD and swelling pressure development are not entirely clear at such low EMDD, use of the relationships shown in Figure 77 and Equation 61 provide a basis for estimating DBF behaviour. Eventually, a further series of tests to confirm the EMDD- P_s relationship will be needed to confirm that assumption.

4.7 MECHANICAL PROPERTIES OF LOW ALKALINITY CONCRETE

Low Heat High Performance Concrete (LHHPC) was designed as a low alkalinity concrete (LAC) suitable for use in massive pours, such as emplacement room plugs. The low heat (of hydration) reduces the potential for thermal cracking and dehydration due to high temperatures.

The LHHPC has been used in several applications. In addition to development testing (Gray and Shenton 1998), LHHPC has been used in a large (20 m³) block cast on surface as a test for the TSX (Chandler et al. 2002), a concrete bulkhead in the TSX (Martino et al. 2008), and testing of varied temperature and saturation conditions after initial curing (Martino et al. 2006).

The chemical hydration reaction of curing is affected by many parameters. These tests have allowed measurement of properties resulting from a variety of conditions; however environmental effects during curing are not fully understood. Conditions that will prevail during most pours in a repository have not been duplicated in these tests. Other than the TSX bulkhead and the large concrete block, curing has taken place under idealized conditions where temperature is constant (20-23°C) and humidity is 100 percent. The TSX concrete was not examined until after the test so initial *in situ* curing conditions are not clearly understood.

LLHPC trial casting was compared to High Fly Ash Concrete (HFAC) and Standard High Performance Concrete (SHPC) (Table 17). An engineering scale trial in 1996 (Chandler et al. 2002) consisted of casting 20 m³ blocks of LHHPC and High Fly Ash Concrete (HFAC) in which the concrete was poured into forms constructed of plywood with steel I-beam bracing. These tests were conducted at the Underground Research Laboratory site. The blocks remain after 14 years however sample holes drilled in the upper sections have allowed freeze-thaw damage to cause cracks. The remaining volume of the blocks is intact and could be sampled for the presence of carbonation over time, as this process is not fully understood in low alkalinity concretes. The comparison of strength from the laboratory cured cylinders (a) and the block samples (b) are shown in Figure 87. In all concrete types, strength continued to increase with time over the period tested.

Table 17: Comparison of Material Content of High Performance Concrete Types

Materials	High Fly Ash Concrete Content (kg/m³)	Standard HPC (SHPC) Content (kg/m³)	Low Heat HPC (LHHPC) Content (kg/m³)
Portland cement	194 (CSA Type 10)	497 (CSA Type 50)	97 (CSA Type 50)
Silica fume	-	49.7	97
Fly ash	194	-	-
Silica flour	-	-	194
Superplasticizer	1.5	7.1	10.3
Fine aggregate	895	703	895
Coarse aggregate	1040	1100	1040
Water	128	124	97
W/CM	0.33	0.23	0.50

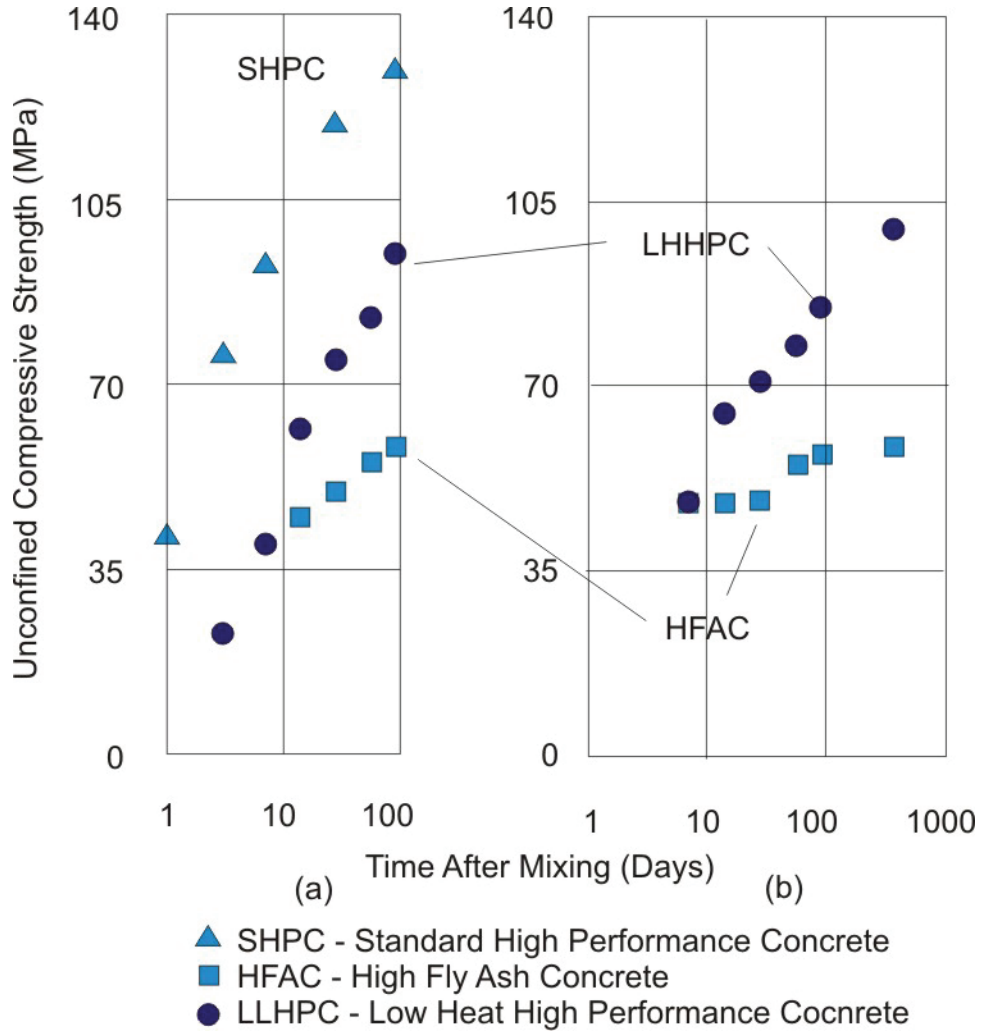


Figure 87: Unconfined Compressive Strength of Low Heat High Performance Concrete (LHHPC), Standard High Performance Concrete (SHPC), Pulverized Fly Ash Concrete (PFAC) Mixes (a) Laboratory Cured Cylinders (b) Cored Samples from Blocks

Table 18 shows the unconfined compressive strength, tensile strength, elastic modulus, Poisson's Ratio and Hoek and Brown parameters of SHPC and LHHPC samples.

Table 18: Mechanical Properties Comparison of Standard High Performance Concrete and Low Heat High Performance Concrete

Property	SHPC	LHHPC
Unconfined Compressive Strength (28 days and 23°C)	122 MPa	75 MPa
Unconfined Compressive Strength (28 days and 50°C)	87 MPa	68 MPa
Unconfined Compressive Strength (28 days and 90°C)	77 MPa	67 MPa
Direct Tensile Strength (28 days and 23°C)	4.5 MPa	3.3 MPa
90-day drying shrinkage (μ) (after 7 days curing)	440	330
Tangent Elastic Young's Modulus (28 days at 40% of unconfined strength)	40 GPa	36 GPa
Young's Modulus in Tension (at 40% of direct tensile strength)	43 GPa	31 GPa
Poisson's Ratio	0.2	0.16
Hoek-Brown Failure Parameter m (at 23° C with s=1)	14.9 MPa	8.2 MPa

Table 18 provides a basic set of mechanical properties for the LHHPC at ambient and elevated temperatures. Based on unpublished testing, the permeability of these concrete samples was 10^{-12} m/s. Similarly, *in situ* testing of the blocks determined values of k ranging from 2×10^{-14} to 4×10^{-14} m/s (Chandler et al. 2002). Permeability can affect durability as a lower permeability can reduce the rate of water migration into and through the concrete. These samples were cured at room temperature and in high humidity conditions before heating. This is not similar to what would be experienced in a repository, where humidity at the pour locations would likely be lower and temperatures likely more elevated.

Repository concrete used in emplacement room seals will be expected to be in service for long time periods (Martino 2006). In order to understand how low alkalinity concrete behaves in the long term, a series of long-term strength tests were conducted (Martino and Keith 2005). Samples were cured for the first 28 days in room temperature and high humidity conditions, which are not the conditions expected in a repository. A series of tests were conducted to determine the effect of heat on the uniaxial compressive strength of concrete cylinders cast of sulphate resistant Portland cement-based concrete (RC) and Low Heat High Performance Concrete (PC) (Table 19). Following an initial 28 days of curing in a room at 100% humidity and a temperature of $\sim 23^\circ\text{C}$, concrete cylinders were placed in one of four environments: dry/ambient (no water added, room temperature); wet/ambient (placed in a water bath at room temperature); dry heat (oven heated in geotechnical ovens) or immersed heat (placed in a heated water bath). Humidity was not controlled during the testing. Water used for immersing

samples was either fresh potable water or Standard Canadian Shield Saline Solution (SCSSS) with a 55 g/L total dissolved solids content. Unconfined compressive strength testing was conducted on the concrete cylinders after one, two, six and twelve months of curing in these various environments.

Both PC and RC types of concrete tested in all curing environments showed an increase in strength with increasing curing time relative to the 28-day average strength values. The responses to the different environments varied between concrete types. The RC samples stored in the heated immersed environment showed an increase in average strength, but the other RC samples showed only slight change. The PC stored in the heated immersion environment showed a rapid increase in strength at one month but then remained essentially unchanged through the 12 month test series. For the other environments, the PC showed some increases in strength over time. Samples immersed in Standard Canadian Shield Saline Solution (SCSSS) did not show differences in strength from those in potable water, however, the time period may have been too short for sulphates and chlorides in the SCSSS to make a noticeable difference. The SCSSS used in the test consisted of an initial batch of 150 L of distilled water to which were added 750 mL of pre-mix solution containing K, Sr, CO₃ and NO₃ and 8.25 kg CaCl₂, 1906.5 g NaCl, 304.2 g MgSO₄·x7(H₂O) and 23.1 g Na₂SiO₂. These results suggest that the strength of LLHPC concrete can be expected to increase for at least the first year if moisture is available. It appears that the concrete cured in dry conditions tends to be stronger than the wet cured conditions. The reason for this is not clear, as a concrete that has water freely supplied to it should have a higher strength. This behaviour warrants further investigation.

Table 19: Average Unconfined Compressive Strength Values (MPa)

Sample Type	28-Day Curing	Months After 28-Day Curing			
		1	2	6	12
PC Oven Heated Immersed	-	121	-	121	121
PC Oven Heated Dry	-	121	125	128	138
PC Ambient Air Temp. Immersed	-	80	89	114	116
PC Ambient Air Temp. Dry	73.4	89	94	112	125
RC Oven Heated Immersed	-	57	-	63	68
RC Oven Heated Dry	-	58	61	60	65
RC Ambient Air Temp. Immersed	-	56	58	67	63
RC Ambient Air Temp. Dry	46.8	60	60	64	63

No correlation was found between Poisson's ratio or Young's modulus with the various environments or curing time. The measured Poisson's ratios averaged 0.25. The Young's

Modulus of the immersed samples averaged approximately 47 GPa and the non-immersed samples averaged approximately 48 GPa.

The TSX provided an opportunity to examine LHHPC concrete that had been installed in conditions similar to a repository. During the first 10 days of curing, water was supplied to the front face of the bulkhead only. The bulkhead was 3.5 m thick and installed in a 4.4 m wide by 3.5 m high tunnel with a “keyed” section 1.5 m high with a wedge shaped cross section. Water was supplied nearly continuously to the back end of the concrete starting 13 days after casting the concrete at pressures that reached 4 MPa after several years (1998 to 2002). The water was heated (2002 to 2003) before the experiment was decommissioned. The concrete was sampled in 2004. Based on sonic velocity measurements and areas of reduced porosity (Martino et al. 2008) an assumed wetting front existed due to water supplied during curing to the front face of the bulkhead and from the water in the pressurized tunnel on the upstream end of the bulkhead. The assumed extent of the two wetting fronts is shown in Figure 93.

Compressive test results are also plotted in Figure 88. The results confirm what was observed with the laboratory samples, where LHHPC exposed to heated and water increased in strength with time. However, the ultimate strength was lower than what was seen in laboratory cylinders cured for a shorter time.

In the TSX bulkhead, Young’s modulus values ranged from 29.8 to 43.8 GPa and Poisson’s ratio ranged from 0.16 to 0.31 from samples taken at the end of the test, when the concrete was approximately five to six years old. Much of the variation can be attributed to placement of the gauges over various combinations of matrix material and aggregate. The Poisson’s Ratio and elastic modulus did not show a clear variation with sample location in the bulkhead, likely because of the variation in material under the strain gauges. Acoustic velocity tests were conducted on samples taken at the end of the test and the dynamic modulus was determined under compressive and tensile loading. The dynamic modulus showed similar results under both loading conditions ranging from 29.4 to 48.8 GPa (compressive) and 27.4 to 45.1 GPa (tensile). These modulus results confirm what was seen in the compressive strength results.

Both the compressive tests and the static and dynamic modulus results indicate that scaling up from laboratory scale mixing may be an issue in achieving desired results with concrete in repositories. This issue warrants further investigation.

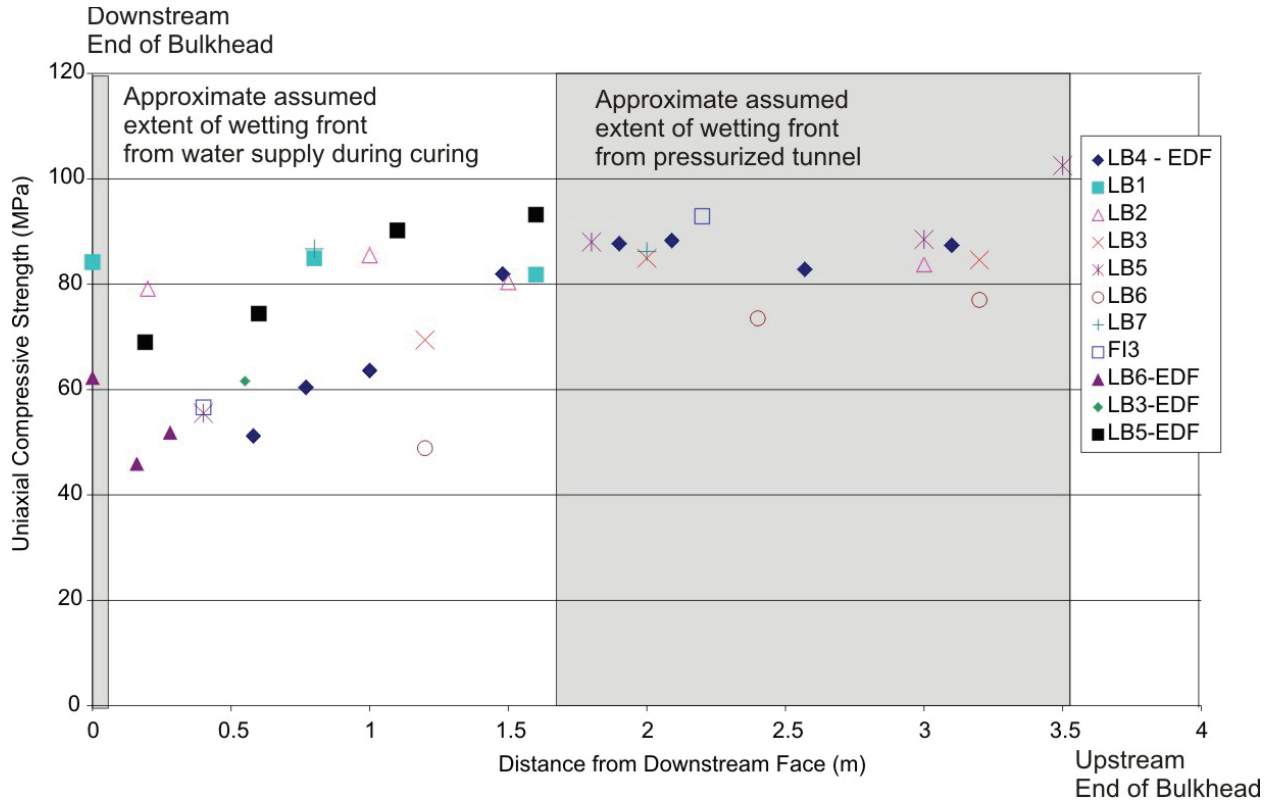


Figure 88: Unconfined Compressive Strength of Low Heat High Performance Concrete (LHHPC), Standard High Performance Concrete (SHPC), Pulverized Fly Ash Concrete (PFAC) Mixes (a) Laboratory Cured Cylinders (b) Cored Samples from Blocks

Strain development, particularly from shrinkage, is an important factor in concretes. The development of strain can determine whether cracks form in a concrete and to what degree the concrete-rock interface may open from shrinkage of the concrete material. Early age shrinkage of low pH concrete differs from regular concretes, due to the different chemical makeup of this type of concrete. The shrinkage of LHHPC is five times that of normal concrete ($250 \mu\epsilon$ compared to $50 \mu\epsilon$ after 28 days) in dry conditions. This shrinkage is typical for high performance concretes that substitute pozzolans for Portland cement (Aitcin 1998). However if LHHPC is cured underwater, then it will expand much greater than normal concrete ($350 \mu\epsilon$ compared to $100 \mu\epsilon$ after 28 days). This is also typical behaviour for a high performance concrete (Aitcin 1998).

Unless a concrete bulkhead can be prevented from undergoing any water loss for the entire period of curing then at some point shrinkage must be expected. Suggestions to avoid autogeneous shrinkage by coating the concrete with an impervious film (Bisonette et al. 1997) are not readily applicable to repository bulkheads as most surfaces are not accessible and introduction of a new chemical compound may not be desirable. Results from the TSX suggest that some degree of interface opening is to be expected even when water is freely supplied to the concrete (Martino et al. 2008). In the case of the TSX, the upstream end was fully exposed to water during the experiment but still experienced shrinkage ($167 \mu\epsilon$).

Other countries have investigated low alkalinity concrete as well. Some work has been done in the US program for low pH tunnel liner concrete mortar. In that work the amount of ordinary Portland cement was reduced by 50% to 70% and blended with varying amounts of Blast Furnace Slag, Fly Ash and Silica Fume. The 28 day strengths ranged from an average of 23.1 to 36.9 MPa, all blends continued to show strength gains to the last testing period at 3 months. These strengths are similar to the high fly ash concrete studied by AECL and noted in Figure 92.

More recently work has been ongoing in Sweden for a variety of concrete uses including mass poured and pneumatically placed concrete. The pneumatically placed concrete has been developed for tunnel plugs and for rock support (shotcrete) (García-Siñeriz et al. 2008). From this work two blends were chosen for the pneumatically placement. One was a 60% ordinary Portland cement (OPC) and 40% silica fume blend with a 90 day pH of 11.1 and 28 day strength of 20.6 MPa. The second was a 35% OPC, 35% silica fume and 30% fly ash blend with a 90 day pH of 10.9 and 28 day strength of 11.4 MPa. These strengths are significantly lower than the LHHPC. This could partly be related to mix design. In pneumatically placed concrete if the concrete not mixed, i.e. water is only added at the nozzle – that would be another important factor in strength. Work done with samples immersed in groundwater from the Äpsö facility in Sweden indicated an increase in porosity over a one year period, but this porosity increase did not increase the hydraulic conductivity (1.03×10^{-10} m/s). This a relatively high value compared to the LHHPC (10^{-12} to 10^{-14} m/s).

Work was done for mass poured concrete in Sweden as well but the work has not yet been published. The Swedish concrete is a self compacting type with a high slump so it is self levelling. Different binder contents were examined, 150, 200 and 300 kg binder using cement, silica fume and limestone filler. The 200 kg and 300 kg binder were examined in detail. Preliminary results indicate that at 28 days of curing the strength was 43.4 MPa and 68.1 MPa for the 200 kg and 300 kg binder respectively. Laboratory testing of water penetration following standard Swedish test methods indicated a hydraulic conductivity in the order of 10^{-10} m/s.

A number of gaps exist in the knowledge of low alkalinity concrete mechanical properties.

- A gap exists in the understanding the sensitivity of the properties (strength, modulus, strain) to variation in both mix design and component qualities. Variability in mixes are likely in a production setting, especially when scaling from laboratory scale blends were more careful control can be exercised to a large scale were more variability would be expected.
- The sensitivity of key properties, such as strength and pH to scaling and variation of components should be determined. With the addition of sedimentary rock masses to the geologic options to host a DGR, the affect on the mix and the type of aggregate used (sedimentary versus granitic) should also be considered. LHHPC has been mainly developed using granitic aggregates and washed glacial pit sand. Chemical and mechanical testing of aggregates from representative sedimentary rock should be undertaken.
- Curing in dry and elevated temperature conditions similar to what may exist in a drier repository has not been examined.
- A gap exists in understanding the evolution of LHHPC. This gap applies to both low and high salinity conditions. The evolution of LHHPC is also required to provide an understanding of the behaviour of mechanical and chemical properties. The

understanding of the mechanical properties is needed due to the long service life of the concrete and the potential long open time of a repository of up to 300 years (NWMO 2005) where concrete will play a role in restraining engineered barrier material. The understanding of the chemical evolution of low alkalinity concrete needs further development both during the operating period of the repository and after closure so that its affect on engineered barrier materials can be understood.

- Related to the understanding of the chemical evolution is the need to locate and examine natural analogues that may simulate aspects of the chemical composition of a low alkalinity concrete. This has been done for regular concrete in repository studies (Smellie 1998).
- The ability to model the durability of low pH concrete requires development and links to the need to understand the low alkalinity concrete evolution. This would also allow better input to safety cases.
- A gap exists in establishing a standardized method for determining the pH of concrete leachate.
- A low pH shotcrete based on Canadian materials has not been developed. The need for this material will depend on the rock mass ultimately selected for a deep geologic repository, however the low pH shotcrete should be developed as even in the most competent rock, shotcrete could be required for excavations through fracture zones, as was the case in the Canadian URL vent raise shaft.

4.8 MECHANICAL PROPERTIES OF LOW ALKALINITY CEMENTIOUS GROUT

A low alkalinity, high performance grout (UF41-14-4) has been developed (Arenius et al. 2008) in Europe. It has the ability to penetrate fine fractures of less than 100 μm . In terms of pH, a material must have a pH of less than 11 to be accepted as a low alkalinity cementitious material (Arenius et al. 2008, Baumgartner 2006 b). A Canadian grout was designated a high performance grout for use in repositories (Onofrei et al. 1993), but it has a pH of 11.5 to 11.9 (Onofrei et al. 1988) in laboratory tests and so is not a low alkalinity grout by this definition.

An extensive testing program was conducted to determine the preferred mix for the European low alkalinity grout (Arenius et al. 2008), including work with a cement based grout, a grout with 15% silica for cement substitution (for a reduced pH grout) and a 41% silica for cement substitution. The UF41-14-4 grout is comprised of 59% Ultrafin (UF) 16 cement and 41% silica fume. This includes 4% naphthalene sulphonate superplasticizer (by weight of the aggregate and binder) with a 1.4 water to binder ratio. Table 20 shows the mechanical properties of the grout. The Ultrafin 16 is a sulphate resistant cement typically used in grouting applications. The silica fume is a micro silica fume (trade name Grout Aid). A coarse, dry silica fume variant is under consideration for wider aperture fractures.

Table 20: Properties of UF41-14-4 Low Alkalinity Grout

Property	Unit	UF41-14-4
Density	Kg/m ³	1354
Marsh Cone fresh grout	s	44
Marsh Cone +1 h grout	s	61
Penetration (min)	µm	42
Penetration (crit)	µm	247
Shear 6 h	kPa	1.1
Shear 24 h	kPa	157
UCS 1 d	MPa	0.7
UCS 28d	MPa	17.0
UCS 91 d	MPa	22.4
Viscosity	MPas	10.9
	MPas	15.3
Yield Stress	Pa	12.1
	Pa	13.8

As a comparison, the 90/10 high performance grout materials were selected for their small mean particle size and the ability to be made fluid by a superplasticizer at low water/cementitious-materials ratios. In case of the 90/10 grout the ratio was set at 0.4 w/c. The cement powder is a re-ground sulphate resistant cement, ground to a Blaine fineness of 600 kg/m³. It has an initial setting time of 10 to 16 h and a final setting time of 12 to 20 h depending on temperature. The strength will reach 20 to 60 MPa at 28 days dependant on the water to cement ratio (0.4 to 0.6 water to cement ratio), time and temperature with a hydraulic conductivity of less than 10⁻¹² m/s. This grout had been demonstrated to penetrate fractures in field applications.

At the high pHs imposed by cement hydration, silica fume provides a reactive material that generates silicate. Silicate reacts readily with available lime and/or portlandite (CH) and forms CSH phases. CH is the most soluble of all the cement hydration products. By removing the CH, silica fume addition creates a hardened grout with improve leach resistance. Moreover, an excess of residual silica in the hardened grout will not impair, and may improve, the long-term leach resistance of the grout (Onofrei et al. 1992). The 90/10 grout was developed with the assumption that the higher pH of the grout would be buffered by silica saturated groundwaters in the granitic rock. However, this assumption does not account for a situation where groundwater causes water movement into a tunnel adjacent to grouting where buffering may be reduced by the proximity of the inflow to backfill. Additionally, the properties of groundwater in other rock types, such as sedimentary formations, were not considered.

A low alkalinity grout using materials available in Canada should be developed and its properties defined. The effect of temperature on the grout setting and strength properties should be investigated on a low alkalinity Canadian grout. It is known that lower temperatures coupled with the chemical composition of the groundwater will retard setting of low pH grouts (Karttunen and Raivo 2008).

4.9 SUMMARY OF MECHANICAL PROPERTIES

Table 21 provides a summary of mechanical properties for the various sealing materials. This includes average values where appropriate.

Table 21: Summary of Mechanical Properties

Property	BSB	LBF	HCB	GF	DBF	Concrete
Strength						Fig. 87,88 Table 18-20
c' (MPa)	0.088	0.060 Fresh 0.071 Saline			0.048	
ϕ'_{oc}	14°	13° Fresh 20° Saline	13° (<1 MPa) 7° (>1 MPa)		28°	
ϕ'_{cs}	13° - 16°	13° Fresh 22° Saline			28°	
M_{cs}	0.49 - 0.61	0.47 Fresh 0.86 Saline			1.1	
CSL	Eqs. 32, 33, 36-38					
Elasticity						
E (MPa)	141±47	88.7 ¹	31-46 @ EMDD=1.74 117- 533 @ EMDD=1.85		178*	
G (MPa)	43±14	35			57.5*	
K (MPa)	4.6 to 65.5	61.6				
ν	0.38 to 0.45 ¹	0.26 ¹				0.25
Yield Loci	Fig. 30	Fig. 62				
Flow Rule	Associated					
Hardening						
κ	0.022	0.004 (50- 200 kPa)				
λ	0.3142	0.5			0.13*	
C_c		Fig. 66, 67 Table 11	Fig. 67, 70, Table 12		Fig. 67, 85, Table 18	
C_s		Fig. 66, 67 Table 11	Fig. 67, 70, Table 12		Fig. 67, 85, Table 18	
1D Modulus		Fig. 68	Fig. 68		Fig. 68	
Unsaturated						
M^b and ϕ^b	Table 6					
E_{unsat} (MPa)	Fig. 43-47					
G_{unsat} (MPa)	111.2-275.8					
ν_{unsat}	0.18					
κ_{unsat}	0.003 - 0.015					
λ_{unsat}	Fig. 50					
$C_r/(1+e_0)$	0.006					
$C_d/(1+e_0)$	0.140 (3.7-4.5 MPa suction)					
$C_o/(1+e_0)$	0.005					
Yield Loci	Fig. 53-57	Fig. 69			Fig. 86	
LC, LSY	Fig. 55, 59			Fig. 74, 75		
Swelling Pressure (MPa)	Fig. 70	Fig. 70	Fig. 71, 72	Fig. 79		

Note: - TBD – to be determined - NA – not applicable
 - ¹ calculated from elastic theory equations - * – preliminary

5. KNOWLEDGE GAP SUMMARY

A number of gaps have been identified in the above review of sealing material properties and behaviour. This section summarizes the properties and behaviour that require further characterization. The summary tables at the end of the thermal, hydraulic and mechanical properties sections highlight the gaps for each material. Particularly, there are gaps in the information required to apply state-of-the-art unsaturated elastic-plastic models to the clay based sealing materials. Internationally, models such as the BBM, BeXM and BGM are being applied, but insufficient data is available to confidently determine all of the incorporated parameters.

Additionally, a previous and more general review was conducted during a 2006 workshop , where overall issues for repository sealing systems were identified (Table 23). The issues were divided into short and long term development goals. Most material properties issues are under items 7 and 8 in that discussion. However, the properties and the ability to achieve those properties are related to the other items identified in that study.

One of the primary near-term needs identified at the 2006 workshop was to define the importance of host rock pore water chemistry as it relates to the performance of clay-based and concrete seals. Considering sedimentary rock as a potential host medium presents groundwater chemistry environments for which the effect on clay-based or concrete-based seals is insufficiently understood (e.g., high salinity in sedimentary formations, and limestone water chemistry in particular). Chemistry effects include the influence on permeability, cation exchange, swelling/healing, design life, stability and cementation. Tools for site suitability assessment would include improved conceptual and numerical models to understand the effect of the groundwater flow and groundwater chemistry on the performance of repository sealing systems. Characterization of the materials under high salinity conditions and identification of the tools is the first step in the process. Subsequently, development of these tools would occur over the long term.

The literature review presented in this document has indicated that a significant amount of work had been done to address this knowledge gap in the effect of pore water chemistry, especially in terms of hydraulic conductivity, hardening and swelling pressure. However, knowledge gaps exist with respect to yielding and strength behaviour for several of the proposed materials. These, along with others, are summarized below.

Table 22: Repository Sealing Systems

Engineering Issues on Repository Sealing Systems	Near-term	Long-term
Required for siting preferences identification or tools for site selection		
1. Defining water influx conditions required allowing seal installation and short-term system stability.	X	
2. Influence of rock competence/fracturing on tunnel or shaft seal performance.	X	X
3. Influences of groundwater chemistry on seal performance.	X	
Required for engineering conceptual or detailed design		
4. Transient unsaturated period effects (e.g., effect on microbes, clay drying/cracking, or clay cementation) with respect to defining guidelines for acceptable repository saturation rates.	X	
5. Influence of sedimentary rock volume increase or decrease due to degree of saturation on seal design and performance.		X
6. Chemical cementation and chemical alteration of bentonite-based seals, concrete-clay interactions, and iron-bentonite interaction.		X
7. Definition of methods and specifications for placement of clay-based materials (design requirements; specific material density, composition, swelling pressure, emplacement method).	X	X
8. Development of concrete-mix designs, placement methods and design requirements for concrete components of repository sealing systems (including grout).	X	X
9. Microbial activity and sealing system design (transient period effects on microbial activity and movement, clay density criteria for limiting microbial activity, microbial activity in sedimentary rock) (including input from container corrosion testing).	X	
10. Demonstration of sealing system component performance (including long-term testing and modelling).		X
11. Development and testing of numerical modelling tools to evaluate sealing system performance	X	X
12. Mitigating long-term erosion of sealing materials.		X
13. Gas generation effects on seal performance.		X
14. Concrete and clay seal design lifetimes and material longevity		X
15. Effect of construction-related structures (e.g., concrete floor, shotcrete or room liners) on sealing.		X
16. Produce and compile supporting evidence to show that material specifications are relevant, achievable and will be maintained throughout their design life.	X	X

Bentonite-sand buffer (BSB) is sufficiently characterized to allow for the calibration of unsaturated, elastic-plastic models such as the BBM, BGM or BExM. As such, only a limited number of tests are recommended for confirmatory testing of BSB. The following specific knowledge gaps were highlighted by the literature review.

- The coefficient of thermal expansion for BSB has not been measured.
- The effect of chemistry on the unsaturated, elastic plastic behaviour of BSB should be confirmed for the expected extreme conditions.

For **light backfill (LBF)** the following specific knowledge gaps were highlighted by the literature review, although extending the range of density examined for BSB could provide clarification to many of the questions still outstanding.

- The thermal conductivity and coefficient of thermal expansion for LBF have not been measured.
- The SWCC for LBF requires characterization.
- Further testing of LBF is required to confirm modulus values derived in the elastic range for both fresh and saline pore water.
- The yield locus for LBF has not been specifically investigated to date.
- Isotropic hardening behaviour of LBF should be confirmed for both fresh and saline pore water.
- The properties of unsaturated LBF have not been investigated to date.

For **highly compacted bentonite (HCB)** the following specific knowledge gaps were highlighted by the literature review.

- A general need to develop a clearer understanding of the stress-strain properties of HCB.
- Further testing is required to define the yield locus for HCB for both fresh and saline pore water.

Little development and experiment work has been done for **gap fill (GF)** the following specific knowledge gaps were highlighted by the literature review.

- Clear identification of to what extent GF can be described using HCB properties information, particularly after it is compressed by adjacent materials.
- Identification of what effects fabric and particle alignment due to compaction or construction will have on materials performance.
- GF has a low thermal conductivity. Further research and testing is required to identify ways for increasing thermal conductivity of material. This is the subject of testing that is planned for 2010.
- The SWCC for GF requires characterization.
- Further testing is required to define the yield locus and strength envelope for GF for both fresh and saline pore water.
- 1D and isotropic hardening behaviour has not been investigated.

- The properties of unsaturated GF have not been investigated to date.

For **dense backfill (DBF)** the following specific knowledge gaps were highlighted by the literature review.

- The thermal conductivity and coefficient of thermal expansion for DBF have not been measured.
- The SWCC for DBF has not been characterized.
- Further testing of DBF is required to confirm modulus values derived in the elastic range for both fresh and saline pore water.
- The yield locus for DBF has not been specifically investigated to date.
- Isotropic hardening behaviour of DBF should be confirmed for both fresh and saline pore water.
- The properties of unsaturated DBF have not been investigated to date.
- The swelling behaviour of DBF has not been investigated.

For **cementitious materials** the following specific knowledge gaps were highlighted by the literature review.

- The thermal conductivity and coefficient of thermal expansion for the proposed cementitious have not been measured.
- A gap exists in understanding the sensitivity of key properties, such as strength, strain and pH to scaling and to the variation of component materials. Variability in mixes are to be expected in a production setting. Determining how much variance can be accepted and still produce the desired properties should be determined. With the addition of sedimentary rock masses to the geologic options to host a DGR, the affect on the mix and the type of aggregate used (sedimentary versus granitic) should also be considered. LHHPC has been mainly developed using granitic aggregates and washed glacial pit sand. Chemical and mechanical testing of aggregates from representative sedimentary rock should be undertaken.
- A gap exists in understanding the evolution of LHHPC. This gap applies to both low and high salinity conditions, and in exposure of the low alkalinity concrete to saline water in early curing. The chemistry of low alkalinity concrete requires study as the components of low alkalinity concrete differ from regular concrete. Testing under low and high saline conditions with petrographic analysis of samples and measurement of properties on specimens should be conducted.
- Because the properties of the low alkalinity concrete will be an issue for repository function for long time periods, long term tests lasting 10 or more years should be conducted to provide and better understanding of the evolution of the material.
- The ability to model the durability of low pH concrete requires development and links to the need to understand the low alkalinity concrete evolution. This would also allow better input to safety cases.
- Related to the understanding of the chemical evolution is the need to locate and examine natural analogues that may simulate aspects of the chemical composition of a low alkalinity concrete.

- A gap exists in establishing a standardized method for determining the pH of concrete leachate.
- A low pH shotcrete based on Canadian materials has not been developed. The need for this material will depend on the rock mass ultimately selected for a deep geological repository, however the low pH shotcrete should be developed as even in the most competent rock, shotcrete could be required for excavations through fracture zones, as was the case in the URL vent raise.
- A low pH grout using materials available in Canada, should be developed and its properties defined.
- The effect of temperature on the grout setting and strength properties should be investigated on a Canadian grout. It is known that lower temperatures coupled with the chemical composition of the groundwater will retard setting of low pH grouts.

These points compliment the gaps identified at the 2006 workshop, which include, but are not limited to: durability, mix design, shotcrete design, curing in warm environments, material compatibility in a sedimentary host rocks, and developing mix designs and/or placement methods to reduce the potential for shrinkage or incomplete curing during hydration.

Activities that address concrete issues will ultimately lead to the development of concrete design and placement specifications specific to repository sealing systems. Because of the long lead time for chemical and property evolution those tests should be initiated in the near term. Some development such as determination of low pH measurement is underway in other programs and participation in that area can be undertaken in the near term as well.

6. CONCLUSIONS

In order to effectively and defensibly model the behaviour of repository sealing designs, detailed characterization of sealing material properties and behaviour is required. This includes identifying the appropriate constitutive models and measurement of the constitutive parameters for the expected range of conditions in a repository. The sealing system will be required to perform in an environment with high temperatures, potentially high groundwater salinities and will experience a transition from an unsaturated state to eventual saturation. Coupled thermal-hydraulic-mechanical (THM) and chemical modeling techniques are being developed and employed since changes in moisture, groundwater chemistry and temperature change the physical properties of the materials.

A great deal of work has been conducted over the last 25 years to define materials for use in a deep geological repository. As repository concepts evolved new material combinations or variants on existing materials were required. In some cases, such as highly compacted bentonite and 50:50 bentonite-sand buffer, this knowledge base is well developed. Other sealing materials being considered require further characterization. Knowledge gaps exist in the store of knowledge for both clay-based and cement-based repository sealing materials.

This report provides a review of material properties available in the literature, and highlights the gaps in those knowledge areas that require further investigation. The following is a list of conclusions regarding the state of knowledge for each type of sealing material being considered in the Canadian used fuel management program.

- **Bentonite-sand buffer (BSB)** has been the subject of a considerable volume of research in Canada. The thermal and hydraulic properties of BSB are well characterized. Its mechanical behaviour is best described by an unsaturated elastic-plastic model (for example, the Blatz-Graham Model (BGM)). Extensive testing has provided the necessary material properties and constitutive parameters to effectively model this material. Some confirmatory testing should be conducted to validate saturated-unsaturated models, including at the expected extreme geochemical conditions. However, future research should focus on other materials, using the extensive testing experience gained during the characterization of BSB.
- **Light backfill (LBF)** is very similar to BSB, except for its lower dry density and EMDD. Much of the work conducted on BSB can be extended to LBF. As such, characterization of LBF in an elastic-plastic framework will be efficient, building on previous experience with BSB. Future testing of LBF should focus on confirmation of constitutive parameters under the extremes and average of expected conditions.
- **Highly compacted bentonite (HCB)** has been the subject of considerable international research. Many of the properties and constitutive parameters for HCB are readily available, especially with respect to thermal and hydraulic behaviour. Future testing should focus on determining the constitutive saturated and unsaturated parameters of the BGM.
- **Gap fill (GF)** is essentially HCB, except for its lower dry density and EMDD due to its placement in pellet form in areas where compaction will be difficult. Similar to LBF, future testing of GF should focus on certain extreme conditions to confirm its behaviour.
- **Dense backfill (DBF)** has received relatively less research attention compared to the above materials. Further thermal, hydraulic and mechanical testing is required.
- **Low alkalinity concrete (LAC)** has received less attention than clay-based materials to date. Testing is required to better understand this material. Development of a shotcrete variant of this material is also required.
- **Low alkalinity cementitious grout (LACG)** requires development in Canada. The grout developed in Canada is not a low pH grout.

Detailed testing programs designed to address the gaps identified in this document will be the subject of subsequent studies.

ACKNOWLEDGEMENTS

The authors gratefully acknowledge the support of NWMO in the preparation of this report and the reviews of David Dixon, Neil Chandler and Gary Simmons.

REFERENCES

- Alonso, E.E., A. Gens and D.W. Hight. 1987. Special problem soils - General report. Proc. 9th European Conf. Soil Mech. Fdn. Engng., Dublin, 3, 1087-1146.
- Alonso, E.E., A. Gens and A. Josa. 1990. A constitutive model for partially saturated soils. *Géotechnique*, 40(3), 405-430.
- Alonso, E.E., A. Lloret, A. Gens and D.Q. Yang. 1995. Experimental behaviour of highly expansive double-structure clay. Proc. 1st Int. Conf. on Unsaturated Soil, Balkema, Paris, 1, 11-16.
- Alonso, E.E., J. Vaunat and A. Gens. 1999. Modelling the mechanical behaviour of expansive clays. *Engineering Geology*, 54, 173-183.
- Anderson, D.E.S. 2003. Evaluation and comparison of mechanical and hydraulic behaviour of two engineered clay sealing materials. M.Sc. Thesis, University of Manitoba.
- Arenius, M., J. Hansen, P. Juhola, P. Karttunen, K. Koskinen, A. Lehtinen, T. Lyytinen, J. Mattila, S. Paratamies, P. Pitkänen, P. Raivio, U. Sievänen, U. Vuorinen, M. Vuorio. 2008. R20 summary report: the groundwater inflow management in ONKALO – the future strategy. Working Report 2008-44, Posiva Oy, Olkiluoto, FI-27160 EURAJOKI.
- Atomic Energy of Canada Limited (AECL). 1994. Environmental impact statement on the concept for disposal of Canada's nuclear fuel waste. Atomic Energy of Canada Limited Report, AECL-10711, COG-93-1. Chalk River, Ontario.
- Barbour, S.L. and N. Yang. 1993. A review of the influence of clay-brine interactions on the geotechnical properties of Ca-montmorillonitic clayey soils from western Canada. *Canadian Geotechnical Journal*, 30, 920-934.
- Baumgartner, P. and G.R. Snider. 2002. Seal evaluation and assessment study (SEAS): light backfill placement trials. AECL Technical Record, TR-793.
- Baumgartner, P., D.G. Priyanto, J.R. Baldwin, J.A. Blatz, B.H. Kjartanson and H. Batenipour. 2008. Preliminary results of one-dimensional consolidation testing on bentonite clay-based sealing components subjected to two pore-fluid chemistry conditions. Nuclear Waste Management Organization Report NWMO TR-2008-04. Toronto, Canada.
- Baumgartner, P. 2006a. Emplacement-room-sealing system requirements. Ontario Power Generation Report 06819-PDR-01110-00001-R00.
- Baumgartner, P. 2006b. Bulkhead-sealing system requirements. Ontario Power Generation Report 06819-PDR-01110-00003-R00.
- Baumgartner, P. 2006c. Tunnel-, service-area-, shaft- and ramp-sealing system requirements. Ontario Power Generation Report 06819-PDR-01110-00004-R00.
- Baumgartner, P. 2006d. Borehole-sealing system requirements. Ontario Power Generation Report 06819-PDR-01110-00002-R00.

- Baumgartner, P. 2006e. Generic Thermal-Mechanical-Hydraulic (THM) Data for Sealing Materials - Volume 1: Soil – Water Relationships”, Ontario Power Generation Report 06819-REP-01300-10122-R00.
- Baumgartner, P. 2005. Scoping analyses for the design of a deep geologic repository in sedimentary rock. Ontario Power Generation, Nuclear Waste Management Division Report, 06819-REP-01300-10093-R00.
- Blatz, J.A. 2000. Elastic-plastic modelling of unsaturated high plastic clay using results from a new triaxial test with controlled suction. Ph.D. Thesis, Department of Civil Engineering, University of Manitoba, Winnipeg, Canada.
- Blatz, J.A. and J. Graham. 2000. A system for controlled suction in triaxial tests. *Géotechnique*, 50(4), 465-478.
- Blatz, J. A. and J. Graham. 2003. Elastic-plastic modelling of unsaturated high-plastic clay using results from a new triaxial test with controlled suction. *Géotechnique*, 53(1), 113-122.
- Blatz, J.A., J. Graham and N.A. Chandler. 2002. Influence of suction on the strength and stiffness of compacted sand-bentonite. *Canadian Geotechnical Journal*, 39, 1005-1015.
- Blatz, J.A., G. Siemens and A. Man. 2008. Triaxial characterization of light and dense backfill to determine material properties for use in numerical modeling. NWMO, Technical Report No: NWMO TR-2008-05.
- Bodén, A., G. Bäckblom, M. Eriksson, F. Karlsson, B. Lagerblad, R. Riekkola, P. Sellin and H. Stille. 2001. Qualification of low-alkali cementitious products in the deep repository results of the pre-study and plans for the feasibility study. TD-01-57, Svensk Kärnbränslehantering AB, Swedish Nuclear Fuel and Waste Management Co, Box 5864, SE-102 40 Stockholm Sweden.
- Börgesson, L. and R. Pusch. 1987. Rheological properties of calcium smectite. SKB Technical Report 87-31.
- Börgesson, L., H. Hormark and O. Kamand. 1988. Rheological properties of sodium smectite. SKB Technical Report 88-30.
- Börgesson, L., A. Fredrikson and L-E. Johannesson. 1994. Heat conductivity of buffer materials. SKB Technical Report 94-29.
- Chandler, N.A., A. Cournut, D.A. Dixon, C. Fairhurst, F. Hansen, M. Gray, K. Hara, Y. Ishijima, E.T. Kozak, J.B. Martino, K. Masumoto, G. McCrank, Y. Sugita, P.M. Thompson, J. Tillerson and B. Vignal. 2002. The five year report of the Tunnel Sealing Experiment: an international project of AECL, JNC, ANDRA and WIPP. Atomic Energy of Canada Limited Report, AECL-12727.* Atomic Energy of Canada Limited, 2251 Speakman Drive, Mississauga, ON, Canada L5K 1B2.

- Cho, W.J., J.O. Lee and P.S. Hahn. 1995. Backfill material for low and intermediate level radioactive waste repository. *Journal of the Korean Nuclear Society*.
- Cho, W.J., J.O. Lee and C.H. Kang. 2002. A compilation and evaluation of thermal and mechanical properties of bentonite based buffer materials for high-level waste repository. *Journal of the Korean Nuclear Society*, 34(1), 90-103.
- Davis, R.O. and A.P.S. Selvadurai. 1995. *Elasticity and Geomechanics*. Cambridge: Cambridge University Press.
- Delage, P. and J. Graham. 1996. Understanding the behaviour of unsaturated soils requires reliable conceptual models. State-of-Art Report, Session 1, Soil Properties. In *Proceedings of the 1st International Conference on Unsaturated Soils, Paris, France, September 1995* (E.E. Alonso & P. Delage, Eds.) A.A. Balkema, Rotterdam, The Netherlands, 3, 1223-1256.
- Di Maio, C. and Fenelli, G.B. 1994. Residual strength of kaolin and bentonite: the influence of their constituent pore fluid. *Géotechnique*, 44(4), 217-226.
- Di Maio, C. and R. Onorati. 1999. Prove di laboratorio: influenza di composizione del liquido di cella. *Rendiconti del XX Convegno Nazionale di Geotecnica, Parma*, 87-94.
- Dixon, D.A. and M.N. Gray. 1985. The engineering properties of buffer material – research at Whiteshell Nuclear Research Establishment. In *Proceedings of the 19th Information Meeting of the Nuclear Fuel Waste Management Program. Volume 3*, 513-530. Atomic Energy of Canada Limited Technical Record, TR-350.
- Dixon, D.A., M.N. Gray, P. Baumgartner and G.L. Rigby. 1986. Pressures acting on waste containers in bentonite-based materials. In *Proceedings of the 2nd International conference on Radioactive Waste Management, Winnipeg, MB, Canada, September*.
- Dixon, D.A. 1995. Towards an understanding of water structure and water movement through dense clays. Ph.D. Thesis, Department of Civil and Geological Engineering, University of Manitoba, Winnipeg, Canada.
- Dixon, D.A., J. Graham and M.N. Gray. 1999. Hydraulic conductivity of clays in confined tests under low hydraulic gradients. *Can. Geotech. J.*, 36, 815-825.
- Dixon, D.A. 2000. Pore water salinity and the development of swelling pressure in bentonite-based buffer and backfill materials. Posiva OY Working Report, 2000-04.
- Dixon, D.A., N.A. Chandler and P. Baumgartner. 2002. The influence of groundwater salinity and interfaces on the performance of potential backfilling materials. 6th International Workshop on Design and Construction of Final Repositories “Backfilling in Radioactive Waste Disposal”. Brussels.
- Dixon, D.A., B. Kjartanson, P. Baumgartner and J. Martino. 2003. The role of interfaces and permeant salinity on the hydraulic behaviours of bentonite-based barriers. In *Proc. 56th Canadian Geotechnical Society Conference, Winnipeg*.

- Dixon, D.A. and S. Stroes-Gascoyne. 2005. Status of developing light backfill and gap fill materials designed to limit microbial activity. OPG TM No. 06819(UF)-03782.02-T10.
- Dixon, D.A., S. Stroes-Gascoyne, B. Kjartanson and P. Baumgartner. 2005. Development of sealing materials for application as engineered barriers in a deep geologic repository for used fuel disposal: filling the gaps. Canadian Nuclear Society Conference, Ottawa, May 8-11.
- Dueck, A. 2004. Hydro-mechanical properties of a water unsaturated sodium bentonite. Laboratory study and theoretical interpretation. Doctoral Thesis. Lund University, Sweden.
- Engelhardt, L. and S. Finsterle. 2003. Thermal-hydraulic experiments with bentonite/crushed rock mixtures and estimation of effective parameters by inverse modeling. *Applied Clay Science*, 23, 111-120.
- Fredlund, D.G. and N.R. Morgenstern. 1977. Stress-state variables for unsaturated soils. *J. Geotech. Eng. Division, Am. Soc. Civil Engineers*, 103, 447-466.
- García-Siñeriz, J.L., M. Cruz Alonso, J. Alonso. 2008. Application of low pH concrete in the construction and the operation of underground repositories. Euradwaste '08 conference.
- Gens, A. and E.E. Alonso. 1992. A framework for the behaviour of unsaturated expansive clays. *Can. Geotech. J.*, 29, 1013-1032.
- Graham, J., D.H. Shields and B.C.C. Sun. 1985. Stress strain properties in sand-clay buffer materials. Report to AECL, Contract WS-24J-18735.
- Graham, J., M.N. Gray, B.C.C. Sun and D.A. Dixon. 1986. Strength and volume change characteristics of a sand-bentonite buffer. Proceedings of the Second International Conference on Radioactive Waste Management, Winnipeg, Canada.
- Graham, J., F. Saadat, M.N. Gray, D.A. Dixon and Q.Y. Zhang. 1989. Strength and Volume change behaviour of a sand-bentonite mixture. *Can. Geotech. J.*, 26, 292-305.
- Graham, J., J.M. Oswell and M.N. Gray. 1992. The effective stress concept in saturated sand-clay buffer. *Canadian Geotechnical Journal*, 29, 1033-1043.
- Graham, J., N.A. Chandler, D.A. Dixon, P.J. Roach, T. To and A.W.L Wan. 1997. The buffer/container experiment: results, synthesis, issues. AECL Report 11746, COG-97-46-I.
- Hedin, A. 2004. Integrated near-field evolution model for a KBS-3 repository. SKB Report R-04-36. Swedish Nuclear Fuel and Waste Management Co., Stockholm.
- Ho, Y.A. 1985. The effects of brine contamination on the properties of soils. M.Sc. Thesis, Department of Civil Engineering, University of Saskatchewan, Saskatoon.

- Hoffmann, C., E.E. Alonso and E. Romero. 2007. Hydro-mechanical behaviour of bentonite pellet mixtures. *Physics and Chemistry of the Earth*, 32, 832-849.
- Hueckel, T.A. 1997. Chemo-plasticity of clays subjected to stress and flow of a single contaminant. *International Journal for Numerical and Analytical Methods in Geomechanics*, 21, 43-72.
- Imbert, C and M.V. Villar. 2006. Hydro-mechanical response of a bentonite pellets/powder mixture upon infiltration. *Applied Clay Science*, 32, 197-209.
- Japan Nuclear Cycle Development Institute (JNC), 2000a. H12 Project to Establish Technical Basis for HLW Disposal in Japan – Project Overview Report, JNC TN 1410 2000-001. JNC, Tokyo, Japan.
- Japan Nuclear Cycle Development Institute (JNC), 2000b. H12 Project to Establish Technical Basis for HLW Disposal in Japan – Repository Design and Engineering Report, JNC TN 1410 2000-003. JNC, Tokyo, Japan.
- Karnland, O., U. Nilsson, H. Weber and P. Wersin. 2008. Sealing ability of Wyoming bentonite pellets foreseen as buffer material – Laboratory results. *Physics and Chemistry of the Earth*, 33, S472-S475.
- Kjartanson, B.H., D.A. Dixon and S. Stroes-Gascoyne. 2003. Effects of container/buffer gap fill on buffer performance. Ontario Power Generation, Nuclear Waste Management Division, TR No. 06819-REP-01200-10102-R00.
- Kjartanson, B.H., D.A. Dixon and C.L. Kohle. 2005. Placement of bentonite pellets to fill repository sealing system voids and gaps. Ontario Power Generation, Nuclear Waste Management Division, TR No. 06819-REP-01200-10136-R00.
- Kronlöf, A. 2005. Injection grout for deep repositories - low pH cementitious injection grout for larger fractures: Testing technical performance of materials. Posiva Working Report : 2004-45.
- Lingnau, B.E. 1993. Consolidated undrained triaxial behaviour of a sand-bentonite mixture at elevated temperature. Ph.D. thesis, University of Manitoba.
- Lingnau, B.E. and J.Graham. 1994. Synopsis of stress-strain properties of saturated buffer. University of Manitoba, Department of Civil and Geological Engineering.
- Loret, B., T. Hueckel and A. Gajo. 2001. Chemo-mechanical coupling in saturated porous media: elastic-plastic behaviour of homoionic expansive clays. *International Journal of Solids and Structures*.
- Maeda, M., M. Ito and M. Tanaka. 1997. Consolidated undrained triaxial test of the Ca-exchanged bentonite. Power Reactor and Nuclear Fuel Development Corporation. PNC TN8410 97-314.
- Man, A.G. 2005. The effect of changes in pore fluid chemistry on the elastic-plastic behaviour of Lake Agassiz clay. Ph.D. thesis, University of Manitoba.

- Marcial, D., P. Delage and Y.J. Cui. 2002. On the high stress compression of bentonites. *Can. Geotech. J.*, 39, 812-820.
- Martino, J.B. 2006. Issues affecting the durability of concrete in a deep geologic repository. Nuclear Waste Management Organization Report No.: 06819-REP-01200-10143-R00.
- Martino, J.B., D.A. Dixon, S. Stroes-Gascoyne, R. Guo, E.T. Kozak, M. Gascoyne, T. Fujita, B. Vignal, Y. Sugita, K. Masumoto, T. Saskura, X. Bourbon, A. Gingras-Genois, and D. Collins. 2008. The Tunnel Sealing Experiment 10 year summary report. URL-121550-REPT-001. Atomic Energy of Canada Limited, 2251 Speakman Drive, Mississauga, ON, Canada L5K 1B2
- Metcalf, R. and C. Walker. 2004. Proceedings of the International Workshop on Bentonite-Cement Interaction in Repository Environments, 14-16 April 2004, Tokyo, Japan, NUMO-TR-04-05, Nuclear Waste Management Organization of Japan.
- Neville, A.M. 2000. *Properties of Concrete*, 4th edition. Prentice Hall.
- Nuclear Waste Management Organization (NWMO). 2005. Choosing a way forward. The future management of Canada's used nuclear fuel. Nuclear Waste Management Organization. (Available at www.nwmo.ca).
- NUKEM. 2003. Deep geological in-floor borehole emplacement. Design changes from in-room emplacement concept. RWE NUKEM Limited Report 89125/REP/02. November, 2003.
- Olson, R.E. 1974. Shearing strength of kaolinite, illite and montmorillonite. *ASCE Journal of the Geotechnical Engineering Division*, 100(GT11), 1215-1229.
- Onofrei, M., M.N. Gray, L.D. Keil and R. Pusch. 1988. Studies of cement grouts and grouting techniques for sealing a nuclear fuel waste disposal vault. In *Proceedings of Materials Research Society 1988 Fall Meeting Boston*, Nov. 28 to Dec. 03.
- Onofrei, M., M.N. Gray, R. Pusch, L. Borgesson, O. Karnland, B. Shenton, B. Walker. 1993. Sealing properties of cement-based grout materials used in the rock sealing project. Atomic Energy of Canada Limited Report AECL-10815. COG-93-444.
- Onofrei, M., M.N. Gray, W.E. Coons, S.R. Alcorn. 1992. High performance cement-based grouts for use in a nuclear waste disposal facility. *Waste Management*, 12, 133-154.
- Onofrei, M., M.N. Gray, D. Breton, G. Ballivy. 1991. The effect of leaching on the pore structure of cement-based grouts for use in nuclear fuel waste disposal. *Mat. Res. Soc. Symp. Proc.* Vol. 212, Materials Research Society.
- Oscarson, D.W., D.A. Dixon and M. Onofrei. 1997. Aspects of clay/concrete interaction. Atomic Energy of Canada Limited Report, AECL-11715.*
- Oswell, J.M. 1991. Elastic-plastic behaviour of a sand-bentonite mixture. Ph.D. thesis, University of Manitoba.

- Priyanto, D.G. 2007a. Development and application of new constitutive models to simulate the hydraulic-mechanical behaviour of unsaturated swelling clay. Ph.D. Thesis, University of Manitoba.
- Priyanto, D.G., J.A. Blatz, G.A. Siemens, R. Offman, J.S. Boyle and D.A. Dixon. 2008a. The effects of initial conditions and liquid composition on the one-dimensional consolidation behaviour of clay-based sealing materials. Nuclear Waste Management Organization Report NWMO TR-2008-06. Toronto, Canada.
- Priyanto, D.G., J.A. Blatz, G.A. Siemens, R. Offman, J.S. Powell and D.A. Dixon. 2008b. The effects of fluid composition on the one-dimensional consolidation behaviour of clay-based sealing materials. Nuclear Waste Management Organization Report NWMO TR-2008-20. Toronto, Canada.
- Pusch, R. 1983. Stress/strain/time properties of highly compacted bentonite. Div. of Soil Mechanics, University of Luefå.
- Pusch, R. 1982. Chemical interaction of clay buffer materials and concrete. KBF-KBS-SFR-82-01.
- Radhakrishna, H.S. 1984. Thermal properties of clay-based buffer materials for a nuclear fuel waste disposal vault. AECL-7805.
- Roscoe, K.H. and J.B. Burland. 1968. On the generalized stress-strain behaviour of 'wet' clay. In J. Heyman and F. Leckie (Eds.), *Engineering Plasticity* (pp. 535-609). Cambridge: Cambridge University Press.
- Russell, S.B. and G.R. Simmons. 2003. Engineered barrier system for a deep geologic repository in Canada. International High Level Radioactive Waste Management Conference, Las Vegas, NV.
- Saadat, F. 1989. Constitutive modelling of the behaviour of a sand-bentonite mixture. Ph.D. Thesis, Department of Civil and Geological Engineering, University of Manitoba, Winnipeg, Canada.
- Siemens, G.A. 2006. Influence of boundary conditions on the hydraulic-mechanical behaviour of an unsaturated swelling soil. Ph.D. Thesis. University of Manitoba.
- SKI (Swedish Nuclear Power Inspectorate). 2005. Engineered barrier system – Long-term stability of buffer and backfill. Report from a Workshop in Lund, Sweden, 2004 November 15-17, Swedish Nuclear Power Inspectorate SKI Report 2005:48.
- Smellie, J.A.T. 1998. MAQARIN natural analogue study: Phase III. SKB Technical Report TR-98-04. Svensk Kärnbränslehantering AB, Swedish Nuclear Fuel and Waste Management Co., Box 5864, SE-102 40 Stockholm Sweden.
- Sun, B.C.C. 1986. Stress-strain properties in sand-clay buffer materials. M.Sc. Thesis, University of Manitoba.

- Takaji, K. and W. Taniguchi. 1999. Dynamic mechanical properties of buffer material. Japan Nuclear Cycle Development Institute. JNC-TN8400 99-042.
- Tang, G.X. 1999. Suction characteristics and elastic-plastic modelling of unsaturated sand-bentonite mixture. Ph.D. Thesis, Department of Civil Engineering, University of Manitoba, Winnipeg, Canada.
- Tang, G.X. and J. Graham. 2000. A method for testing tensile strength in unsaturated soils. *ASTM Geotech. Test. J.*, 23(3), 377-387.
- Tang, G.X., J. Graham, J. Blatz, R.K.N.D. Rajapakse and M.Gray. 1998. Suction characteristics of unsaturated sand-bentonite. International Workshop on Key Issues in Waste Isolation Research, Barcelona, Spain, December 1998.
- Tang, G.X. and J. Graham. 2002. A possible elastic-plastic framework for unsaturated high plastic clay soils. *Can. Geotech. J.*, 39(4), 894-907.
- Tang, G.X., J. Graham, J. Blatz, M.Gray and R.K.N.D. Rajapakse. 2002. Suctions, stresses and strengths in unsaturated sand-bentonite. *Engineering Geology*, 66, 147-156.
- Terzaghi, K. 1936. The shear resistance of saturated soils. In Proc. 1st Int. Conf. Soil Mech. Found. Eng., 1, pp. 54-56. Cambridge, MA.
- Vieno, T. 2004. Main issues in the use of cement in a spent fuel repository – what are we seeking answers for? In Proceedings of the International Workshop on Bentonite-Cement Interaction in Repository Environments, 14-16 April 2004, Tokyo, Japan, NUMO-TR-04-05, Nuclear Waste Management Organization of Japan.
- Villar, M.V. 2002. Thermo-hydraulic-mechanical characterization of a bentonite from Cabo de Gata: a study applied to the use of bentonite as sealing material in high level radioactive waste repositories. ENRESA Technical Publication 04/2002.
- Wan, A. W-L. 1987. Compaction and strength characteristics of sand-clay buffer material formed at swelling pressure-water content equilibrium. M.Sc. Thesis, Department of Civil and Geological Engineering, University of Manitoba, Winnipeg, Canada.
- Wan, A. W-L. 1996. The use of thermocouple psychrometer to measure in situ suctions and water content in compacted clays. Ph.D. Thesis, Department of Civil and Geological Engineering, University of Manitoba, Winnipeg, Canada.
- Wersin, P., L.H. Johnson, I.G. McKinley. 2007. Performance of the bentonite barrier at temperatures beyond 100 °C: A critical review. *Physics and Chemistry of the Earth*, 32, 780-788.
- Wiebe, B.J. 1996. The effect of confining pressure, temperature, and suction on the strength and stiffness of unsaturated buffer. M.Sc. Thesis, Department of Civil Engineering, University of Manitoba, Winnipeg, Canada.

- Wiebe, B.J., J. Graham, G.X.Tang and D. Dixon. 1998. Influence of pressure, saturation, and temperature on the behaviour of unsaturated sand-bentonite. *Canadian Geotechnical Journal*, 35, 194-205.
- Yarechewski, D.S. 1993. Constant mean effective stress tests on sand-bentonite specimens at elevated temperature. M.Sc. Thesis, University of Manitoba.
- Yin, J.H. 1990. Constitutive modelling of time-dependent stress-strain behaviour of soils. Ph.D. Thesis, University of Manitoba.
- Yin, J.H. and J. Graham. 1989. Viscous elastic plastic modelling of one-dimensional time dependent behaviour of clays. *Canadian Geotechnical Journal*, 26, 199-209.
- Yin, J.H. and J. Graham. 1994. Equivalent times and one-dimensional elastic visco-plastic modelling of time-dependent stress-strain behaviour of clays. *Canadian Geotechnical Journal*, 31.